Node Cluster Stability in Vehicular Ad hoc Networks

by

Khadige Hussein Abboud

A thesis
presented to the University of Waterloo
in fulfillment of the
thesis requirement for the degree of
Doctor of Philosophy
in
Electrical and Computer Engineering

Waterloo, Ontario, Canada, 2015

I hereby declare that I am the sole author of this thesis. This is a true copy of the thesis, including any required final revisions, as accepted by my examiners.

I understand that my thesis may be made electronically available to the public.

Abstract

In recent years, efforts have been made to deploy communication capabilities in vehicles and the transport infrastructure, leading to a potential of vehicular ad hoc networks (VANETs). In the envisioned VANET, communications among vehicles will enhance the intelligent transportation systems (ITS) and support not only public-safety applications, but also a wide range of infotainment applications. Urban roads and highways are highly susceptible to a large number of vehicles and traffic jams. Therefore, the networking protocols for VANETs should be scalable to support such large sized networks. Node clustering (i.e., organizing the network into smaller groups of nodes) is a potential approach to improve the scalability of networking protocols for VANETs. However, high relative vehicle mobility and frequent network topology changes inflict new challenges on maintaining stable clusters.

The communication links between network nodes play an essential role in determining the VANET topology. This thesis presents a stochastic microscopic vehicle mobility model to capture the time variations of the distance between two consecutive vehicles on a highway. The proposed mobility model is used to characterize the length and the duration of a communication link connecting two nodes in the network for different vehicular traffic flow conditions. Vehicle trajectory data from real and simulated highways are used for performance evaluation.

In a highly dynamic VANET, vehicles join and leave clusters along their travel route, resulting in changes in cluster structure. This thesis investigates the impact of vehicle mobility on node cluster stability. A lumped stochastic model is proposed to describe the temporal variations of a system of intervehicle distances, where each intervehicle distance is represented by the proposed microscopic mobility model. Two metrics are used to measure cluster stability: the time period of invariant cluster-overlap state between two neighboring clusters as a measure of external cluster stability, and the time period of invariant cluster-membership as a measure of internal cluster stability. Using the proposed lumped stochastic model, the two cluster stability metrics are probabilistically characterized for different vehicular traffic flow conditions. Additionally, the limiting behavior of a system of two neighboring clusters is modeled, and the steady-state number of common/unclustered nodes between two clusters is approximately derived. To the best of our knowledge, this is the first mathematical characterization of node cluster stability which takes account of the effect of microscopic vehicle mobility.

In addition to the impact of vehicle mobility on node cluster stability, the notion of cluster stability is also related to the network protocol requirements. This thesis explores

the effect of cluster characteristics (cluster size and cluster-overlap) on minimizing the generic routing overhead. Furthermore, using the derived cluster stability metrics, the impact of cluster instability on intra- and inter- cluster routing overhead is investigated.

The proposed vehicle mobility model is a useful tool for mathematically analyzing the impact of mobility and node density on the performance of network protocols in VANETs. The node cluster stability analysis and the proposed the external and internal cluster stability metrics provide a useful tool for the development of efficient clustering algorithms for VANETs.

Acknowledgements

I would like to express my deep gratitude to my supervisor, Prof. Weihua Zhuang. Thank you for your continuous guidance, support, and encouragement throughout my PhD study. Without your guidance, advice, and valuable input on my research ideas and writings, this work would have not been possible.

I gratefully acknowledge my PhD committee members, Prof. Jelena Mišić, Prof. Bruce Hellinga, Prof. Otman Basir, and Prof. Liang-Liang Xie for their valuable comments and insightful suggestions that helped increase the quality of the thesis.

I sincerely thank Prof. Sherman (Xuemin) Shen and my colleagues at the Broadband Communications Research (BBCR) group, both past and current BBCR members. I feel lucky that I have met and worked with you all. I want to thank you for your friendship, support, and beneficial discussions, especially in the VANET BBCR subgroup.

From the bottom of my heart, I thank my parents for their prayers, support, care, and unconditional love. There is nothing I can do to thank you enough. So lucky, I am, that I was born in this family. I am and will always remain in debt for you. I also want to thank my little sister, Fatima Abboud, who owns a special spot in my heart. Gratitude is due to my brothers and their families for their support and encouragements throughout these years. I want to thank my sister, Zeinab Abboud, for being there for me when I ranted and complained without making me feel that I am being judged. Once again, we have synchronized our start and end of another education level! Good luck in your new adventure as a graduate student.

I want to thank my dearest friend, Nosayba El-Sayed, for her thoughtfulness, support, and encouragement throughout these years. Despite the small number of times that we have actually met, they were enough to leave an encouraging, an enriching, and an uplifting trace on me. I am grateful to have a friend like you.

Last but not least, I want to thank Ali-Akbar Samadani. Thank you for your love, for your encouragement, and for being there for me during the good and the bad. I could not ask for a better company during this PhD trip. I cherish our laughs, our own dictionary of words, our long aimless walks, and our coffee.

Dedication

To my parents

Table of Contents

List of Tables

List of Figures

List of Abbreviations and Symbols

Abbreviations

1D	1-dimensional
CCH	Control channel
CCM	Common Cluster member
cdf	Cumulative distribution function
CH	Cluster head
CM	Cluster member
DSRC	Dedicated Short Range Communications
ETSI	European Telecommunications Standards Institute
FCC	Federal Communications Commission of the U.S.
i.i.d.	Independent and identically distributed
ITS	Intelligent Transportation Systems
LR	Linear regression
MAC	Medium Access Control
NGSIM	Next generation simulation
NHTSA	National Highway Traffic Safety Administration of the U.S.
pdf	Probability density function

pmf	Probability mass function
r.v.	Random variable
RREQ	Route request
s.p.	Stochastic process
s.t.	such that
SCHs	Service channels
TDMA	Time Division Multiple Access
U.S.	United States (of America)
UN	Unclustered node

Symbols

()	Sequence notation
α	Location parameter for the distribution of the inter-vehicle distance (the minimum distance headway) in meters
α_l	Location parameter for the distribution of the cluster length (L_c)
$\bar{v}$	The maximum relative speed between vehicles in meters per second
β	State dependency parameter of the probability transition matrix
Δt	An arbitrary time period in seconds
δ_c	Rate of cluster maintenance updates in packets per second
δ_j	Absorbing probability of lumped state $\Omega_j \in \Omega_{NOV}$
$\delta_{E'_e}$	Absorbing probability δ_{E_e} weighted by the stationary distribution π_i
δ_{E_e}	Absorbing probability of lumped state $\Omega_e \in \Omega_E$

δ_{Inter}	Rate of inter-cluster topology updates in packets per second
δ_{Intra}	Rate of intra-cluster topology updates in packets per second
δ_{L_l}	Absorbing probability of lumped state $\Omega_l \in \Omega_L$
ϵ	A constant for the truncation of the distribution of L_c
$\eta(m)$	A stochastic process with state space $\{-1, 1\}$ representing the cluster-overlap state (s.p.)
$\Gamma(z, x)$	The upper incomplete gamma function
$\gamma(z, x)$	The lower incomplete gamma function
$\Gamma(x)$	Gamma function
λ	Scale parameter for the mesoscopic probability distribution of the distance headway in near-capacity traffic flow conditions
λ_l	Scale parameter for the distribution of the cluster length (L_c)
λ_u	The u^{th} non-unit eigenvalue of M
$\lambda_u^{(j)}$	The u^{th} non-unit eigenvalue of $M^{(j)}$
$\lceil x \rceil$	The smallest integer greater than x
$\lfloor x \rfloor$	The largest integer smaller than x
$\mathbb{A}_J(n)$	The set of all possible ordered J-restricted integer partitions of n
$\mathbb{A}_J^i(n)$	The i^{th} J-restricted integer partition of n, $\mathbb{A}_J^i(n)$
$\mathbb{A}_{\Psi_{intra,n}}$	A matrix with each row represents a possible number of occurrences of overhead 0,1, or 2 pkt/f for the n sampled nodes
$\mathbb{B}_m$	A matrix of two columns and rows representing the frequencies of parts 2 and 3 in all possible integer partition of m into at most L parts, where each part is either 2 or 3
$\mathbb{K}_J(N_H)$	The set of all J-combinations of the set $\{0, 1, \ldots, N_H\}$

$\mathbb{S}_E$	A set of states of the edge lumped Markov chain for system $\mathbb{X}_{CM}$ corresponding to initial state of the system
$\mathbb{X}_{\mathbb{N}_\mathbb{E}}$	The system of distance headways between the two gateways (s.p.)
$\mathbb{X}$	Sequence of N distance headways(s.p.)
$\mathbb{X}_c(m)$	Sequence of distance headways between two CHs at the m^{th} time step (sequence of r.v.s)
$\mathbb{X}_H$	Sequence of $(N_H + 1)$ distance headways between the reference node and its hop edge node (s.p.)
$\mathbb{X}_{CM_E}$	Sequence of distance headways of the CH and the nodes on one side of the cluster when the first cluster-membership change occurs due to a node entering the cluster (s.p)
$\mathbb{X}_{CM_L}$	Sequence of distance headways of the CH and the nodes on one side of the cluster when the first cluster-membership change occurs due to a node leaving the cluster (s.p)
$\mathbb{X}_{CM}$	Sequence of distance headways of the CH and the N_{CM_r} nodes (s.p.)
$\mathbb{X}_c$	Sequence of distance headways between two CHs (s.p.)
$\mho_i$	Stationary distribution of lumped state Ω_i
μ	Mean distance headway in meters
ν_n	Sum of n distance headways (r.v.)
ω	Packet generation rate per node in packet per second
Ω'_e	The lumped state for system $\mathbb{X}_{CM_E}$ corresponding to lumped state Ω_e for $\mathbb{X}_{CM}$
Ω'_l	The lumped state for system $\mathbb{X}_{CM_L}$ corresponding to lumped state Ω_l for $\mathbb{X}_{CM}$
Ω_i	The i^{th} lumped state in the lumped Markov chain.
Ω_E	A set of lumped states in the Edge lumped Markov chain of system $\mathbb{X}_{CM}$ corresponding to a node entering the cluster

Ω_I	A set of lumped states in the Edge lumped Markov chain of system $\mathbb{X}_{CM}$ corresponding to the initial states of the cluster
Ω_L	A set of lumped states in the Edge lumped Markov chain of system $\mathbb{X}_{CM}$ corresponding to a node leaving the cluster
Ω_{NOV1}	A subset of lumped states in Ω_{NOV} that are directly accessible from lumped states in Ω_{OV}
Ω_{NOV2}	A subset of lumped states in Ω_{NOV} that are not directly accessible from lumped states in Ω_{OV}
Ω_{NOV}	A set of lumped states in the lumped Markov chain of system $\mathbb{X}_c$ corresponding to non-overlapping clusters
Ω_{OV1}	A subset of lumped states in Ω_{OV} that are directly accessible from lumped states in Ω_{NOV}
Ω_{OV2}	A subset of lumped states in Ω_{OV} that are not directly accessible from lumped states in Ω_{NOV}
Ω_{OV}	A set of lumped states in the lumped Markov chain of system $\mathbb{X}_c$ corresponding to overlapping clusters
Ω_{R^c}	A set of lumped states in the fully lumped Markov chain of system $\mathbb{X}_{CM}$ corresponding to the hop edge node leaving the cluster
Ω_R	A set of lumped states in the fully lumped Markov chain of system $\mathbb{X}_{CM}$ corresponding to a distance less than R between the CH and the hop edge node
$\otimes$	General matrix multiplication notation
ϕ_i	Absorbing probability of lumped state $\Omega_i \in \Omega_{OV}$
Φ_{CH}	Number of packets needed to broadcast a CH packet to a neighbouring CH
π_i	Stationary distribution of the i^{th} state in the 1D-Markov chain
$\pi_{E,i}$	Stationary distribution of the i^{th} lumped state in the edge lumped Markov chain

$\prod$	Product notation (when used for matrices, it denotes Hadamard matrix multiplication)
Ψ	A row vector of size $\tilde{N'}_L$ in which the j^{th} element equals δ_j
ψ_c	Clustering overhead in packets per second (r.v.)
ψ_T	Total cluster-based routing overhead in packets per second (r.v.)
$\psi_{f,n}$	Number of packets needed to flood a packet to $n-1$ nodes
Ψ_{inter}	The intercluster routing overhead due to mobility per route request of length L measured in packets (r.v.)
$\Psi_{intra,i}$	The intracluster routing overhead due to vehicle mobility for node i in packets per frame (r.v.)
ψ_{Intra}	Inter-cluster routing overhead in packets per second (r.v.)
ψ_{Intra}	Intra-cluster routing overhead in packets per second (r.v.)
ψ_{pp}	The total routing overhead for generic proactive-proactive protocol in packets per second (r.v.)
ψ_{pr}	The total routing overhead for generic proactive-reactive protocol in packets per second (r.v.)
ψ_{rp}	The total routing overhead for generic reactive-proactive protocol in packets per second (r.v.)
ψ_{rr}	The total routing overhead for generic reactive-reactive protocol in packets per second (r.v.)
ρ	Intensity factor
σ	Standard deviation of the distance headway in meters
$\sum$	Sum notation
τ	The duration of the time step in the Markov chain model in seconds
τ_F	Duration of the time frame in seconds

τ_L	The time interval between successive route requests of the same source-destination pairs
θ_i	The length of the i^{th} cluster-non-overlapping period (r.v.)
$\tilde{M'}_{N_c}$	The probability transition matrix of the absorbing lumped Markov chain, when lumped states in Ω_{OV} are merged into a single absorbing state
$\tilde{M}_E$	Probability transition matrix of the lumped Markov chain representing system $\mathbb{X}_{\mathbb{N}_\mathbb{E}}$
ζ_i	The length of the i^{th} cluster-overlapping period (r.v.)
$\{\}$	Set notation
$a_j(i)$	The j^{th} part of the i^{th} J-restricted integer partition of n, $\mathbb{A}_J^i(n)$
A_{k-1}	The interarrival time between customers $k-1$ and k (r.v.)
B_k	The buffer content at the beginning of the k^{th} cycle (r.v.)
$C(l)$	The event that there exists at least one node within distance l from a reference node
$C^c(l)$	The event that there are no nodes within distance l from a reference node (the complement of event $C(l)$)
$c_{T_{Ii}}$	The coefficient of variation of T_{Ii}
$c_{T_{Io}}$	The coefficient of variation of T_{Io}
D	Vehicle density over the highway lane in vehicle per kilometer
$E[Y]$	The expectation of random variable Y
$e_1(m)$	The event that at least one of the distance headways of set $\mathbb{X}_H$ is in state N_{ED} at the m^{th} time step, resulting in a link disconnection
$e_2(m)$	The event that at least J distance headways of set $\mathbb{X}_H$ are in states that construct a J-restricted integer partition of an integer that is greater or equal to N_{ED} with parts at most equal to N_R
E_D	The event that the link between a reference node and its hop edge node, separated by N_H nodes, disconnects given $\mathbb{X}(0)$

$E_{D,V}(m)$	A set of events, each corresponding to set $\mathbb{X}_H$ being in a set of states that construct one of the rows of V at the m^{th} time step, given $\mathbb{X}_H(0)$
$e_{i_l 2}$	The event that a vehicle enters the leading cluster from the left side of its CH
e_{i_l}	The event that a vehicle enters the cluster from the left side of the CH
$e_{i_r 1}$	the event that a vehicle enters the following cluster from the right side of its CH
e_{i_r}	The event that a vehicle enters the cluster from the right side of the CH
e_{o_l}	The event that a vehicle leaves the cluster from the left side of the CH
e_{o_r}	The event that a vehicle leaves the cluster from the right side of the CH
$Erlang(a, b)$	Erlang distribution with shape parameter a and scale parameter b
$Exp(a)$	Exponential distribution with parameter a
$F_Y(y)$	The cumulative distribution function of random variable Y
$f_Y(y)$	The probability density function of random variable Y
G_i	The length of the i^{th} gap from a reference node in meters (r.v.)
H_i	The length of the i^{th} hop from a reference node in meters (r.v.)
I	The identity matrix of size equal to that of $\tilde{N'}_L$
I_c	The super state of system $\mathbb{X}_c$ when the cluster formation is finished (at the 0^{th} time step)
I_{CM}	The super state of system $\mathbb{X}_{CM}$ when the cluster formation is finished (at the 0^{th} time step)
K	Cluster size parameter in hops
K^*	Cluster size parameter in hops that minimizes the average cluster based routing overhead
$K_J(N_H)$	The number of combinations of set $\{0, 1, \ldots, N_H\}$ (the size of $\mathbb{K}_J(N_H)$)

$k_j(v)$	The j^{th} element of the v^{th} combination in the set $\mathbb{K}_J(N_H)$
K_{max}	Maximum cluster size parameter in hops
L	The cluster-level length of the route between a source-destination pair in terms of number of clusters
L_c	Cluster length in meters (r.v.)
$L_J(n)$	The total number of ordered J-restricted integer partitions of n (the size of set $\mathbb{A}_J(n)$)
L_o	Length of the overlapping range between neighboring clusters in meters (r.v.)
l_o	The overlapping factor
l_o^*	Overlapping factor that minimizes the average cluster based routing overhead
L_s	The length of the range covered by each state in the 1D-Markov chain measured in meters
L_{HWY}	Length of the highway segment in meters
Lf	The length of the path from the root node to a leaf node in the intercluster routing overhead rooted tree model (r.v.)
M	Probability transition matrix of the 1D-Markov chain
M'	The probability transition matrix of the absorbing 1D-Markov chain
$M^{(j)}$	The upper left $(j+1)\times(j+1)$ portion of the probability transition matrix, M, with $q_j = 0$ and $r_j = 1$
M_1	A column vector of ones with size $\tilde{N'}_L$
M_{N_c}	The probability transition matrix of the lumped Markov chain describing the system $\mathbb{X}_c$
$M_{N_{CM}}$	The probability transition matrix of the edge lumped Markov chain describing the system $\mathbb{X}_{CM}$

N	An arbitrary number of Markov chains
N_E	The number of nodes between the GWR and GWL connecting the two neighboring clusters (r.v.)
N_H	The number of nodes between a reference node and its hop edge node at the 0^{th} time step
N_i	Number of CMs that are i hops away from the CH (r.v.)
$N_i(\Delta t)$	The number of nodes entering the overlapping region during an arbitrary time period, Δt (r.v.)
$N_i(\zeta_k)$	The number of nodes entering the buffer during the k^{th} cluster-overlapping period (r.v.)
n_j	The number of time steps at which the distance headway is in state j in the NGSIM/VISSIM trajectory data
N_l	The number of nodes in a road segment of length l (r.v.)
$N_o(\Delta t)$	The number of nodes leaving the unclustered region during an arbitrary time period, Δt (r.v.)
$N_o(\theta_k)$	The number of nodes leaving the buffer during the k^{th} cluster-non-overlapping period (r.v.)
$N_{\max}$	Number of states in the 1D-Markov chain
N_{th}	The integer number of the states that cover distance headways within an arbitrary threshold value in the distance headway's 1D-Markov chain
N_{CCM}	Number of common cluster members between two neighboring overlapping clusters (r.v.)
N_{CH}	Number of clusters on the highway segment
N_{CM_r}	The number of CMs on the right side of a cluster (r.v.)
N_{CM}	Number of nodes in the cluster (r.v.)
N_c	The number of nodes between two neighbouring CHs

N_{ED}	The minimum integer value that causes event E_D to occur when it is partitioned into the state indices of the distance headways set, $\mathbb{X}_H$
N_{HWY}	Number of vehicles on the highway (r.v.)
$n_{j,j'}$	The number of transitions of a distance headway from state j to state j' within a time step of length τ in the NGSIM/VISSIM trajectory data
N_L	The state space size of the lumped Markov chain
$N_{UN,\max}$	The maximum number of unclustered nodes between two neighboring clusters
N_{UN}	Number of unclustered nodes between two neighboring disjoint clusters (r.v.)
$Norm(\mu, \sigma^2)$	Normal distribution with mean μ and variance σ^2
$O(\Omega_i)$	A function that maps a lumped state from edge lumped markov chain to the corresponding one in the fully markov chain
o_p	Routing protocol optimizing factor with a value $\in [0, 1]$
p	Density dependent parameter for the transition probability from state j to $j+1$ in the 1D-Markov chain
P_H	The probability that a CM's local neighborhood changes during a cycle
p_j	transition probability from state j to state $j+1$ in the 1D-Markov chain within one time step
p_s	Parameter of the geometric approximation of the number of common/ unclustered nodes that depends on the cluster overlap state between neighboring clusters
$P_Y(y)$	The probability mass function of random variable Y
P_{C0}	The limiting probability that there is zero common CMs between neighboring clusters
P_{CCM}	The limiting probability of the randomly selected node being a common cluster member

P_{che}	The probability that a route of length L clusters is cached
P_{CH}	The limiting probability of the randomly selected node being a cluster head
P_{CM}	The limiting probability of the randomly selected node being a cluster member
P_E	The probability that two neighbouring clusters are connected via gateways
P_{Hn}	The probability that none of the nodes in the cluster detect a change in their one-hop neighborhood
$p_{j,j'}$	The transition probability from state j to j' in the NGSIM/VISSIM trajectory data
P_{nov}	The limiting cluster-overlapping probability
P_{ov}	The limiting cluster-non-overlapping probability
P_{U0}	The limiting probability that there is zero unclustered nodes between neighboring clusters
P_{UN}	The limiting probability of the randomly selected node being an unclustered node
$Pears(a, b, c)$	Pearson type III distribution with scale, shape, and location parameters a, b, and c, respectively
$Pois(a)$	Poisson distribution with parameter a
q	Density dependent parameter for the transition probability from state j to $j-1$ in the 1D-Markov chain
q_j	transition probability from state j to state $j-1$ in the 1D-Markov chain within one time step
$Q_Y(y)$	The probability generating function of random variable Y
R	Transmission range in meters
r_j	return probability of state j back to itself in the 1D-Markov chain within one time step

s_i	i^{th} state in the the 1D-Markov chain
S_{k-1}	The service time of customer $k-1$ (r.v.)
$T(e)$	The first occurrence time of event e (r.v.)
T_H	The time period between two successive changes in node's one-hop neighborhood
T_{CM1_l}	First occurrence time of the first change in cluster-membership (after cluster formation) due to a vehicle leaving and entering the cluster from the left side of the CH (r.v.)
T_{CM1_r}	First occurrence time of the first change in cluster-membership (after cluster formation) due to a vehicle leaving and entering the cluster from the right side of the CH (r.v.)
T_{CM1}	Time for the first change in cluster-membership to occur after cluster formation (r.v.)
$T_{CM1}(\Omega_k)$	Time for the first change in cluster-membership to occur after cluster formation, given that system $\mathbb{X}_{CM}$ is initially in state Ω_k (r.v.)
T_{CM}	The time interval between two consecutive membership changes of a cluster (r.v.)
T_{Ii}	The interarrival time of nodes to the overlapping region (r.v.)
T_{Io}	Node interdeparture time from the unclustered region that causes the number of unclustered nodes to decrease (r.v.)
T_i	The first arrival time of nodes to the overlapping region (r.v.)
$T^i_{j,j'}$	The first passage time of the distance headway X_i to state j' given that the distance headway is in state j at the 0^{th} time step
$T_{nov1}(\Omega_j)$	The time interval from the instant that the clusters become non-overlapping till the first time instant that the two clusters become non-overlapping, given that system of distance headways between the two CHs, $\mathbb{X}_c$, is initially in lumped state Ω_j (r.v.)
T_{nov}	Cluster-non-overlapping time period (r.v.)

T_{ov1}	The time interval from the instant that the clusters are initially formed till the first time instant that the two clusters are no longer overlapping (r.v.)
$T_{ov1}(\Omega_k)$	The time interval from the instant that the clusters are initially formed till the first time instant that the two clusters are no longer overlapping, given that system of distance headways between the two CHs, $\mathbb{X}_c$, are initially in lumped state Ω_k (r.v.)
T_{ov}	Cluster-overlapping time period (r.v.)
V	the union of the two matrices, $V^{'}$ and $V^{''}$
$V(m)$	The virtual waiting time (buffer content) at an arbitrary time step m (r.v.)
$V(v)$	The v^{th} row of V
$V^{''}$	A matrix with $N_H + 1$ columns and rows consisting of all possible ordered J-restricted partitions of integers $N_{ED} + 1, N_{ED} + 2, ..., (N_H + 1)N_{ED}$, each with the largest part less than or equal to N_{ED}
$V^{'}$	A matrix with $N_H + 1$ columns and rows consisting of J-restricted partition of N_{ED} and $(N_H - J + 1)$ zeros
X	Arbitrary distance headway in meters (s.p.)
X_i	The distance headway between node i and node $i + 1$ in meters (s.p.)
$X_i(m)$	The distance headway between node i and node $i + 1$ in meters at the m^{th} (r.v.)
x_j	The quantized distance headway length of the j^{th} state in the 1D-Markov chain measured in meters
$X_{\max}$	The maximum value of the distance headway in meters
z	Shape parameter for the mesoscopic probability distribution of the distance headway in near-capacity traffic flow conditions
z_l	Shape parameter for the distribution of the cluster length L_c
$\text{erf}(\cdot)$	The error function

$\tilde{M}_{N_c}$	The probability transition matrix of the absorbing lumped Markov chain, when lumped states in Ω_{NOV} are merged into a single absorbing state
$\tilde{M}_{N_{CM}}$	The probability transition matrix of the absorbing edge lumped Markov chain, when lumped states in Ω_L and Ω_E are merged into one single absorbing state
$\tilde{N'}_L$	The number of states in the absorbing lumped Markov chain, when the lumped states in Ω_{OV} are merged into one absorbing state
$\tilde{N}_L$	The number of states in the absorbing lumped Markov chain, when the lumped states in Ω_{NOV} are merged into one absorbing state
M''_{N_c}	The probability transition matrix of the absorbing lumped Markov chain, when lumped states in Ω_{NOV} are made absorbing without merging them into a single state
M'_{CM}	The probability transition matrix of the absorbing edge lumped Markov chain, when lumped states in Ω_L and Ω_E are made absorbing without merging them into a single state
M'_{N_c}	The probability transition matrix of the absorbing lumped Markov chain, when lumped states in Ω_{OV} are made absorbing without merging them into a single state

Chapter 1

Introduction

1.1 Vehicular ad hoc networks (VANETs)

Newly manufactured vehicles are no longer the simple mechanical devices that we once knew. Each vehicle is a smart body of various sensors that can measure different attributes. Recently, efforts have been made to deploy communication capabilities in vehicles and the transport infrastructure, leading to a potential of vehicular ad hoc networks (VANETs). In 1999, the United States Federal Communications Commission (FCC) allocated 75 MHz of radio spectrum in the 5.9 GHz band to be used for Dedicated Short Range Communication (DSRC) by intelligent transportation systems (ITS). The DSRC spectrum has seven 10MHz channels, one control channel (CCH) and six service channels (SCHs). In 2008, the European Telecommunications Standards Institute (ETSI) allocated 30 MHz of spectrum in the 5.9 GHz band for ITS. In 2014, the U.S. National Highway Traffic Safety Administration (NHTSA) announced that it had been working with the U.S. department of transportation on regulations that would eventually mandate vehicular communication capabilities in new light vehicles by 2017 [2]. An envisioned VANET will consist of *i)* vehicles with on-board sensing and transmitting units which form the network nodes; *ii)* stationary road side units (RSUs) deployed on the sides of roads and connected to the Internet; and *iii)* a set of wireless channels from the DSRC spectrum. An illustration of a VANET infrastructure is shown in Figure 1.1.

The embedded wireless communication capabilities will enable both vehicle-to-vehicle (V2V) and vehicle-to-infrastructure (V2I[1]) communications. Many new ITS applications

[1]V2I communications refer to the bidirectional communications between a RSU and a vehicle.

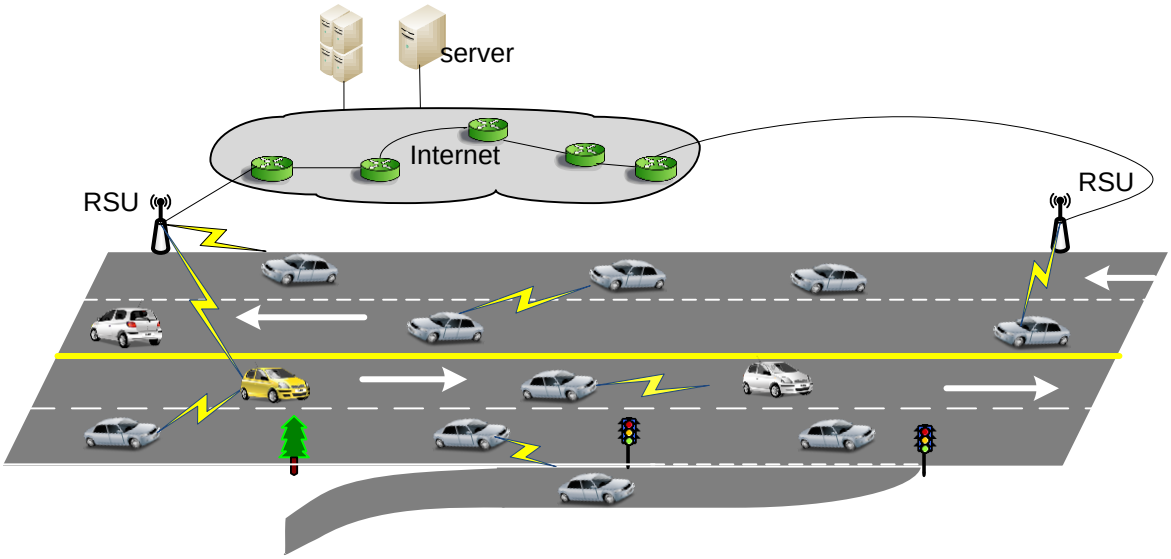

Figure 1.1: An illustration of VANET infrastructure

will emerge with the support of V2V and V2I communications. ITS applications include on-road safety and infotainment applications. Examples of safety applications include emergency warning, lane changing assistance, and intersection coordination. On the other hand, infotainment applications can provide *i)* drivers with information about weather, maps, and directions to nearby petrol stations/restaurants, and *ii)* passengers with Internet access that includes web-surfing and multimedia applications [3].

The implementation of VANET applications is dependent on the development of networking protocols that can guarantee reliable and efficient V2V and V2I communications. VANETs are susceptible to a large number of nodes, traffic[2] jams, and traffic density variations from time-to-time and from point-to-point on the same roads. Therefore, the networking protocols for VANETs should be scalable to support such large sized networks.

VANETs have specific characteristics that impose new challenges to the network development and operation when compared with traditional mobile ad hoc networks (MANETs). Unlike traditional networks, where nodes are either static or move independently with low speeds, nodes in VANETs move with very high speeds, causing network fragmentations and rapid changes in the network topology. Additionally, the movement of vehicular nodes is dependent on driver behaviors and the interaction with neighboring vehicles.

[2]The term traffic refers to vehicle traffic in this thesis.

1.2 Node clustering in VANETs

Node clustering is a network management strategy in which nearby nodes are grouped into a set called *cluster*. In each cluster, a node is elected to manage the cluster. This node is called cluster head (CH). The remaining nodes are called cluster members (CMs), each belonging to one or multiple clusters. A communication between a pair of nodes in the same cluster is referred to as intracluster communication, whereas an intercluster communication takes place between nodes in different clusters. The CH may elect some of its CMs as gateway nodes that facilitate the intercluster communications among neighbouring clusters. Therefore, node clustering is a process that transforms a flat network infrastructure into a two-tier infrastructure. The first tier consists of CHs and gateways, whereas the second tier is composed of the CMs.

When the number of nodes increases in a network, the performance of flat-network protocols starts degrading [4, 5]. Node clustering has been shown to be an effective strategy to improve scalability in traditional ad hoc networks [6, 7]. For medium access control (MAC) protocols, the CH can act as a central coordinator that manages the access of its CMs to the wireless channel(s) [7]. For routing protocols, CHs can be made responsible for the discovery and maintenance of routing paths, thus limiting the number of control-message overhead in these processes [6].

There are different ways to cluster network nodes. Different clustering algorithms in the literature have different rules that govern the CH/gateway election, the membership to a cluster, and the type of inter-/intra- cluster communications. However, regardless of the algorithm-specific clustering rules, the formed clusters may share some characteristics. An important characteristic of node clusters is the cluster size. The size of a cluster is usually defined by its coverage area. The area is represented by a radius from the reference node (i.e., the CH). The radius covers either a single hop [8] or multiple hops [9, 10]. As a result, the size of the cluster is directly related to the transmission range. A larger cluster size produces a smaller number of clusters, with a larger number of nodes to manage within each cluster. The overlapping state between neighboring clusters is another important characteristic. The overlapping state determines the type of intercluster communication between neighboring clusters. In the literature, the overlapping between neighboring cluster takes one of three states: complete disjoint, partial overlap, or complete overlap. In the complete disjoint state, no node belongs to more than one cluster [11]. In this case, gateway nodes should be elected in each cluster and the intercluster communications is done via gateway-to-gateway communications as shown in Figure 1.2(a). In the partial overlap state, neighboring clusters share common gateway nodes [12–15]. In this case, gateway-to-CH communications is used to connect neighboring clusters. In the complete

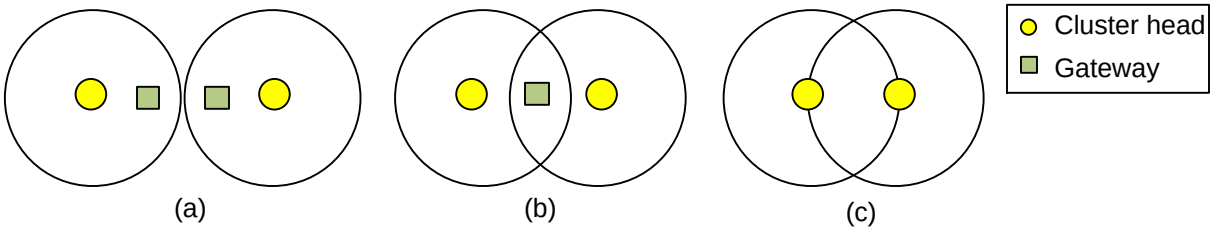

Figure 1.2: Cluster-overlap states: (a) disjoint, (b) partial overlap, (c) complete overlap.

overlap state, the neighboring two CHs are within the communication range of each other and communicate directly.

In general, a non-overlapping clustered structure produces a relatively small number of clusters and reduces the design complexity of the network protocols that run on the clusters. For example, two clusters may utilize the same channel resources at the same time if they are non neighboring clusters [16] [17]. On the other hand, a highly overlapping clustered structure may cause complexity in the channel assignment, lead to a broadcast storm, and form long hierarchical routes. Additional channel resources ought to be used to prevent intercluster interference due to cluster overlapping. For example, assigning different time frames for neighboring clusters [18] and assigning different transmission codes to CMs located in a possibly overlapping region [19]. In developing a clustering algorithm, the choice of cluster characteristics, such as the cluster size and the overlapping state between clusters, should comply with the requirements of network protocols. The choice of the cluster characteristics should balance the cost-efficiency trade-off for the supported network protocols.

Despite the potential benefits of node clustering, the formation and maintenance of clusters require explicit exchange of cluster-control messages [16]. In order to form clusters, nodes must exchange some local information (*e.g.,* node location or ID). This is done in the form of cluster-control messages. For example, one of the basic clustering techniques is to choose the CH with the lowest ID among its neighbors [16]. To form lowest ID clusters, neighboring nodes must exchange their ID information. Therefore, a portion of the network radio resources is used for cluster formation. Node clustering groups nearby nodes into clusters; hence the proximity of CMs to the CH is very important in maintaining the cluster structure. Changes in the relative position of CMs can alter the cluster structure. To track cluster changes, a CH should always announce its existence to its CMs, and each CM should continuously reply back to its CH. This signaling uses a portion of the network radio resources.

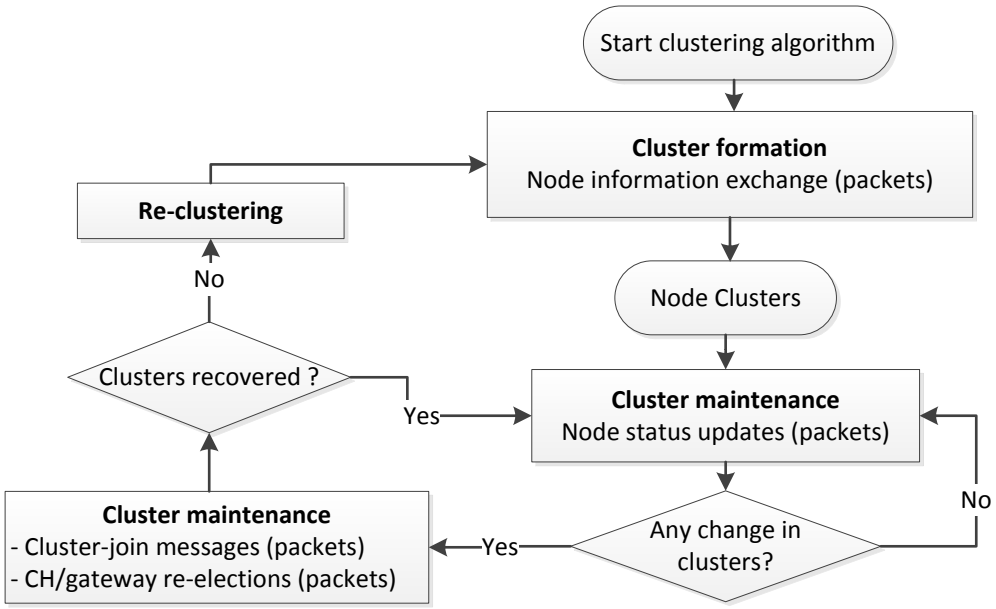

Figure 1.3: Clustering cost.

The node status update information can be utilized to perform local updates on the cluster structure, such as joining a new cluster and/or re-electing new CHs or gateways. This signaling along with the node status update messaging use a portion of the network radio resources, i.e., the cluster maintenance cost. In some cases, the cluster changes cannot be resolved locally; hence a re-clustering is triggered (i.e., a new cluster formation). Frequent re-clustering consumes the network radio resources and causes service disruption for the cluster-based network protocols. Figure 1.3 shows a flow chart of the clustering cost, where a formation cost is paid whenever re-clustering is triggered. As the number of cluster-control messages increases, the network bandwidth drains, leaving insufficient available resources for implementing upper layer applications [16]. Therefore, there exists a cost-efficiency trade-off for implementing node clustering for network protocols.

Considering the susceptibility of VANETs to a large number of nodes, traffic jams, and variable traffic density, the network protocols should be scalable. Node clustering, just as in traditional ad hoc networks, is a potential approach to improve the scalability of networking protocols such as for routing and medium access control in VANETs [11–13, 15, 18, 20–36]. Nevertheless, forming and maintaining the clusters in VANETs is not an easy task. In VANETs, vehicles move with high and variable speeds causing frequent changes in the network topology, which can significantly increase the cluster maintenance cost. As a

result, cluster stability is a crucial measure of the efficiency of clustering algorithms for VANETs.

1.3 Node cluster stability

Cluster stability is a major issue in node clustering for VANETs. Traditional clustering algorithms have a high maintenance cost in dynamic networks [23]. This calls for new clustering approaches that produce long lasting clusters in a highly mobile network. The research on clustering in VANETs [11–13, 15, 20–23] has tackled stability in the formation and/or the maintenance stages of clustering. Existing clustering algorithms for VANETs that tackle stability in the cluster formation stage utilize mobility information mainly in the CH election. The basic idea is to increase the lifetime of the cluster by choosing the CH that is more likely to have a long time connection to most of the CMs [11–15, 18, 22, 23]. Given a set of clusters, regardless of the clustering algorithm, node mobility can change the originally formed clusters. Strategies that enhance cluster stability at the maintenance stage are mainly a set of event-driven rules that aim to prevent or postpone triggering re-clustering [12, 15, 23].

In a highly dynamic VANET, vehicles join and leave clusters along their travel route, resulting in changes in cluster structure. The temporal changes in cluster structure are either internal or external [37]. An internal change in the cluster structure is concerned with a change inside the cluster such as when vehicles join or leave the cluster, resulting in a change in cluster-membership. Frequent changes in the internal cluster structure consume network radio resources and cause service disruption for the cluster-based network protocols (e.g., in intracluster resource allocation, route discovery, and message delivery). Therefore, analyzing the impact of vehicle mobility on the rate at which nodes enter and leave a cluster is an important measure of internal cluster stability. This metric has been adopted by researchers to evaluate the performance of their proposed clustering algorithms through simulations [15, 23, 38]. A higher rate of cluster-membership changes indicates a smaller time period of invariant cluster-membership and, therefore, lower internal cluster stability.

On the other hand, an external change in the cluster structure is concerned with the relationship of a cluster with other clusters in a network. One metric that evaluates the external relationship of a cluster is its overlapping ranges with neighboring clusters. The time variations of the distance between two neighboring CHs, due to vehicle mobility, can cause the coverage ranges of the clusters to overlap. As the overlapping range between two clusters increases, the two clusters may merge into a single cluster [12, 15, 36]. Frequent splitting and merging of clusters increase the control overhead and drain the radio resources

[13, 22, 38]. Although researchers have favored forming a non-overlapping (or a reduced overlapping) clustered structure [13] [22] [12] [19], encountering overlapping clusters during the network runtime is inevitable, especially in a highly mobile network. Overlapping clusters have received significant attention since the work by Palla et al. [39]. It is shown that real networks are better characterized by well-defined statistics of overlapping and nested clusters rather than disjoint clusters. Regardless of whether or not cluster overlapping is preferred, characterizing the overlapping state between neighboring clusters and its changes over time becomes crucial in the presence of node mobility. A higher rate of cluster-overlap state change indicates a shorter time period of unchanged cluster-overlap state and, therefore, lower external cluster stability.

Despite the importance of cluster stability as a measure of clustering algorithm efficiency in VANETs, characterizing cluster stability has taken the form of simulations [15, 23, 38] or case studies [40] in the literature.

1.4 Vehicle mobility

Vehicle mobility is a major component of the VANET structure. The impact of node mobility on network topology dynamics and, consequently, on cluster stability and network protocol performance should be considered. Despite its high speed and randomness, the vehicle movement is restricted by road topology, speed limits, traffic rules, and movement of nearby vehicles. Therefore, based on these metrics, vehicle movement follows certain patterns [1]. Modeling vehicle traffic characteristics has attracted great attention from researchers in transportation engineering for many years. From the various vehicle traffic characteristics, the distance headway and its variations over time play an essential role in changing the network topology. The distance headway (or the intervehicle distance) is the distance between identical points on two consecutive vehicles on the same lane. In general, vehicle mobility models in the literature can be categorized into three (microscopic, mesoscopic, and macroscopic) types according to the detail level of the interactions among vehicles that the model characterizes [1, 41, 42]. A macroscopic distance headway model describes the average distance headway over a highway. The average distance headway is equal to reciprocal of the vehicle density. The vehicle density (D) is defined as the average number of vehicles per lane occupying a segment of the roadway [1]. The value of the vehicle density defines the traffic flow condition, an important metric for modelling vehicular traffic flow. Table 1.1 lists the traffic flow conditions corresponding to different traffic density ranges.

Mesoscopic traffic flow models describe the traffic flow with more details than macro-

scopic models. On a mesoscopic level, the behaviors of individual vehicles are characterized independently [1, 43]. A mesoscopic mobility model describes the distance headways of individual vehicles by independent and identically distributed random variables [1, 44]. That is, on a mesoscopice level, the traffic appears as a snap shot over the considered road segment. Different mesoscopic models have been proposed for different traffic flow conditions [1].

A microscopic model specifies time variations of a distance headway according to the driver behaviors and interactions with neighboring vehicles [1, 41]. On a microscopic level, the details of individual vehicle behaviors are modeled. The level of details include vehicular behaviors resulting from interacting with nearby vehicles. These behaviors include accelerating, decelerating, reacting to slowing leading vehicles, decisions on changing lanes, overpassing vehicles, etc. There are mainly two types of microscopic traffic flow models: the car following models and the cellular automata (CA) models. Car following models basically revolve around one simple rule: *keeping a safe distance ahead*.

Despite the accuracy of modelling the following-behavior of vehicles, there are several factors that limit the generality of car following models [45]. At a long distance headway, the interaction between vehicles is very low. In this case, vehicle behavior is not affected by the leading vehicle and will be in a free-driving mode which is not captured by a car-following model. Even in a highly dense situation, when the distance headway is small, a following vehicle may desire to move at a lower speed from the leading vehicle, and hence will not be in the following mode [45]. While car-following models are continuous models, CA-models are discrete. A CA-model describes a single lane road as a lattice of a number of equal sized cells [46]. The model includes a set of event-driven rules that define how a vehicle on road changes its speed and acceleration to traverse through cells (i.e., road segments).

In order to characterize the stability of clusters, a model that captures the time variations of distance headways need to be considered. Deterministic microscopic models (e.g. GM car following models [1]) do not reflect the realistic randomness in driver behavior. The two main factors that affect changes of a distance headway over time, i.e., the driver

Table 1.1: Traffic flow state for different vehicle densities [1]

Density (veh/ml/lane)	**Traffic flow condition**
$0 - 42$	Uncongested flow conditions (low)
$42 - 67$	Near-capacity flow conditions (intermediate)
$67 - 100$	Congested flow conditions (high)

behaviors and interactions with neighboring vehicles, are both random. Furthermore, the correlation between a distance headway and its changes over a time period is not captured in a mesoscopic model. Therefore, to accurately model the cluster stability, a microscopic mobility model should be used. As pointed out earlier, microscopic mobility models in the literature include a set of deterministic and/or probabilistic rules that define how a vehicle on road changes its speed and/or acceleration in reaction to its neighboring vehicles' behaviors [1]. As such a model depends on the behaviors of neighboring vehicles over time, the analysis tends to take the form of case studies (e.g., [44]).

1.5 Cluster-based routing in VANETs

Routing is a process of selecting paths in a network along which data is transmitted between network entities. When a source node wants to send data packets to a certain destination, a routing protocol is responsible for establishing and maintaining a route between the source and the destination. A route consists of a sequence of relay nodes from the source to the destination. Routing protocols use some path selection algorithms such as shortest path algorithms.

Generally, in a multi-hop wireless network, source messages are relayed by intermediate nodes in order to reach the destination. To establish a path between network entities in a multi-hop network, many routing protocols have been proposed in the literature [47]. A routing protocol can be proactive (table-driven), reactive (on demand), or hybrid (a mix of both) [48] and is implemented along with a Hello protocol. In a Hello protocol, each node periodically broadcasts its local topology information (*e.g.,* neighbor nodes list, link state information, and/or mobility information) to its one hop neighbors.

In a proactive routing protocol, every node shares its local topology information with every other node in the network. Therefore, each node maintains the topology map of the whole network and builds a table of routes to every other node in the network. Sharing topology information is periodic or is triggered when topology changes occur. On the other hand, a reactive routing protocol is on-demand for data transmission. Routes between nodes are found only when they are needed to forward packets. When a source node has data to send, a route discovery process is initiated by broadcasting a route request (RREQ) packet throughout the network until a route to a destination is found [49].

Due to the high vehicle speeds and the frequent network topology changes in VANETs, finding and maintaining a long route are not easy tasks. Wireless links switch between connection and disconnections because of the relative speed between the nodes, thus increasing

the routing overhead associated with topology updates and route discovery processes. Additionally, the large number of nodes in VANETs makes flooding control messages (RREQ and topology update packets) consume a large portion of the radio bandwidth; hence scalability is another issue to be considered when developing a reliable routing protocol for VANETs.

One way of minimizing the routing overhead is to use a hierarchical infrastructure. In a clustered network, CHs and gateways create a virtual backbone that can be made responsible for the discovery and maintenance of routing paths, thus limiting the number of control-message overhead in these processes. Additionally, if a link of an established route breaks, a CH can take the responsibility of fixing the route locally within the cluster.

In a cluster-based routing protocol, different routing strategies can be used for intra- and inter- cluster routing. For example, if a proactive routing strategy is used for intracluster communication [24, 26, 27], each node in the cluster maintains a topology map of the cluster. If a source node has data to send to a destination that is in the same cluster as the source, the route information is readily available. On the other hand, if a reactive strategy is used for intracluster routing [28], a source node floods an RREQ packet within its cluster if the destination is within the cluster. Existing protocols in the literature differ in the routing strategy used for intercluster communications. Some protocols use reactive routing [24, 27], while in other protocols, CHs proactively share their cluster membership information and hence the RREQ is flooded only among the series of clusters towards the destination [28]. Cluster-based routing protocols proposed in the literature aim to minimize the routing overhead and scale to an increased node density, using various cluster characteristics. For example, non-overlapping multi-hop clusters are considered in [24], while single-hop possibly overlapping clusters are assumed in [27]. Cluster characteristics have direct impact on the routing protocol performance.

Although node clustering is a potential solution for minimizing routing overhead, unstable clusters can increase the control signaling overhead associated with the discovery and maintenance of routing paths. Due to vehicle mobility, a node may leave or enter a cluster, triggering updates to the intracluster routes. Frequent changes in the internal cluster structure increase the number of control messages required to establish and maintain routes between cluster members, thus, increasing the intracluster routing overhead. On the other hand, changes in the cluster-overlap state affect the routing overhead. A highly overlapping clustered structure may increase the intracluster routing overhead, as common nodes need to report to both clusters. Disjoint clusters may result in longer hierarchical routes between CHs and a failure of route discovery processes [49]. Therefore, analyzing the impact of cluster instability, due to vehicle mobility, on the routing overhead is crucial for validating the effectiveness of clustering for routing in VANETs.

1.6 Research objectives and thesis outline

Due to the lack of mathematical basis of node cluster stability in VANETs as discussed in previous sections, this research is a step towards building a framework for node cluster stability in VANETs and has the following objectives:

- to characterize the communication link in VANETs as a corner stone in determining the topology of VANET and its change over time, and to develop a stochastic microscopic vehicle mobility model that can be utilized in analyzing the impact of mobility and node density on network protocols in VANETs;
- to model node cluster stability in terms of the cluster's internal relation with its CMs and the cluster's external relation with neighboring clusters; and
- to investigate the impact of cluster characteristics on the routing overhead, and to employ the cluster stability model for determining the impact of cluster instability on the routing overhead.

The rest of the thesis is organized as follows. Chapter 2 describes the system model under consideration. Chapter 3 presents probabilistic analysis of the communication link in VANETs for three vehicle density ranges. Mesoscopic mobility models are utilized to obtain the communication link length. In addition, a microscopic vehicle mobility is introduced to describe the time variation of the distance headway on a single lane highway, which is consistent with highway data patterns from empirical and simulated data sets [50, 51]. Chapter 4 introduces a stochastic analysis of single-hop cluster stability in terms of two metrics that measure external and the internal cluster stability [52, 53]. Chapter 5 first investigates the impact of cluster characteristics on generic routing overhead, then analyzes the impact of cluster instability on generic routing overhead, where clusters are formed using the results of the first part [54, 55]. Finally, Chapter 6 concludes this research and identifies some further research topics.

Chapter 2

System model

Consider a connected VANET on a multi-lane highway of length L_{HWY} with no on or off ramps. We focus on a single lane with lane changes implicitly captured in the adopted mobility model. We choose a single lane from a multi-lane highway instead of a single-lane highway, in order to be more realistic in a highway scenario. A vehicle can overtake a slower leading vehicle, if possible, and accelerate towards its desired speed[1]. Let N_{HWY} be the total number of vehicles on the highway. Assume that the highway is in a steady traffic flow condition defined by a time-invariant vehicle density. Let D denote the vehicle density in vehicle per kilometer. We consider three levels of D: low, intermediate, and high vehicle densities as in Table 1.1. However, we do not consider the case when the vehicle density is changing between the three levels. Additionally, we do not consider the case of increasing/decreasing vehicle density within the same level of density. In our system model we focus only on a single direction traffic flow. Due to large relative speeds between vehicles flowing in opposite directions, a cluster consists of vehicles moving in the same direction, i.e., each direction of the highway is clustered separately [23]. All the vehicles have the same transmission range, denoted by R. Any two nodes at a distance less than R from each other are one hop neighbours. The length of a hop is defined as the distance to the furthest node within the transmission range of a reference node, which is upper bounded by R. Let H_i denote the i^{th} hop length with respect to a reference node, $i \geq 1$. Assume that the transmission range is much larger than the width of the highway such that a node can communicate with any node within a longitudinal distance of R from it[2].

[1] In a single-lane highway, the vehicle traffic gradually converges into a number of platoons lead by the slower vehicles on the highway [56].

[2] Typically, the transmission range covers a circular area with a radius R centred at the node. However, since the transmission range is much larger than the width of the road, the area covered by the transmission

Consider a single DSRC channel which supports a high data rate of $6 - 27$Mbps and a transmission range up to 1000 meters (m). Time is partitioned with a constant step size. Let X_i be the distance headway between node i and node $i+1$, $i = 0, 1, 2, \ldots$. The distance headway is the distance between two identical points on two consecutive vehicles on the same lane. Define $X_i = \{X_i(m), m = 0, 1, 2 \ldots\}$ to be a discrete-time stochastic process of the i^{th} distance headway, where $X_i(m)$ is a random variable representing the distance headway of node i at the m^{th} time step. At any time step, $X_i(m) \in [\alpha, X_{\max}]$ for all $i, m \geq 0$, where α and $X_{\max}$ is the minimum and maximum distance headway, respectively. Furthermore, assume that X_i's are independent with identical statistical behaviors for all $i \geq 0$. For notation simplicity, we omit index i from X_i and H_i when referring to an arbitrary distance headway and an arbitrary hop, respectively. Let μ and σ be the mean and the standard deviation of the distance headway in meters, respectively, where $\mu = 1000/D$ and σ are constant system parameters and take different values according to the vehicle density. Throughout this thesis, $F_Y(y), P_Y(y), f_Y(y), Q_Y(y)$, and $E[Y]$ are used to denote the cumulative distribution function (cdf), the probability mass function (pmf), the probability density function (pdf), the probability generating function, and the expectation of random variable Y, respectively.

2.1 Node clusters

The nodes on the highway are clustered by some clustering algorithm into possibly overlapping, K-hop clusters, where K is the cluster size parameter. The range of each cluster extends K-hops on both sides of the CH. Let L_c be the length of the cluster in meters. We define L_c such that the K^{th} hops of a cluster are of length R, in order to control overlapping between clusters (more details in Subsection 5.1.2). Figure 2.1 illustrates the clusters under consideration. Let N_{CM} denote the total number of nodes in a cluster. Let N_{CH} be the number of clusters formed on the highway. A CH elects the hop edge node, i.e., the furthest node within its hop, as a gateway node that is responsible to facilitate inter-cluster communications. We refer to the side of the cluster that is following the CH as the *left* side, while the leading side of the cluster is referred to as the *right* side. Therefore, GWR and GWL are the right and the left gateways of a cluster, respectively, as illustrated in Figure 2.1(a). Together the CHs and the gateways form the backbone nodes. At the end of the cluster formation, the vehicles are distributed on the highway according to a stationary probability distribution of the distance headways. In our analysis, the 0^{th} time step refers to the time when the cluster formation has just completed. Define the cluster-overlap state

range can be approximated by a rectangular area with length $2R$.

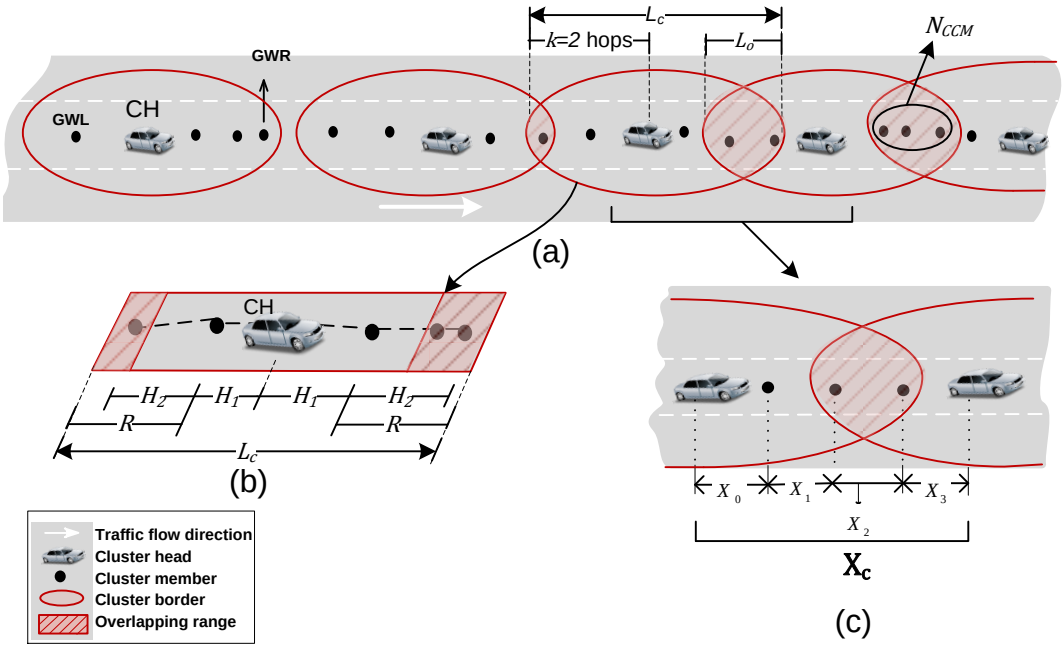

Figure 2.1: An illustration of the clusters under consideration for $k = 2$ hops.

between two neighbouring clusters to be *i)* overlapping, when the distance between the two CHs is less than $2R$; or *ii)* non-overlapping (or disjoint), otherwise. For two neighboring clusters, we define the following variables.

- Let L_o denote the length of the overlapping range between two neighboring clusters;
- Let l_o denote the overlapping fraction of the cluster length with a neighboring cluster (i.e., $l_o = {}^{L_o}/_{L_c}$). The overlapping state between neighboring clusters is determined by the value of $l_o \in [0, 0.5]$, where $l_o = 0$ and $l_o = 0.5$ correspond to complete disjoint and complete overlap states, respectively;
- Let $\mathbb{X}_c$ denote the sequence of distance headways between two neighboring CHs as illustrated in Figure 2.1(c);
- Let N_{CCM} denote the number of common cluster members between two neighbouring overlapping clusters;
- Let N_{UN} denote the number of unclustered nodes between two neighboring disjoint clusters (assume that $N_{UN} = 0$ at the end of the initial cluster formation).

We assume that the clusters are initially overlapping and the CHs remain the same over a time interval of interest. Throughout this thesis, the cluster size K and the overlapping ratio l_o are referred to as cluster characteristics, whereas $N_{CM}, N_{CCM}, L_c,$ and L_o are referred to as cluster parameters.

2.2 Node mobility

In this research, we are interested in the distance headway and the spatial distribution of vehicles along the road. Therefore, the adopted vehicular mobility model is used to describe the distance headway. Unless otherwise mentioned, on a macroscopic level, we consider three different traffic flow conditions: uncongested, near-capacity, and congested. We study each of the three traffic flow conditions separately, without considering the case of changing traffic flow condition. Each traffic flow condition corresponds to a range of vehicle densities according to Table 1.1 [1]. The uncongested, near capacity, and congested traffic flow conditions correspond to low, intermediate, and high vehicle densities, respectively. Additionally, each traffic flow condition corresponds to a unique microscopic and a unique mesoscopic distance headway model. On a microscopic level, we propose to model the time variations of the distance headway by a discrete-time finite-state Markov chain. Details of the microscopic model are given in Chapter 3.

Mesoscopic mobility model

Main mesoscopic models in the literature focus on the time-headway, which is the elapsed time of the passage of identical points on two consecutive vehicles [1]. For an uncongested traffic flow condition, the exponential distribution has been shown to be a good approximation for the time headway distribution [1]. With a low vehicle density, interactions between vehicles are very low and almost negligible. As a result, vehicles move independently at a maximum speed [1]. It is reasonable to assume that, over a short time interval of interest, vehicles move at constant velocity and do not interact with each other [57], [58]. Therefore, for a low vehicle density, we assume that the distance headway has the same distribution as the time headway with parameters properly scaled. The inter-vehicle distances X_i's at any time step are independent and identically distributed (i.i.d.) with an exponential probability density function (pdf)

$$f_{X_i}(x) = \frac{1}{\mu} e^{-\frac{x}{\mu}}, \quad x \geq 0. \tag{2.1}$$

In this case, the mean and the standard deviation of the distance headway is $\mu = \sigma = \frac{1000}{D}$. According to the distribution, $P(X_i \leq \alpha) > 0$; however, for simplicity, we ignore the effect of this probability[3].

In the literature, the Gaussian distribution is used to model the time headway for a congested traffic flow condition [1]. Although the time headway is almost constant for a high vehicle density, driver behaviors cause the time headway to vary around that constant value. Therefore, the Gaussian distribution model for the time headway characterizes the driver attempt to drive at a constant time headway [1]. With the same argument, we assume that the distance headways vary around a constant value with a Gaussian distribution. The pdf of the distance headway is approximately given by

$$f_{X_i}(x) = \frac{1}{\sqrt{2\pi}\sigma} e^{-\frac{(x-\mu)^2}{2\sigma^2}}, \quad x \geq 0. \tag{2.2}$$

The standard deviation σ for a high vehicle density is given by[4] $\sigma = \frac{(\mu-\alpha)}{2}$.

For a near-capacity traffic flow condition, empirical pdfs for inter-vehicle distances show that neither an exponential nor a Gaussian distribution is a good fit [59]. Hence, we assume that the inter-vehicle distances follow a general distribution, Pearson type III, that was originally proposed for time headways [1]. With an intermediate vehicle density, the pdf of the distance headway is approximately given by

$$f_{X_i}(x) = \frac{\lambda^z}{\Gamma(z)} (x-\alpha)^{z-1} e^{-\lambda(x-\alpha)}, \quad x \geq \alpha \tag{2.3}$$

where λ and z are the scale and shape parameters of the general Pearson type III distribution, respectively, and $\Gamma(z) = \int_0^\infty u^{z-1} e^{-u} du$ is the gamma function. The parameters λ and z are related to μ and σ according to the following relations [1]

$$\lambda = \frac{\mu - \alpha}{\sigma^2}, \quad z = \frac{(\mu-\alpha)^2}{\sigma^2}. \tag{2.4}$$

[3] $P(X_i \leq \alpha) = 1 - e^{-D\alpha}$. For example, for $D = 6$ veh/km and $\alpha = 6.7$ meters [1], $P(X_i \leq \alpha) = 0.04$. The probability $P(X_i \leq \alpha)$ increases with D.

[4] We use the same guidelines for calculating the variance of time headway as given in [1]. With $\sigma = \frac{(\mu-\alpha)}{2}$, $P(X_i > \alpha) = 0.977$ [1]. For a congested traffic flow condition (i.e., $D \geq 42$ veh/km) and $\alpha = 6.7m$ [1], $P(X_i \leq 0) \leq 2.8 \times 10^{-3}$.

2.3 Summary

In this chapter, the system model under consideration in this research has been presented. In specific, a highway VANET is considered with focus on a single lane. As this research does not target the performance evaluation of a specific clustering algorithm, the cluster characteristics and parameters of the formed clusters have been defined in this chapter. The nodes on the highway are clustered by some clustering algorithm into possibly overlapping, K-hop clusters. Furthermore, the vehicle mobility under consideration has been introduced. Three vehicle traffic flow conditions are considered, each corresponding to a range of vehicle densities. For each traffic flow condition, we employ the associated mesoscopic distance headway model when a snapshot of the highway traffic is studied. On the other hand, when studying the temporal variations in the vehicle traffic, a microscopic mobility model is used, which is presented in the following chapter.

Chapter 3

Communication link characteristics

Unlike traditional mobile ad hoc networks, the high node mobility in VANETs can cause frequent network topology changes and fragmentations. Moreover, VANETs are susceptible to vehicle density variations from time to time throughout the day. This imposes new challenges in maintaining a connection between vehicular nodes. The length of the communication link and its duration between network nodes play a crucial role in determining node cluster stability. As discussed in Section 1.3, any change in cluster structure is directly or indirectly related to the duration of communication links between network nodes and the switching of the links between connection and disconnection. This section presents a probabilistic analysis of the communication link in VANETs for three vehicle density ranges. Firstly, we propose a stochastic microscopic mobility model that captures time variations of inter-vehicle distances (distance headways). A discrete-time finite-state Markov chain with state dependent transition probabilities is proposed to model the distance headway. Secondly, the stationary distribution of the communication link length is derived using mesoscopic mobility models. Thirdly, the proposed stochastic microscopic model and first passage time analysis are used to derive the probability distribution of the communication link lifetime. Finally, we simulate highway vehicular traffic using microscopic vehicle traffic simulator, VISSIM, and demonstrate that the analytical results of our model match well with simulation results.

3.1 Microscopic vehicle mobility model

We model the stochastic process, X_i, as a discrete-time finite-state Markov chain, inspired by [59, 60]. The Markov chain, illustrated in Figure 3.1, has $N_{\max}$ states corresponding

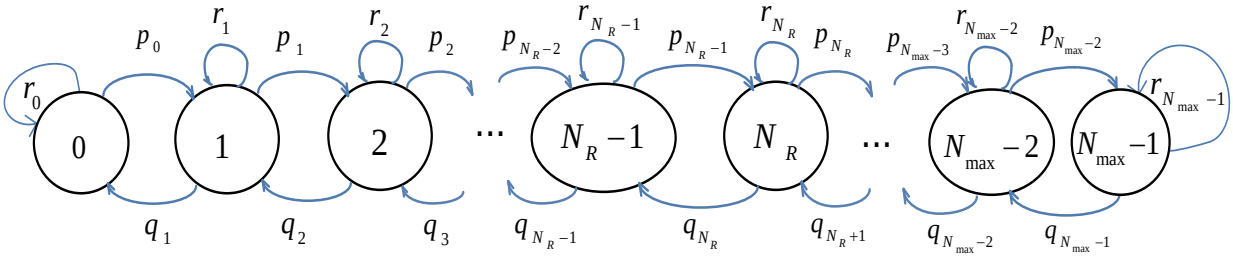

Figure 3.1: An illustration of the proposed discrete-time $N_{\max}$-state Markov chain model of the distance headway

to $N_{\max}$ ranges of a distance headway. The length of the range covered by each state is a constant, denoted by L_s in meters. The j^{th} state covers the range $[x_j, x_j + L_s)$, $0 \leq j \leq N_{\max} - 1$, where $x_j = \alpha + jL_s$. At any time step, $X_i(m) = x_j$ denotes that the distance headway X_i is in the j^{th} state, for all $i, m \geq 0$, and $0 \leq j \leq N_{\max} - 1$. Let $N_R = \frac{R-\alpha}{L_s}$ be the integer number of states that cover distance headways within R. Hence, the states with indices $j \in \{0, 1, 2, \ldots, N_R - 1, N_R, N_R + 1, \ldots, N_{\max} - 2, \text{ and } N_{\max} - 1\}$ correspond to the quantized distances $x_j \in \{\alpha, \alpha + L_s, \alpha + 2L_s, \alpha + 3L_s, \ldots, \alpha + (N_R - 1)L_s, R, \alpha + (N_R + 1)L_s, \ldots, X_{\max} - L_s, \text{ and } X_{\max}\}$, respectively. Within a time step, a distance headway in state j can transit to the next state, the previous state, or remain in the same state with probabilities p_j, q_j, or r_j, $0 \leq j \leq N_{\max} - 1$, respectively. Without loss of generality, assume that probability transition matrix is a positive-definite tri-diagonal and is given by

$$M = \begin{pmatrix} r_0 & p_0 & 0 & \ldots & \ldots & 0 \\ q_1 & r_1 & p_1 & 0 & \ldots & \vdots \\ 0 & q_2 & r_2 & p_2 & 0 & \vdots \\ \vdots & \ddots & \ddots & \ddots & \ddots & 0 \\ 0 & \ldots & 0 & q_{N_{\max}-2} & r_{N_{\max}-2} & p_{N_{\max}-2} \\ 0 & \ldots & \ldots & 0 & q_{N_{\max}-1} & r_{N_{\max}-1} \end{pmatrix}. \tag{3.1}$$

The tri-diagonal structure of M is due to the fact that the values of a distance headway at consecutive time steps are highly correlated, for a short time step, such as $\tau \leq \frac{L_s}{\bar{v}}$,

where $\bar{v}$ is the maximum relative speed between vehicles[1]. We propose to use the following state-dependent transition probability functions

$$\begin{aligned} p_j &= p\left(1-\beta\left(1-\frac{x_j}{X_{\max}}\right)\right) \\ q_j &= q\left(1-\beta\left(1-\frac{x_j}{X_{\max}}\right)\right) \\ r_j &= 1-p_j-q_j, \qquad 0 \le j \le N_{\max}-1,\ 0 \le p,q,\beta \le 1 \end{aligned} \tag{3.2}$$

where p, q, and β are constants that depend on the vehicle density. For a low vehicle density, β is close to zero, and therefore the transition probabilities are independent of the state value, x_j. The value of β increases as the vehicle density increases, and thus increases the dependency on the state value. Eq.(3.2) can be explained as follows. In a low vehicle density, distance headways are relatively large. Hence, a vehicle moves freely with a desired speed [1]. In such a scenario, the distance headway value does not affect the driver's choice to keep/change the speed, since the distance headway is large enough. On the other hand, in a high vehicle density situation, distance headways are relatively small. Hence, vehicles move with high constraints to keep a safe distance ahead. In such a scenario, the distance headway value has a high impact on the driver's behavior and his/her choice to keep/change the speed (and consequently the distance headway). The constant β is comparable with the driver strain constant used in [41], whereas $\beta = 0$ in [42]. The transition probabilities of the distance headway to neighboring states increase with the distance headway value, when $\beta > 0$ in (3.2). This is due to the fact that a larger distance headway results in less constraints in driving.

In order to verify the dependency of the distance headway transition probability on its current state, we compute the transition probability matrix using i) empirical vehicle trajectory data collected from highways provided by Next Generation Simulation (NGSIM) community and available online [61], and ii) simulated vehicle trajectory data generated by VISSIM microscopic vehicle traffic simulator. The vehicles in VISSIM simulator move according to Wiedemann's microscopic mobility model. Wiedemann is psycho-physical car-following model that describes behaviors of individual vehicles according to their interactions with neighboring vehicles, their desired relative speeds, their relative positions, and some driver-dependant behaviors. The Wiedemann model accounts for four differ-

[1]Consider an i.i.d. desired vehicle speed with a mean of 100 kilometer per hour and a standard deviation of 10 kilometer per hour, i.e., $P(\bar{v} \le 36) = 0.99$. In this case, the choice of $\tau = 2$ seconds for $L_s = 20$ meters, reduces the transition probability of the distance headway to a non-neighboring state to less than 0.0054

ent driving modes: free driving, approaching, following, and breaking [62]. We adopt the Wiedemann 99 model which is designed for a highway scenario with its parameters set to the default values suggested in [63]. We use two NGSIM data sets: *I-80-Main-Data* and *US-101-Main-Data*, which were collected from a seven lane highway for a section of 500 and 640 meters, respectively. From the NGSIM data sets, we exclude data points associated with vehicles 1) on an on-ramp lane, 2) on an off-ramp lane, 3) at the end of the section, or 4) undertaking a lane change. The VISSIM data set was obtained via six 30-minute simulations of a three-lane highway traffic for different vehicle densities. The highway is a closed loop, and the vehicles enter the highway with a traffic flow of (3052.8, 1914.2, 854.6, 683.7, and 379.8) vehicle per hour per lane for 1000 seconds, resulting in vehicle densities of (42, 26, 16, 9, and 5), respectively. The VISSIM data points associated with vehicles entering the highway or changing lanes are not included in our analysis. To obtain the transition probabilities, the NGSIM and VISSIM data sets are mapped into a sequence of quantized state values (x_j) with a predefined state length L_s, where $x_j \in [0, X_{\max}]$ in meters and $0 \leq j \leq N_{\max} - 1$. The NGSIM data sets is only available with intermediate-to-high vehicle densities with $X_{\max} = 100$ meters. For each state j, the transition probabilities for the distance headway are determined by counting the number of occurrences of each transition. Let $n_{j,j'}$ be the number of transitions of a distance headway from state j to state $j', 0 \leq j' \leq N_{\max} - 1$, within a time step of length τ, and $n_j = \sum_{j'=0}^{N_{\max}-1} n_{j,j'}$ be the number of time steps at which the distance headway is in state j. The transition probability from state j to j' is calculated by $p_{j,j'} = \frac{n_{j,j'}}{n_j}, \quad 0 \leq j, j' \leq N_{\max} - 1$.

Figure 3.2 plots the transition probabilities (and their standard deviation) from state j to its direct neighboring states and to itself for different x_j values, with the default data recording values: $L_s = 1$ meter and $\tau = 0.1$ seconds for the NGSIM data set, and $L_s = 2$ meters and $\tau = 0.2$ seconds for the VISSIM data set. The results show a dependency of the transition probabilities on the x_j value. The weighted linear regression (LR) is used to fit the transition probabilities in Figure 3.2, with $n_{j,j'}$ being the weight of each $p_{j,j'}$ data point. The transition probabilities p_j and q_j increase with the quantized state value, x_j, which agrees with (3.2). The values of p, q, and β are calculated according to the resulting weighted LR fit and are given in the figure legends. The results show that $p_{j,j'}$ is smaller than 10^{-3} for $|j - j'| > 1$, and is therefore neglected, which is consistent with the tri-diagonal transition matrix assumption given in (3.1). Figure 3.3 plots the transition probability matrix calculated from the NGSIM data for $x_j, x_{j'} \in [110, 120]$, $L_s = 0.1$ meters, and $\tau = 0.1$ seconds. It is observed from Figure 3.3 that, for a reduced value of the ratio L_s/τ, $p_{j,j'}$ increases for $|j - j'| > 1$. Figure 3.4 plots the transition probability to the next state (and its standard deviation) for different x_j values and different vehicle densities. The results show that, the larger the vehicle densities, the higher the state-dependency of the

transition probabilities. The resulting β values for different vehicle densities are plotted in Figure 3.5, which shows an approximate linear relation between β and the vehicle density. This agrees with our proposed transition probability functions in (3.2).

It should be noted that the proposed microscopic model does not explicitly describe how and when lane changes occur nor does it describe impacts of lane-changes on the time variations of distance headways. However, the model implicitly captures the impact of lane changes on maintaining the ability of the vehicles to overtake slower vehicles and accelerate towards their desired speed. This is captured in the parameters p, q, and β which can be tuned from empirical/simulated multi-lane highway trajectory data for one of the lanes as done earlier in this section.

3.2 Distribution of the communication link length

In this section, we present the probability distribution of the communication link length using mesoscopic distance headway models described in Section 2.2. The hop length (or the link length), denoted by H, is the distance from a reference node to the furthest node within the transmission range of the reference node, which is upper bounded by the transmission range R. Given a mesoscopic model, the distance headways X_i's are i.i.d. with probability density function $f_X(x)$ and cdf $F_X(x)$. Let $C(l)$ be the event that there exists at least one node within distance l from a reference node. The event $C(l)$ occurs with probability $F_X(l)$. Let $C^c(l)$ be the complement of event $C(l)$, i.e., the event that there are no nodes within distance l from a reference node. Then, the cdf of H is given by [64]

$$F_H(h) = \frac{P(C^c(R-h), C(h))}{P(C(R))}. \tag{3.3}$$

The pdf can then be calculated by $f_H(h) = \frac{d}{dh_r} F_H(h)$. For a low vehicle density, the distance headway is exponentially distributed with pdf given in (2.1). The pdf of the corresponding hop length is given by [65]

$$f_H(h) = \frac{e^{-\frac{(R-h)}{\mu}}}{\mu(1 - e^{-\frac{R}{\mu}})}, \quad 0 < h < R \tag{3.4}$$

which is a scaled exponential distribution truncated at R. For an intermediate vehicle density, the distance headways are i.i.d., each following the Pearson type III pdf in (2.3).

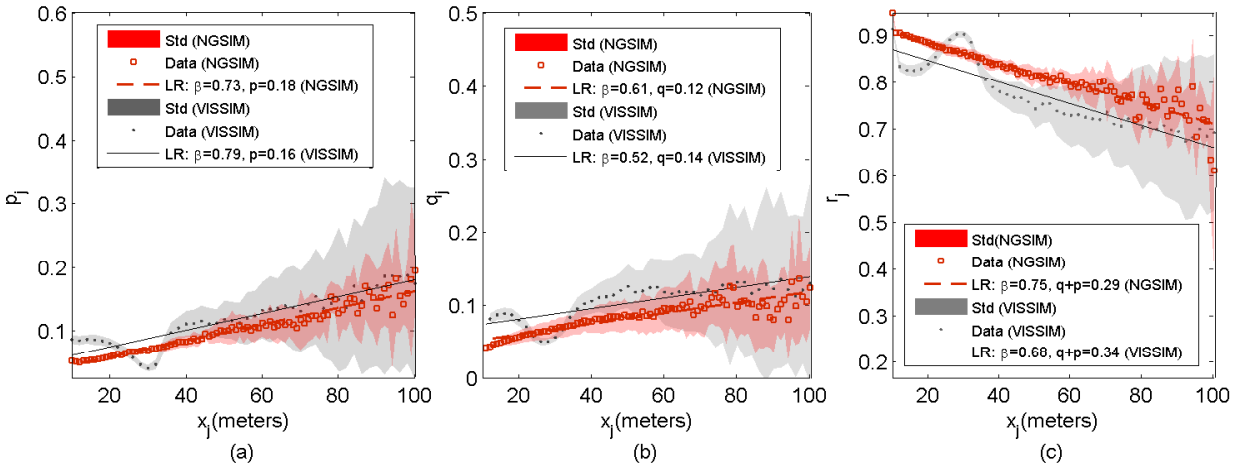

Figure 3.2: **The transition probability from state j to (a) state $j+1$, (b) state $j-1$, and (c) state j, for different x_j values from NGSIM and VISSIM data for intermediate to high vehicle densities. Results for the weighted LR fit model for (3.2) are given in the legends.**

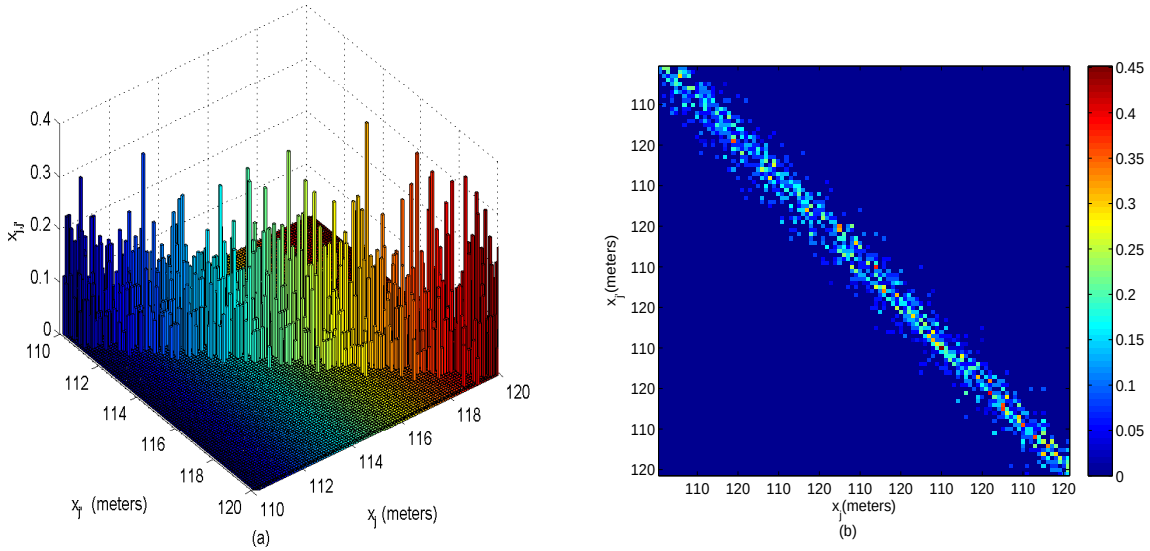

Figure 3.3: **Probability transition matrix for 100 quantized values of $x_j, x_{j'} \in [110, 120]$ with $L_s = 0.1$ meters and $\tau = 0.1$ seconds. The matrix is calculated based on NGSIM data.**

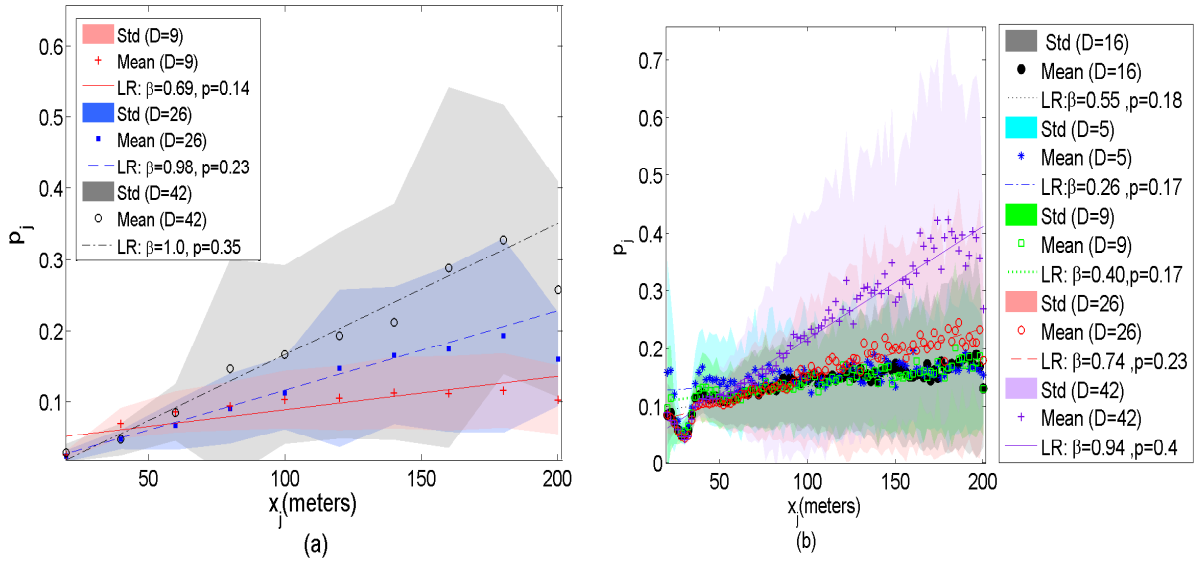

Figure 3.4: Transition probability from state j to state $j+1$, for different x_j values from VISSIM data for vehicle densities of (a) 9, 26, and 42 veh/km with $L_s = 20$ meters and $\tau = 2$ seconds and (b) 5, 9, 16, 26, and 42 veh/km, with $L_s = 2$ meters and $\tau = 0.2$ seconds. Results of the weighted linear regression fit model for (6) are given in the legends.

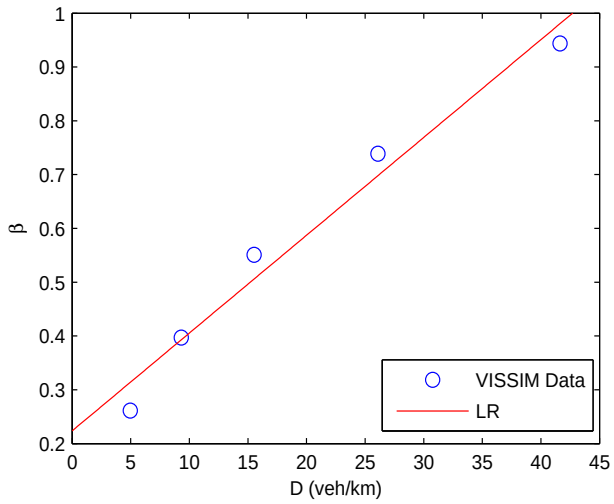

Figure 3.5: State dependency parameter, β for different D values calculated based on VISSIM data.

The cdf for the first hop length can be derived from (3.3) and the corresponding pdf is found to be

$$f_H(h) = \frac{f_X(R-h)\gamma(z,\lambda(h-\alpha)) + f_X(h)\Gamma(z,\lambda(R-h-\alpha))}{\gamma(z,\lambda(R-\alpha))}, \quad \alpha \leq h < R-\alpha \tag{3.5}$$

where $\gamma(z,x) = \int_0^x t^{z-1}e^{-t}dt$ and $\Gamma(z,x) = \int_x^\infty t^{z-1}e^{-t}dt$ are the lower and the upper incomplete gamma functions, respectively, and $f_X(\cdot)$ is given by (2.3). The derivation for $f_H(h)$ is given in Appendix A.1.

For a high vehicle density, the distance headways are i.i.d., each following the Gaussian pdf in (2.2). Using the cdf of the Gaussian distribution, $F_X(x) = \frac{1}{2}\left(1 + \text{erf}\left(\frac{x-\mu}{\sqrt{2}\sigma}\right)\right)$, the cdf for the hop length can be derived from (3.3) and is given by

$$\begin{aligned} f_H(h) \;=\; & \frac{1}{\sqrt{2\pi}\sigma}\left(1+\text{erf}\left(\frac{R-\mu}{\sqrt{2}\sigma}\right)\right)^{-1} \times \left[\text{e}^{-\frac{(h-\mu)^2}{2\sigma^2}}\right. \\ & \times \left(1-\text{erf}\left(\frac{R-h-\mu}{\sqrt{2}\sigma}\right)\right) + \text{e}^{-\frac{(R-h-\mu)^2}{2\sigma^2}} \\ & \left. \times \left(1+\text{erf}\left(\frac{h-\mu}{\sqrt{2}\sigma}\right)\right)\right], \qquad 0 < h < R \end{aligned} \tag{3.6}$$

where $\text{erf}(\cdot)$ is the error function, given by $\text{erf}(x) = \frac{2}{\sqrt{\pi}}\int_0^x e^{-t^2}dt$.

3.3 Communication link lifetime

Consider a communication hop from an arbitrary reference node in the direction of the vehicle traffic flow. The reference node is one hop away from all the nodes within a distance less than R (assuming that an on/off link depends only on the distance between the nodes). Define the communication link lifetime between two nodes as the first time step at which the distance between the two nodes is larger than or equal to R, given that the distance between them is less than R at the 0^{th} time step. For any node within R from the reference node, the communication link lifetime is at least equal to the that of the furthest node from the reference vehicle (referred to as *hop edge node*). A study of the communication link lifetime of the edge vehicle from its reference vehicle is presented in the following.

3.3.1 First passage time between two distance headway states

Let $T^i_{j,j'}, 0 \leq j, j' \leq N_{\max} - 1$, be the first passage time of the distance headway X_i to state j' given that the distance headway is in state j at the 0^{th} time step, i.e., $T^i_{j,j'} = min\{m > 0; X_i(m) = x_{j'}, X_i(0) = x_j\}, 0 \leq j \leq N_{\max} - 1$.In the following, $T_{j,j'}$ is used without superscript i for an arbitrary distance headway. Let M' be an $N_{\max} \times N_{\max}$ matrix equal to M with $q_{N_{\max}-1} = 0$ and $r_{N_{\max}-1} = 1$. Let $\{\lambda_u\}_{u=0}^{N_{\max}-2}$ be the $N_{\max} - 1$ non-unit eigenvalues of M'. The first passage time to state $N_{\max} - 1$, given that $X_i(0) = x_0$, is the sum of $N_{\max} - 1$ independent geometric random variables, each with a mean equal to $\frac{1}{1-\lambda_u}$ [66]. The probability generating function of $T_{0,N_{\max}-1}$ is given by

$$Q_{T_{0,N_{\max}-1}}(v) = \prod_{u=0}^{N_{\max}-2} \left[\frac{(1-\lambda_u)v}{1-\lambda_u v} \right]. \tag{3.7}$$

The pmf of $T_{0,N_{\max}-1}$ is then calculated by $P_{T_{0,N_{\max}-1}}(m) = \frac{Q^{(m)}_{T_{0,N_{\max}-1}}(0)}{m!}$, where $Q^{(m)}_{T_{0,N_{\max}-1}}(0)$ is the value of the m^{th} derivative of $Q_{T_{0,N_{\max}-1}}(v)$ at $v = 0$.

Let $M^{(j)}$ be a $(j+1) \times (j+1)$ matrix, $0 < j < N_{\max} - 1$, equal to the upper left $(j+1) \times (j+1)$ portion of matrix M with $q_j = 0$ and $r_j = 1$. The first passage time of the distance headway to state j, given that the initial distance headway is in state 0, has a probability generating function $Q_{T_{0,j}}(v) = \prod_{u=0}^{j-1} \left[\frac{(1-\lambda_u^{(j)})v}{1-\lambda_u^{(j)}v} \right]$, where $\lambda_u^{(j)}$, $u = 0, 1, \ldots, j-1$, are the j non-unit eigenvalues of $M^{(j)}$. Note that the distance headway cannot move to state $j'(> j)$ before passing through state j in a birth and death process. Using $T_{0,j'} = T_{0,j} + T_{j,j'}$, the passage time to state j' given that the initial distance headway is in state j, $0 \leq j < j' \leq N_{\max} - 1$, can be calculated. The probability generating function of $T_{j,j'}$ is $Q_{T_{j,j'}}(v) = \frac{E\left[v^{T_{0,j'}}\right]}{E\left[v^{T_{0,j}}\right]}$, and is calculated by

$$Q_{T_{j,j'}}(v) = v^{j'-j} \frac{\prod_{u=0}^{j'-1} \left[\frac{(1-\lambda_u^{(j')})}{1-\lambda_u^{(j')}v} \right]}{\prod_{u=0}^{j-1} \left[\frac{(1-\lambda_u^{(j)})}{1-\lambda_u^{(j)}v} \right]}. \tag{3.8}$$

Figure 3.6 plots the pmf's of $T_{0,N_{\max}-1}$, $T_{1,4}$ and $T_{2,3}$ for a nine-state distance headway model. The pmf's are evaluated using MAPLE [67]. Figure 3.6 shows that the probability of the first passage time, $T_{j,j'}$, taking on a small value decreases as the number of states, $|j' - j|$, increases.

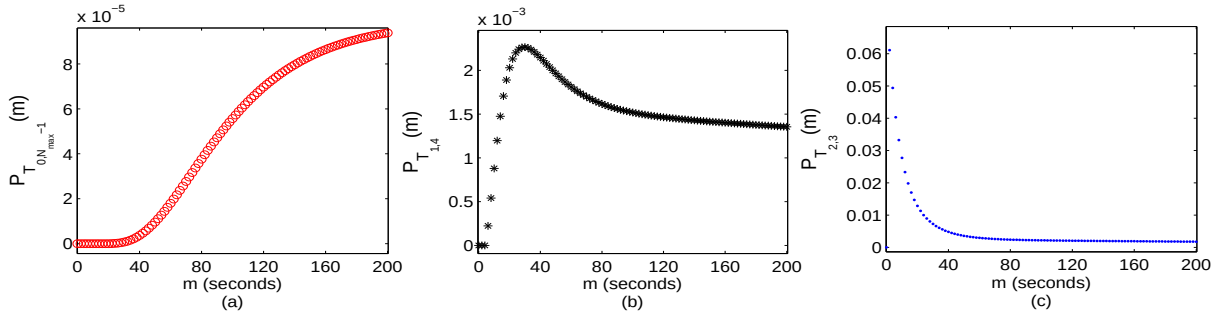

Figure 3.6: Probability mass function of the first passage time for (a) $T_{1,N_{\max}}$, (b) $T_{1,4}$, and (c) $T_{2,3}$, with mean values of $19.8 \times 10^3, 1.24 \times 10^3$, and 318.4 seconds, respectively, with parameters $N_{\max} = 9, L_s = 20$ meters, $\tau = 2$ seconds, $X_{\max} = 160$ meters, $\beta = 0.66$, $p = 0.12$, and $q = 0.26$.

3.3.2 First passage time of the sum of distance headways

The distance between a reference node and its hop edge node is equal to the sum of the distance headways between the two nodes. Let N_H be the number of nodes between a node and its hop edge node at the 0^{th} time step. Label the nodes with IDs: $\{0, 1, ...N_H + 1\}$, where the reference node has ID 0, and the hop edge node has ID $N_H + 1$. Therefore, $R \leq \sum_{i=0}^{N_H+1} X_i(0) < R + X_{N_H+1}(0)$. A node and its hop edge node remain connected until $\sum_{i=0}^{N_H} X_i(m) \geq R$ at some time step m which is the communication link lifetime.

The sum of $(N_H + 1)$ i.i.d. distance headways, where each headway, X_i, is a birth and death Markov chain as illustrated in Figure 3.1, is an $(N_H + 1)$ dimensional Markov chain. The complexity of this Markov chain is obvious especially when N_H is not small, since a non-zero transition probability to a non-neighboring state is possible. For tractability, we use an alternative approach as follows.

3.3.3 Link disconnection events

In this subsection, we present the set of events that cause the disconnection between a reference node and its hop edge node at a certain time step, m. Consider a set $\mathbb{X}_H = \{X_0, X_1, \ldots, X_{N_H}\}$ of $(N_H + 1)$ distance headways (stochastic processes) between the reference node and its hop edge node, where $\mathbb{X}_H = \{\mathbb{X}_H(m), m = 0, 1, 2, \ldots\}$. For notation simplicity, let $\mathbb{X}_H(m) = \{k_0, k_1, \ldots, k_{N_H}\}$ denote $\{X_i(m) = x_{k_i}\}_{i=0}^{N_H}$. Furthermore, let $\{s_0, s_1, \ldots, s_{N_H}\}$ denote the set of state indices of the $(N_H + 1)$ distance headways at the

0^{th} time step, (i.e., $\{X_i(0) = x_{s_i}\}_{i=0}^{N_H}$), where $s_i \in \{0, 1, 2, \ldots, N_R - 1\}$, and $\sum_{i=0}^{N_H} x_{s_i} < R$. Let E_D be the event that the link between a reference node and its hop edge node, separated by N_H nodes, disconnects given $\mathbb{X}_H(0)$, and let $E_D(m)$ be the event that this disconnection occurs at the m^{th} time step. When the hop edge node and the reference node are adjacent to each other, i.e., $N_H = 0$, a link disconnection occurs when the distance headway X_0 transits to state N_R. Therefore, $E_D(m) \equiv \{X_0(m) = x_{N_R} | s_0\}$ for $N_H = 0$.

When $N_H > 0$, consider first the case when $\alpha = 0$. A link disconnection occurs at time step m if $\left\{\mathbb{X}_H(m) = \{k_0, k_1, \ldots, k_{N_H}\}, \sum_{i=0}^{N_H} k_i \geq N_R\right\}$. That is, the set $\{k_i\}_{i=0}^{N_H}$ is an integer partition of a positive integer that is greater than or equal to N_R. In number theory and combinatorics, an ordered integer partition of a positive integer n is a sequence of positive integers whose sum equals n. Each member of the sequence is called a *part*. An ordered J-restricted integer partition of an integer n is an integer partition of n into exactly J parts. Let $\mathbb{A}_J(n) = \{a_1(i), a_2(i), \ldots, a_J(i)\}_{i=1}^{L_J(n)}$ be a set of all possible ordered J-restricted integer partitions of n, where $a_j(i)$, $1 \leq j \leq J$ is the j^{th} part of the i^{th} partition $\mathbb{A}_J^i(n)$, and $L_J(n) = \binom{n-1}{J-1}$ is the total number of such partitions, i.e., the size of set $\mathbb{A}_J(n)$ [68]. For example, $A_2(6) = \{\{1, 5\}, \{5, 1\}, \{2, 4\}, \{4, 2\}, \{3, 3\}\}$, where $A_2^1(6) = \{1, 5\}$, $a_1(1) = 1, a_2(4) = 2$ and $L_2(6) = \binom{6-1}{2-1} = 5$. Furthermore, let $\mathbb{K}_J(N_H) = \{k_1(v), k_2(v), \ldots, k_J(v)\}_{v=1}^{K_J(N_H)}$ be the set of all J-combinations of the set $\{0, 1, \ldots, N_H\}$, where $k_j(v)$, $1 \leq j \leq J$, is the j^{th} element of the v^{th} combination, and let $K_J(N_H) = \binom{N_H+1}{J}$ be the number of such combinations. We define two random events, $e_1(m), e_2(m)$ at the m^{th} time step as follows:

$$e_1(m) \equiv \bigcup_{k_0=0}^{N_H} \left\{X_{k_0}(m) = x_{N_{ED}} \middle| s_{k_0}\right\} \tag{3.9}$$

$$\begin{aligned} e_2(m) \equiv \bigcup_{J=2}^{N_H+1} \bigcup_{i=1}^{L_J(N_{ED})} \bigcup_{v=1}^{K_J(N_H)} \Big\{ & X_{k_1(v)}(m) \geq x_{a_1(i)}, \\ & X_{k_2(v)}(m) \geq x_{a_2(i)}, \ldots, X_{k_J(v)}(m) \geq x_{a_J(i)} \Big| \\ & s_{k_1(v)}, s_{k_2(v)}, \ldots, s_{k_J(v)} \Big\} \end{aligned} \tag{3.10}$$

where $N_{ED} = N_R - \lfloor \frac{\alpha N_H}{(R-\alpha)/N_R} \rfloor$ is an integer such that if set $\mathbb{X}_H$ is in set of states whose indices construct an integer partition of an integer greater than or equal to N_{ED}, the communication link breaks. Note that N_{ED} accounts for the minimum value of the distance headways (i.e., α), and $N_{ED} = N_R$ for $\alpha = 0$. Event $e_1(m)$ occurs when at least one of the distance headways of set $\mathbb{X}_H$ is in state N_{ED} at the m^{th} time step, resulting in a link disconnection. Note that N_{ED} is the least state index required for a distance headway

to reach in order for the link to disconnect. Event $e_2(m)$ occurs when at least J distance headways of set $\mathbb{X}_H$ are in states that construct a J-restricted integer partition of an integer that is greater or equal to N_{ED} with parts at most equal to N_R. Note that N_{ED} accounts for the minimum value of the distance headway, i.e., α. That is, event $e_2(m)$ occurs if J distance headways of set $\mathbb{X}_H$ are in states $\{k_1, k_2, \ldots, k_J\}$ at the m^{th} time step such that $\sum_{i=1}^{J} k_i \geq N_{ED}$ for any $2 \leq J \leq N_H + 1$. An occurrence of event $e_2(m)$ result in a link disconnection at the m^{th} time step, because the sum $N_{ED} + \lfloor \frac{\alpha N_H}{L_s} \rfloor$ is equal to N_R, which indicates that the sum of the J distances is greater than or equal to R. Consequently, a link disconnection occurs at the m^{th} time step when either $e_1(m)$ or $e_2(m)$ occurs, i.e., $E_D(m) = \{e_1(m) \cup e_2(m)\}$.

3.3.4 Probability distribution of the link lifetime

The lifetime or a communication link from a reference node to its hop edge node, separated by N_H nodes, given $\mathbb{X}_H(0)$, is the first passage time of event $E_D(m)$, denoted by $T(E_D)$. Let $T(e_i)$ be the first passage time for the occurrence of event $e_i(m)$, $i = 1, 2$ (i.e., $T(e_i) = \min\{m | e_i(m)\}$). The communication link lifetime is calculated by $T(E_D) = \min\{T(e_1), T(e_2)\}$. For $N_H = 0$, this simplifies to $T(E_D) = T(e_1) = T_{s_0, N_{ED}}$, with pmf $P_{T(E_D)}(m)$ which can be calculated using the m^{th} derivative of (3.7) and (3.8) for $s_0 = 0$ and $s_0 > 0$, respectively.

For $N_H > 0$, the calculation of the pmf of the link lifetime is not straight forward, due to the obvious correlation between $e_1(m)$ and $e_2(m)$. Let $V = \{V^{'} \bigcup V^{''}\}$ be a matrix resulting from the union of two matrices, $V^{'}$ and $V^{''}$, with the three matrices having $N_H + 1$ columns. Each unique row of $V^{'}$ consists of J elements equal to one of the partitions in $\mathbb{A}_J(N_{ED})$ and $(N_H - J + 1)$ zero elements, $1 \leq J \leq N_H + 1$. The number of rows of $V^{'}$ is equal to $\sum_{J=1}^{N_{ED}} \binom{N_H+1}{N_H-J+1} \binom{N_{ED}-1}{J-1}$. Matrix $V^{''}$ is constructed similarly with all possible ordered J-restricted partitions of integers $N_{ED} + 1, N_{ED} + 2, ..., (N_H + 1)N_{ED}$, each with the largest part less than or equal to N_{ED}. For example, for $N_H = 1$, $N_R = 3$, $\alpha = 0$ we have

$$V^{'} = \begin{pmatrix} 3 & 0 \\ 0 & 3 \\ 1 & 2 \\ 2 & 1 \end{pmatrix}, \quad \text{and } V^{''} = \begin{pmatrix} 1 & 3 \\ 3 & 1 \\ 2 & 2 \\ 3 & 2 \\ 2 & 3 \\ 3 & 3 \end{pmatrix}.$$

A link disconnection occurs at the m^{th} time step when the distance headway set $\mathbb{X}_H$ is in states $\{u_1, u_2, \ldots, u_{N_H+1}\}$ such that $\{u_1, u_2, \ldots, u_{N_H+1}\}$ is a row in V. Let $E_{D,V}(m) \equiv \{\mathbb{X}_H(m) = V | \mathbb{X}_H(0)\}$ be a set of events, each corresponding to set $\mathbb{X}_H$ being in a set of states that construct one of the rows of V at the m^{th} time step, given $\mathbb{X}_H(0)$. An event in the set $E_{D,V}(m)$, $E_{D,V(v)}(m)$, $1 < v < |V|$, is the event that the set $\mathbb{X}_H$ is in states that construct the v^{th} row in V at the m^{th} time step, where $|V|$ is the number of rows in V. An occurrence of event $E_{D,V(v)}(m)$ results in a link disconnection at the m^{th} time step. The first passage time of these events is $T(E_{D,V}) = \min\{m | E_{D,V}(m)\}$. The distribution of $T(E_{D,V})$ can be derived to be

$$P_{T(E_{D,V})}(m) = \begin{cases} \prod_{i=0}^{N_H} M'_{s_i+1,v_i+1}, & m = 1 \\ \prod_{i=0}^{N_H} M'^{m}_{s_i+1,v_i+1} - \left[\sum_{n=1}^{m-1} \left\{\prod_{j=0}^{N_H} M'^{n}_{v_j+1,v_j+1}\right\}^t \otimes P_{T(E_{D,V})}(m-n)\right], & m > 1 \end{cases} \tag{3.11}$$

where v_i is the i^{th} column of matrix V and $M'^{m}_{s_i+1,v_i+1}$ is an array with elements equal to the $(v_i+1)^{\text{th}}$ entries of the $(s_i+1)^{\text{th}}$ row of the m^{th} power of matrix M', $1 \leq i, j \leq N_{\max}$, $\{\cdot\}^t$ denotes the transpose matrix operation, and the product notations $\otimes$ and $\prod$ correspond to the general and the Hadamard matrix multiplications, respectively. For $m > 1$, the subtracted term in (3.11) is to guarantee that none of the $E_{D,V}$ events occurs before time step m, i.e., set $\mathbb{X}_H$ does not reach states with indices that construct a row in V before time step m. Since the communication link disconnects if any of the events in $E_{D,V}$ occurs, the pmf of the link lifetime is given by

$$P_{T(E_D)}(m) = \sum_{v=1}^{|V|} P_{T(E_{D,V(v)})}(m) \tag{3.12}$$

where $|V|$ is the number of rows in matrix V and $V(v)$ is the v^{th} row of V.

3.4 Results and discussion

This section presents numerical results for the analysis of the pdf of the communication link length, $f_H(h)$, and the pmf of the link lifetime, $P_{T(E_D)}(m)$. We consider three traffic flow conditions, uncongested, near-capacity, and congested, each corresponding to a set of parameters listed in Table 3.1. We set $\sigma = \frac{1000}{2D}$ for the mesoscopic distance headway models. The parameters for the microscopic Markov-chain distance headway model are

also listed in Table 3.1, where β, p and q follow the VISSIM data fitting results in Section 3.1. Without loss of generality, we set $\alpha = 0$, and $X_{\max} = R$. This is sufficient for communication link analysis, as the link breaks if any X_i's reach state N_R. The values of N_H and $\mathbb{X}_H(0)$, listed in Table 3.1, are first set to their average values. To verify the link lifetime analysis, we compare the analytical link lifetime pmf calculated with (3.11) and (3.12) to that calculated from simulated vehicular traffic. A three-lane highway traffic is simulated using the microscopic vehicle traffic simulator VISSIM as described in Section 3.1. The choice of simulating a three-lane highway instead of a single-lane highway is to achieve a more realistic vehicle mobility in which a vehicle can overtake other vehicles and accelerate towards its desired speed. The desired speed for all vehicles is normally distributed with mean 100 kilometer per hour and standard deviation of 10 kilometer per hour. The pmf of the lifetime of a link with initial conditions N_H and $\mathbb{X}_H(0)$, is calculated by counting the number of occurrences of link breakage at m^{th} time step for $m > 0$ and for all links with initial conditions N_H and $\mathbb{X}_H(0)$. Six 30-minute simulations are obtained for each of the three vehicle densities. The calculation of the link lifetime pmf, $P_{T(E_D)}(m)$, from the VISSIM simulated vehicle traffic data includes the lifetime of the following: 1) a link between a reference vehicle and its corresponding hop edge node on the same lane, independently of changing hop edge node during the link's lifetime as long as the initial hop edge node remains in the link; and 2) a new link between a reference vehicle and its new hop edge node on the same lane when its previous link breaks. A link which involves a lane change during its lifetime is excluded from the pmf calculation. The frequency of a link lifetime at value l is upper bounded by $\frac{T_{sim}N_S}{l}$, where T_{sim} is the simulation time and N_S is the total number of vehicles in the simulation. The frequency of l-valued lifetime occurrences in VISSIM data is normalized accordingly in the link lifetime pmf calculation.

Figure 3.7 plots the pdfs (3.4)-(3.6) of the hop length for three vehicle densities $D = 9, 26$, and 42 veh/km with average hop length equal to $99.2, 121.8$, and 132.2 meters, respectively. The average length of the communication link is larger for a higher vehicle

Table 3.1: System parameters in simulation and analysis of Chapter 3

Traffic flow condition	**D(veh/km)**	$\mathbf{N_H}$	$\boldsymbol{\beta}$	$\mathbf{p, q}$	$\mathbb{X}_{\boldsymbol{H}}(\mathbf{0})$
Uncongested	9	0	0.4	0.17	{5}
Near-capacity	26	3	0.74	0.23	{1,1,1,1}
Congested	42	5	0.94	0.35	{1,1,1,1,1,1}
$\mathbf{R}$ (meter)	$\mathbf{N_R}$	$\mathbf{N}_{\max}$	$\boldsymbol{\alpha}$	$\boldsymbol{\tau}$ (second)	$\mathbf{L_s}$(meter)
160	8	9	0	2	20

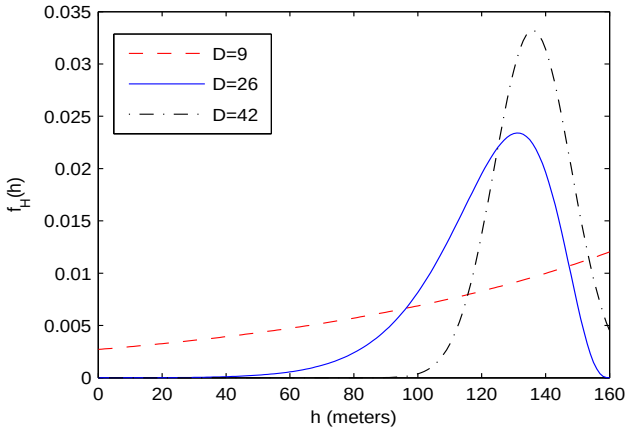

Figure 3.7: The probability density function of the hop length for three traffic flow conditions with vehicle densities of 9, 26, and 42 veh/km.

density, due to a larger average number of nodes between a node and its hop edge node. Using (2.1)-(2.3), the probability for an unavailable link between two vehicles (i.e., $P(X_i > R)$) is $0.23, 5.2 \times 10^{-5}$, and 0 for $D = 9, 26$, and 42 veh/km, respectively. That is, the probability of network fragmentations is higher in an uncongested traffic flow condition than that in a congested traffic flow condition.

Figure 3.8 plots the pmf of the communication link lifetime for the three traffic flow conditions. The theoretical results are obtained using (3.8) for the uncongested traffic flow condition and (3.12) for the near-capacity and congested traffic flow conditions. We use MAPLE to calculate the m^{th} derivative for the generating function in (3.8). For large values of j and/or j' in (3.8), we use the m^{th} derivative of the product rule proposed in [69]. The simulation results are calculated from the generated VISSIM vehicle trajectory data. The simulation results closely agree with the theoretical calculations. However, there exist slight differences between simulation and theoretical results. This is mainly due to lane changes, which are not explicitly accounted for in our model. The effect of lane changes is more notable in the low vehicle density simulation results, where we get zero probability for some large link lifetime values, as shown in Figure 3.8(a). This is due to the high probability of lane change for large link lifetimes, which is excluded from our calculations. The average link lifetime is found to be 335.5, 88.1, and 65.9seconds for the low, intermediate, and high vehicle densities, respectively. Recall from subsection 3.3.3, that the link disconnection event, E_D, depends on the initial conditions N_H and $\mathbb{X}_H(0)$. In order to extend the results for different initial conditions, we conduct the following: 1) discretize the mesoscopic distance headway models in (2.1)-(2.3); 2) using the discretized mesoscopic

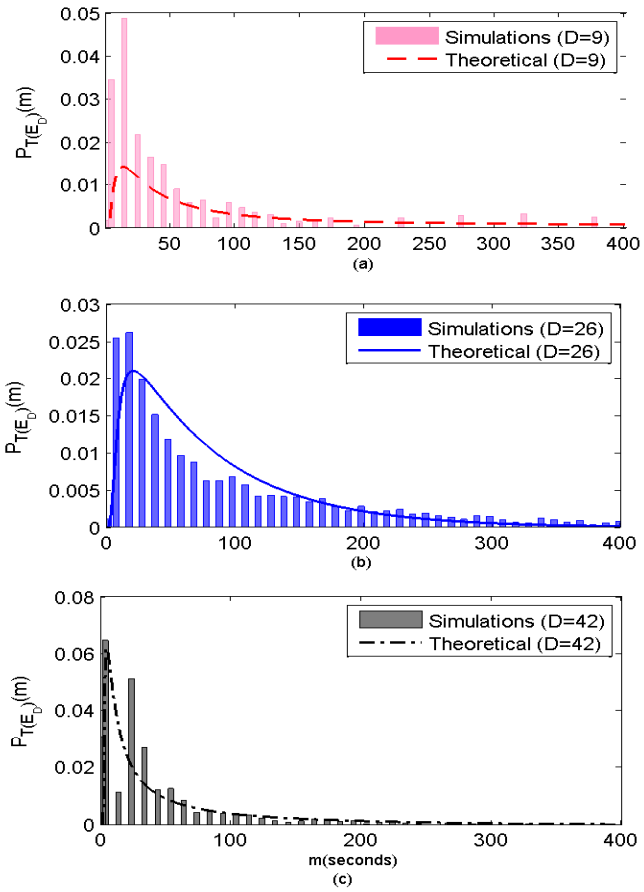

Figure 3.8: Probability mass function of the communication link lifetime for $D =$ (a) 9, (b) 26, and (c) 42 veh/km.

distance headway models, calculate the probability, $P\left(\mathbb{X}_H(0) = \{s_i\}_{i=1}^{n} | N_H = n\right)$, that set $\mathbb{X}_H(0)$ of size n is equal to set $\{s_i\}_{i=1}^{n}$, for $0 \leq s_i \leq N_{\max}$; and 3) using renewal theory, the pmf of the N_H is calculated for each of the mesoscopic distance headway models in (2.1)-(2.3) [70]. Therefore, we extend the results for different initial conditions (i.e., N_H and $\mathbb{X}_H(0)$) for the range of values within which N_H lies with probabilities of 0.94, 0.95, and 0.94 and X lies with probabilities 0.94, 0.97, and 0.99, for $D = 9, 26$, and 42 veh/km, respectively. Finally, the low of total probability is used to find the pmf of the link lifetime over the considered set of initial conditions. The average link lifetime, over the considered range of initial conditions, is found to be 145.50, 46.07, and 44.76 seconds for the low, intermediate, and high vehicle density, respectively. Although, intuitively, it is thought

that a communication link lasts longer with a higher vehicle density, our results indicate the opposite. The reasons are: 1) the impact of a larger number of vehicles within the link, N_H, with a higher vehicle density and therefore multiple mobility factors on the communication link lifetime; and 2) vehicles tendency to move with their maximum desired speed in an uncongested traffic flow conditions. Since the communication link disconnects when the sum of any $J \leq N_H + 1$ distance headways is greater than R, the larger the N_H value, the more frequently a link breakage occurs, for the same distance headway model. Although distance headways are large in a low vehicle density scenario with free driving (Table 1.1), this does not necessarily indicate a large probability of changing speeds (i.e., large p and q). On the contrary, vehicles are more likely to be at their maximum desired speeds, resulting in small p and q values [1]. In a congested traffic flow condition, vehicles are more likely to undergo stop-and-go situations, in which drivers speed up whenever they get an opportunity (i.e., large p and q values). This agrees with VISSIM results shown in Figure 3.4.

From the results shown in Figure 3.7 and Figure 3.8, we conclude the following: For a high traffic density, there is a higher probability of link availability between two nodes (Figure 3.7); however, the link lifetime is shorter (Figure 3.8). This causes the communication link to fluctuate between connection and disconnection more frequently when compared to that in a low vehicle density. This is due to the stop-and-go scenario in a high vehicle density. On the other hand, for a low traffic density, there is a lower probability of link availability between two nodes (Figure 3.7); however, if a link exists, the link lasts longer when compared to the case in a high vehicle density (Figure 3.8). Therefore, when a communication link disconnects in an uncongested traffic flow condition, it has a smaller probability to re-connect than that in a congested traffic flow condition.

3.5 Summary

This chapter presents a stochastic analysis of the communication link in a highway VANET with focus on a single lane. Mesoscopic mobility models are used to derive the stationary probability density of the communication link length for three traffic flow conditions. A stochastic microscopic model is proposed for the distance headway. The model captures time variations of the distance headway based on a discrete-time Markov chain that preserves the realistic dependency of distance headway changes at consecutive time steps. This dependency increases with the vehicle density, which is consistent with highway data patterns from empirical NGSIM and simulated VISSIM data sets. Further, the distance headway model is used to analyze the communication link lifetime. The first passage time

analysis is employed to derive the probability distribution of the communication link lifetime. Numerical results indicate that the communication hop length increases and the link lifetime decreases with an increase in vehicle density. The link length and lifetime statistics are essential to studying the network topology and its temporal variations in VANETs.

Chapter 4

Node cluster stability

This chapter presents a stochastic analysis of single-hop cluster stability. The stochastic microscopic mobility model presented in Section 3.1 is adopted to capture the time variations of distance headways. Firstly, we propose a discrete-time lumped Markov chain to model the time variations of a system of distance headways. Secondly, the first passage time analysis is used to derive probability distributions of the time periods of invariant cluster-overlap state and cluster-membership as measures of external and internal cluster stability, respectively. Thirdly, queueing theory is utilized to model the limiting behaviors of the external cluster stability. The overlapping region between overlapping clusters and the unclustered region between disjoint clusters are modeled as a storage buffer in a two-state random environment. Using G/G/1 queuing theory, the steady-state distributions of the numbers of common and unclustered nodes are approximated. Numerical results are presented to evaluate the proposed models, which demonstrate a close agreement between analytical and simulation results.

4.1 External cluster stability

The cluster-overlap state is governed by the the distance between two neighboring CHs. As this distance decreases, the CHs approach each other causing the two clusters to overlap. On the other hand, as the distance between CHs increases, the CHs move apart from each other causing the two clusters to become disjoint. The distance between two neighboring CHs is equal to the sum of the distance headways between the two nodes. Label the (N_c+2) nodes with IDs $0, 1, \ldots, N_c+1$, where the following CH has ID 0 and the leading CH has ID $(N_c + 1)$. For notation simplicity, let $\mathbb{X}_c = (X_i)_{i=0}^{N_c}$ be the sequence of distance headways

between the two CHs as illustrated in Figure 2.1 (c), where $\mathbb{X}_c(m) = (X_i(m))_{i=0}^{N_c}$, and $\{\mathbb{X}_c(m) \in (s_0, s_1, \ldots, s_{N_c}\ )\} \equiv \{X_i(m) \in s_i, \forall i \in [0, N_c]\}$. Consider initially overlapping clusters, i.e., $\sum_{i=0}^{N_c} X_i(0) < 2R$. Two neighboring CHs remain overlapping until $\sum_{i=0}^{N_c} X_i(m) \geq 2R$ at some time step m. The sequence of $(N_c + 1)$ i.i.d. distance headways is an $(N_c + 1)$-dimensional Markov chain, where each headway, X_i, is a birth and death Markov chain as described in Section 3.1. For clarity, the term *state* refers to a state in the original Markov chain, X, the term *super state* refers to a state in the (N_c+1)-dimensional Markov chain, and the term *lumped state* refers to a set of super states (to be discussed later in this section). Additionally, parentheses ( ) are used for a sequence, while curly brackets { } are used for a set. A super state in the (N_c+1)-dimensional Markov chain is a sequence of size $N_c + 1$, in which the i^{th} element represents the state (in the one dimensional (1D)-Markov chain) that the i^{th} distance headway belongs to. That is, a super state, $(s_0, s_1, \ldots, s_{N_c})$, means that distance headway X_i is in state $s_i \in [0, N_{\max} - 1]$. The sum of $(N_c + 1)$ distance headways representing the distance between the two CHs can be calculated from the $(N_c + 1)$-dimensional Markov chain. The state space size of the $(N_c + 1)$-dimensional Markov chain is equal to $N_{\max}^{(N_c+1)}$, making it subject to the state-space explosion problem when N_c is large [1]. However, since we are interested in the sum of the $(N_c + 1)$ distance headways, the state space can be reduced according to the following theorem.

Theorem 1 *Let X be a discrete-time, birth-death, irreducible Markov chain with N_{max} finite states, and let set $\mathbb{X} = (X_i)_{i=0}^{N-1}$ represent a system of N independent copies of chain X. The N-dimensional Markov chain that represents the system, $\mathbb{X}$, is lumpable with respect to the state space partition $\Omega = \{\Omega_0, \Omega_1 \ldots, \Omega_{N_L}\}$, such that (s.t.) any two super states in subset Ω_i are permutations of the same set of states $\forall i \in [0, N_L - 1]$, where $N_L = \frac{(N_{max}+N-1)!}{N!(N_{max}-1)!}$ is the state space size of the lumped Markov chain.*

The proof of Theorem 1 and following corollaries are given in the Appendix. Since a lumped state, $\Omega_i = \{(s_0, s_1, \ldots, s_{N-1})\}, 0 \leq i \leq N_L - 1$, contains all super states that are permutations of the same set of states, we can write the lumped state as a set of those states $\Omega_i = \{s_0, s_1, \ldots, s_{N-1}\}$. Since the $(N_c + 1)$-dimensional Markov chain is irreducible, the lumped Markov chain is also irreducible [71]. The stationary distribution of the lumped Markov chain can be derived from the stationary distribution of the 1D-Markov chain according to the following Corollary.

[1] This problem can also be solved in similar fashion as that used to calculate the communication link lifetime in Section 3.3. However, since the number of nodes between two neighboring CHs can be much larger than the number of nodes between a node and its hop edge node, the computational complexity of the recursive relation (3.11) becomes large due to the increased size of the matrix V.

Corollary 1 *Consider a system of N independent copies of a finite, discrete-time, birth-death, irreducible Markov chain, X, with stationary distribution $(\pi_i)_{i=0}^{N_{max}-1}$. The stationary distribution of the lumped Markov chain of Theorem 1, representing the system, $\mathbb{X} = (X_i)_{i=0}^{N-1}$, follows a multi-nomial distribution with parameters $(\pi_i)_{i=0}^{N_{max}-1}$.*

4.1.1 Time to the first change of cluster-overlap state

Consider two overlapping clusters. At any time instant, the overlapping range between two neighbouring clusters is equal to $2R - \sum_{i=0}^{N_c} X_i(m)$, $\forall m \geq 0$. Therefore, according to Theorem 1, the time variation of the overlapping range between the two clusters can be described by a lumped Markov chain with lumped states $\Omega_0, \Omega_1, \ldots, \Omega_{N_L-1}$ which represents the system, $\mathbb{X}_c = (X_i)_{i=0}^{N_c}$. Furthermore, divide the lumped states into two sets, Ω_{OV} and Ω_{NOV}. A lumped state $\Omega_i = \{s_0, s_1, \ldots, s_{N_c}\}$ belongs to Ω_{OV} and to Ω_{NOV} if $\sum_{i=0}^{N_c} s_i < 2N_R$ and $\sum_{i=0}^{N_c} s_i \geq 2N_R$, respectively, where N_R is the integer number of the states that cover distance headways within R in the distance headway's 1D-Markov chain. Let the system of the distance headways between the two CHs be initially in super state I_c, i.e., $\mathbb{X}_c(0) \in I_c$, s.t. $I_c \in \Omega_k \in \Omega_{OV}$, $0 \leq k \leq N_L - 1$. Let the time period until the clusters are no longer overlapping be $T_{ov1}(\Omega_k)$, given that the distance headways between them are initially in states $I_c \in \Omega_k$. Then, this time period is equal to the first passage time for the system, $\mathbb{X}_c$, to transit from the lumped state Ω_k to any lumped state $\Omega_{k'}$, s.t. $\Omega_{k'} \in \Omega_{NOV}$. That is, $T_{ov1}(\Omega_k) = \min\Big\{m > 0;\ \mathbb{X}_c(m) \in (k_0, k_1, \ldots, k_{N_c}),\ \sum_{i=0}^{N_c} k_i \geq 2N_R \mid \mathbb{X}_c(0) \in I_c\Big\}$. Let M_{N_c} be the transition probability matrix of the lumped Markov chain describing $\mathbb{X}_c$. One way to find the first passage time is to force the lumped states in Ω_{NOV} to become absorbing, i.e., set the probability of returning to the same lump state, Ω_i, within one time step to one $\forall \Omega_i \in \Omega_{NOV}$. Furthermore, let all the lumped states in Ω_{NOV} be merged into one single absorbing state and let it be the last $(\tilde{N}_L - 1)^{\text{th}}$ state, where $\tilde{N}_L$ is the number of states in the new absorbing lumped Markov chain. The transition probability matrix of the new absorbing lumped Markov chain, $\tilde{M}_{N_c}$, is derived from M_{N_c} as follows: $\tilde{M}_{N_c}(\Omega_i, \Omega_j) = M_{N_c}(\Omega_i, \Omega_j)\ \forall i, j,\ s.t.\ \Omega_i, \Omega_j \in \Omega_{OV}$, $\tilde{M}_{N_c}(\Omega_i, \Omega_{N_L-1}) = \sum_j M_{N_c}(\Omega_i, \Omega_j)$ $\forall i, j,\ s.t.\ \Omega_i \in \Omega_{OV}$ and $\Omega_j \in \Omega_{NOV}$. Let $T_{ov1}(\Omega_k)$ denote the time interval from the instant that the clusters are initially formed till the first time instant that the cluster-overlap state changes, given that the distance headways are in super state $I_c \in \Omega_k$. The cdf of $T_{ov1}(\Omega_k)$ is given by

$$F_{T_{ov1}(\Omega_k)}(m) = \tilde{M}_{N_c}(\Omega_k, \Omega_{\tilde{N}_L-1}) + \sum_{\substack{j \\ \Omega_j \in \Omega_{OV}}} \tilde{M}_{N_c}(\Omega_k, \Omega_j) F_{T_{ov1}(\Omega_j)}(m-1), \quad m \geq 1 \qquad (4.1)$$

where $F_{T_{ov1}(\Omega_k)}(0) = 0$. Equation (4.1) calculates the cdf of $T_{ov1}(\Omega_k)$ recursively. Since $F_{T_{ov1}(\Omega_k)}(m) = \sum_{n=1}^{m} P_{T_{ov1}(\Omega_k)}(m)$, the first term in (4.1) corresponds to the absorption probability within one time step given that the system is initially in lumped state Ω_k, i.e., $F_{T_{ov1}(\Omega_k)}(1) = \tilde{M}_{N_c}(\Omega_k, \Omega_{\tilde{N}_L-1})$. The second term in (4.1) corresponds to $\sum_{n=2}^{m} P_{T_{ov1}(\Omega_k)}(m)$ which is the absorption probability within $(m-1)$ time steps given that the system transited from Ω_k to $\Omega_j \in \Omega_{OV}$ within one time step.

The size of the state space of the lumped Markov chain can still be large with an increased number of nodes between the two CHs, since $N_L = \frac{(N_{\max}+N_c)!}{(N_c+1)!(N_{\max}-1)!}$. However, the state space of the absorbing lumped Markov chain, needed to compute the time period until the overlap state changes between the two neighboring CHs, is bounded according to the following Corollary.

Corollary 2 *Consider a system of N independent copies of an irreducible Markov chain according in Theorem 1, and let the event of interest be that the sum of the states of the N chains be larger than a deterministic threshold N_{th}. The absorbing lumped Markov chain, required to obtain the first occurrence time of the event of interest, has a state space that is bounded by a deterministic function of N_{th}, when $N > N_{th}$.*

Consider the scalability of analyzing a system of N distance headways, $\mathbb{X}_N$, to an increased number of distance headways, N. Using the lumped Markov chain, the scalability of analyzing system $\mathbb{X}_N$ is improved for: *i)* the steady-state analysis - The problem of finding the stationary distribution of a system of distance headway is of constant computational complexity with respect to N (according to Corollary 1); and *ii)* the transient analysis (i.e, the first passage time analysis) - The computational complexity of the first passage time analysis is dependent on the state space size of the considered Markov chain. According to Corollary 2, the state space size of the absorbing lumped Markov chain is upper bounded by the total number of integer partitions of all integer that are less than N_{th} as discussed in Appendix A.3. Figure 4.1 shows the state space reduction using the proposed lumped Markov chain.

In this subsection, we focus on the time interval from the instant that two partially overlapping neighboring clusters are formed till the time instant that they no longer overlap. Given an initial super state of the two neighboring clusters at the end of the cluster formation stage, consider the following: *i)* a proactive re-clustering procedure in which re-clustering is triggered after a fixed period of time, say Δt seconds from the cluster formation; and *ii)* a reactive re-clustering procedure in which re-clustering is triggered

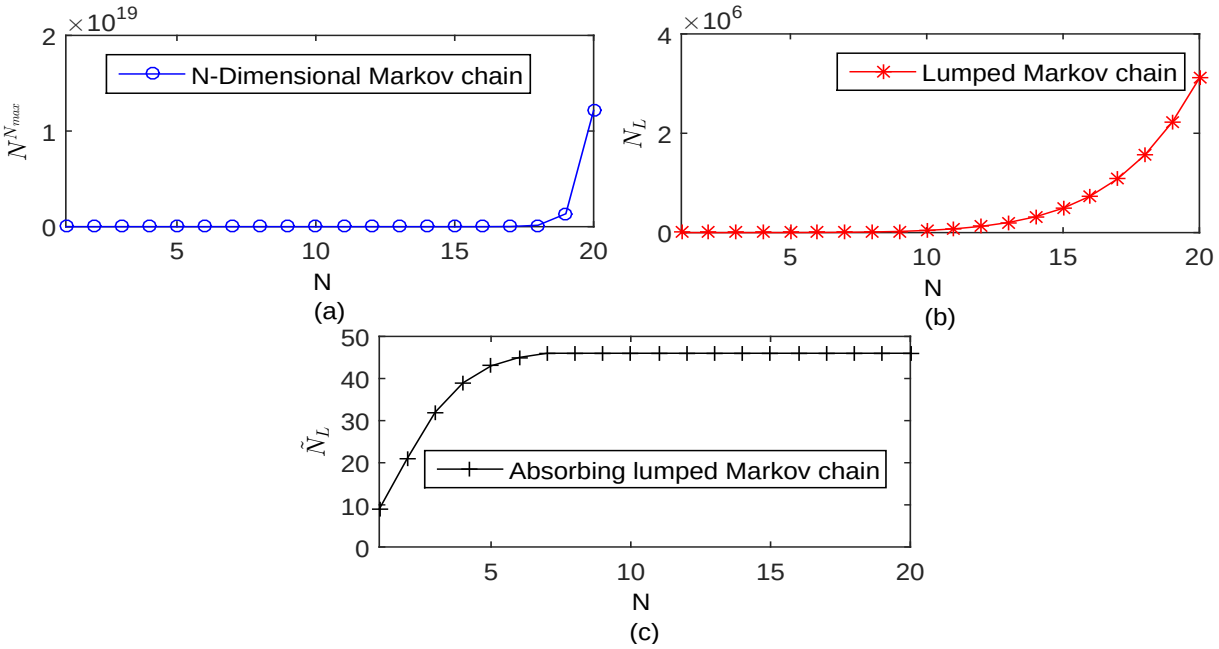

Figure 4.1: The state space size of a Markov chain representing a system of N Markov chains (distance headways), $\mathbb{X}_N$, with $N_{\max} = 9$ when the system $\mathbb{X}_N$ is represented by (a) an N-dimensional Markov chain, (b) a lumped Markov chain according to Theorem 1, and (c) an absorbing lumped Markov chain according to Corollary 2 with $N_{\text{th}} = 8$.

when the cluster-overlap state changes. In *i)*, the probability that the overlap state changes between the two overlapping neighboring clusters before re-clustering is triggered is equal to $F_{T_{ov1}(\Omega_k)}(\Delta t)$. In *ii)*, the re-clustering period is equal to $T_{ov1}(\Omega_k)$ with the cdf calculated by (4.1). Up until now, we have considered a pair of neighboring clusters in a specific super state when they are initially formed. In reality, the initial state of a pair of neighboring clusters is a random variable. For a given N_c, since the distance headways are stationary when the clusters are formed, the probability that two overlapping neighboring clusters are initially in lumped state Ω_i is given by $\mho_i \Big/ \left[\sum_{j,\Omega_j \in \Omega_{OV}} \mho_j\right]$ where $\mho_i$ is given by (B.3) in Appendix A.2. Using the law of total probability, the cdf of the time for the first change

in overlap state to occur between two initially overlapping clusters is given by

$$F_{T_{ov1}}(m) = \frac{\sum\limits_{\substack{j \\ \Omega_j \in \Omega_{OV}}} \mho_j F_{T_{ov1}(\Omega_j)}(m)}{\sum\limits_{\substack{i \\ \Omega_i \in \Omega_{OV}}} \mho_i}, \quad m = 1, 2, \ldots. \tag{4.2}$$

4.1.2 Time period between successive changes of cluster-overlap state

In the preceding subsection, we have analysed the time interval during which two neighboring clusters remain overlapping since the clusters are formed. During this time interval, the cluster-overlap state remains unchanged. Suppose two neighboring clusters overlap in cluster formation and the overlap state changes at time $T_{ov1}(< \Delta t)$ and becomes non-overlapping. The cluster-overlap state may change again before re-clustering is triggered. As a result, the time period between two consecutive changes of cluster-overlap state equals *i)* the cluster-overlapping time period when the overlap state changes from overlapping to non-overlapping, plus *ii)* the cluster-non-overlapping time period when the overlap state changes from non-overlapping to overlapping. During a cluster-overlapping or cluster non-overlapping time periods, the cluster-overlap state remains unchanged indicating how long the cluster remains externally stable.

Cluster-overlapping time period

The second cluster-overlapping time period may not be equal to T_{ov1}, since the initial state may not be the same as that when the clusters are initially formed. We refer to this period as cluster overlapping period, denoted by T_{ov}.

To derive the distribution of T_{ov}, the same approach used to find the distribution of T_{ov1} can be used. Notice that the absorbing lumped Markov chain is the same as that used to calculate the distribution of T_{ov1}. The only difference is the distribution of the initial state, I_c. One way to find the distribution of I_c at the time when the second overlapping state occurs is as follows:

- Make the lumped states in set Ω_{NOV} absorbing, without combining them into one

absorbing state. The corresponding transition probability matrix, ${M''}_{N_c}$, is equal to M_{N_c} with ${M''}_{N_c}(\Omega_j, \Omega_i) = 0$ and ${M''}_{N_c}(\Omega_j, \Omega_j) = 1 \forall i, j,\ s.t.\ \Omega_j \in \Omega_{NOV}$;

- Calculate the absorbing probability δ_j for each absorbing lumped state $\Omega_j \in \Omega_{NOV}$ by

$$\delta_j = \sum_{\substack{i \\ \Omega_i \in \Omega_{OV}}} \frac{\mho_i}{\sum_{\substack{k \\ \Omega_k \in \Omega_{OV}}} \mho_k} \lim_{m \to \infty} {M''}_{N_c}^{(m)}(\Omega_i, \Omega_j) \tag{4.3}$$

where ${M''}_{N_c}^{(m)}(\Omega_i, \Omega_j)$ denotes the $(\Omega_i, \Omega_j)^{\text{th}}$ entry of the m^{th} power of matrix ${M''}_{N_c}$;

- Form another absorbing Markov chain by making the lumped states in set Ω_{OV} absorbing, without combining them into one absorbing state. The corresponding transition probability matrix, ${M'}_{N_c}$, is equal to M_{N_c} with ${M'}_{N_c}(\Omega_i, \Omega_j) = 0$ and ${M'}_{N_c}(\Omega_i, \Omega_i) = 1\ \forall i, j,\ s.t.\ \Omega_i \in \Omega_{OV}$;

- Calculate the absorbing probability ϕ_i for each absorbing lumped state $\Omega_i \in \Omega_{OV}$ by

$$\phi_i = \sum_{\substack{j \\ \Omega_j \in \Omega_{NOV}}} \delta_j \lim_{m \to \infty} {M'}_{N_c}^{(m)}(\Omega_j, \Omega_i). \tag{4.4}$$

The probability that the distance headways between the two neighboring clusters are in state $\Omega_i \in \Omega_{OV}$ at the time when the second overlapping state occurs is equal to ϕ_i. Therefore, the cdf of the cluster-overlapping period is given by

$$F_{T_{ov}}(m) = \sum_{\substack{i \\ \Omega_i \in \Omega_{OV}}} \phi_i F_{T_{ov1}(\Omega_i)}(m), m = 1, 2, \ldots \tag{4.5}$$

where $F_{T_{ov1}(\Omega_i)}(m)$ is given by (4.1). However, using this approach, we lose the advantage of having a single absorbing state and, therefore, a bounded state space (according to Corollary 2). We propose to approximate the distribution of the system initial state at the time when the second overlapping state occurs, ϕ_i, as follows

$$\phi_i \approx \frac{\mho_i \tilde{M}_{N_c}(\Omega_i, \Omega_{\tilde{N}_L - 1})}{\sum_{\substack{i \\ \Omega_i \in \Omega_{OV}}} \mho_i \tilde{M}_{N_c}(\Omega_i, \Omega_{\tilde{N}_L - 1})}. \tag{4.6}$$

The approximated ϕ_i for lumped state $\Omega_i (\in \Omega_{OV})$ is equal to its stationary probability weighted with the absorption probability within one time step. Notice that this weight

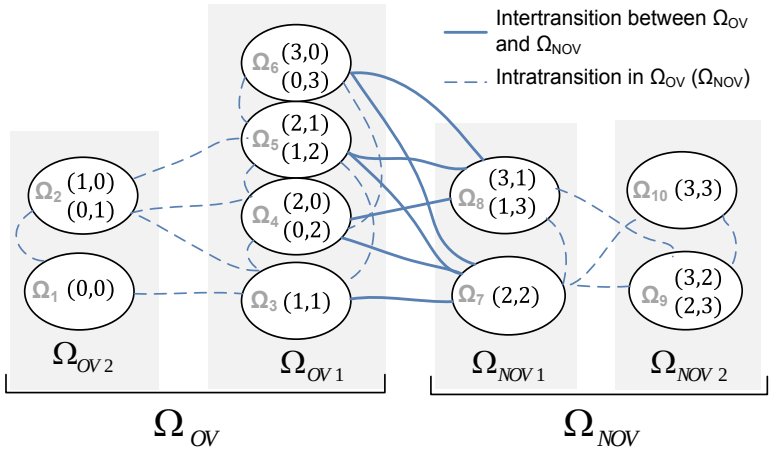

Figure 4.2: An illustration of a lumped markov chain for $N = 2, N_{\mathbf{th}} = 4, N_{\mathbf{max}} = 3$. A line between two lumped states represents a non-zero two-way transition probability in a single time step between the linked states. There exist non-zero transition probabilities between subsets of Ω_{OV1} and Ω_{NOV1}.

eliminates all the lumped states $\Omega_i \in \Omega_{OV}$ that are not directly accessible from states in Ω_{NOV}. Figure 4.2 illustrates an example for a lumped Markov chain, where the directly accessible lumped states are those connected by solid lines, i.e. Ω_{OV1} and Ω_{NOV1}. When the overlapping state of two neighboring clusters changes from non-overlapping to overlapping, the only possible states to be reached first are those in Ω_{OV1}.

Cluster-non-overlapping time period

Consider two initially overlapping clusters, the cluster state can change to become non-overlapping and again to become overlapping. The time period between two consecutive changes of cluster-overlap state equals the cluster-non-overlapping time period when the state changes from non-overlapping to overlapping. Neighboring CHs may move apart from each other and the clusters become disjoint. This may result in disruption to intercluster and/or intracluster communications and/or seizure of the cluster membership status from edge CMs. This produces unclustered nodes that may create their own cluster which can trigger re-clustering and increase the clustering cost. Let T_{nov} denote the cluster non-overlapping time period. The same procedure used to calculate the cdf of T_{ov} can be used

to derive the cdf of T_{nov}, which is given by

$$F_{T_{nov}}(m) = \sum_{\substack{j \\ \Omega_j \in \tilde{\Omega}_{NOV}}} \delta_j F_{T_{nov1}(\Omega_j)}(m), \quad m = 1, 2, \ldots \tag{4.7}$$

where $F_{T_{nov1}(\Omega_j)}(m) = \tilde{M}'_{N_c}(\Omega_j, \Omega_{\tilde{N'}_L - 1}) + \sum_{\Omega_k \in \tilde{\Omega}_{NOV}}^{k} \left[\tilde{M}'_{N_c}(\Omega_j, \Omega_k) F_{T_{nov1}(\Omega_k)}(m-1) \right], m \geq 1$, $\delta_j \approx \frac{\upsilon_j \tilde{M'}_{N_c}(\Omega_j, \Omega_{\tilde{N'}_L - 1})}{\sum_{\substack{j \\ \Omega_j \in \tilde{\Omega}_{NOV}}} \upsilon_j \tilde{M'}_{N_c}(\Omega_j, \Omega_{\tilde{N'}_L - 1})}$, and $\tilde{M'}_{N_c}$ is the probability transition matrix that corresponds to the lumped Markov chain with all states in Ω_{OV} combined into one absorbing state. That is, $\tilde{M}'_{N_c}$ is derived from M_{N_c} as follows: $\tilde{M}'_{N_c}(\Omega_j, \Omega_i) = M_{N_c}(\Omega_j, \Omega_i)\ \forall i, j,\ s.t.\ \Omega_j, \Omega_i \in \Omega_{NOV}$, $\tilde{M}'_{N_c}(\Omega_j, \Omega_{\tilde{N'}_L - 1}) = \sum_j M_{N_c}(\Omega_j, \Omega_i)\ \forall i, j,\ s.t. \Omega_j \in \Omega_{NOV}$ and $\Omega_i \in \Omega_{OV}$. The average cluster-non-overlapping time period is given by [72]

$$E[T_{nov}] = \Psi \left(I - \tilde{M}'_{N_c} \right)^{-1} M_1 \tag{4.8}$$

where Ψ is a row vector of size $\tilde{N'}_L$ in which the j^{th} element equals δ_j, I is the identity matrix of size equal to that of $\tilde{N'}_L$, and M_1 is a column vector of ones with size $\tilde{N'}_L$. The second moment of the cluster-non-overlapping time period is given by[2] [72]

$$E[T^2_{nov}] = 2\Psi \tilde{M}'_{N_c} \left(I - \tilde{M}'_{N_c} \right)^{-2} M_1 + E[T_{nov}]. \tag{4.9}$$

4.2 Internal cluster stability

Due to relative vehicle mobility, two events result in changes to the cluster-membership: *i)* a vehicle leaving the cluster, and *ii)* a vehicle entering the cluster. Let e_{o_r} and e_{o_l} denote the events that a vehicle leaves the cluster from the right side and the left side of the CH, respectively. Let e_{i_r} and e_{i_l} denote the events that a vehicle enters the cluster from the right side and the left side of the CH, respectively. Figure 4.3 illustrates these events. Consider the time for the first change in cluster-membership to occur after cluster formation, and denote this time by T_{CM1}. This time is equivalent to the first occurrence times of one of the four events, i.e., $T_{CM1} = T(e_{o_r} \cup e_{i_r} \cup e_{o_l} \cup e_{i_l})$, where $T(e)$ denotes the first occurrence time of event e. Furthermore, let $T_{CM1_r} = T(e_{o_r} \cup e_{i_r})$ and $T_{CM1_l} = T(e_{o_l} \cup e_{i_l})$

[2]The first and the second moments of the cluster-overlapping period can be calculated similarly by adjusting (4.8)-(4.9) to correspond to the absorbing lumped Markov chain with transition matrix $\tilde{M}_{N_c}$.

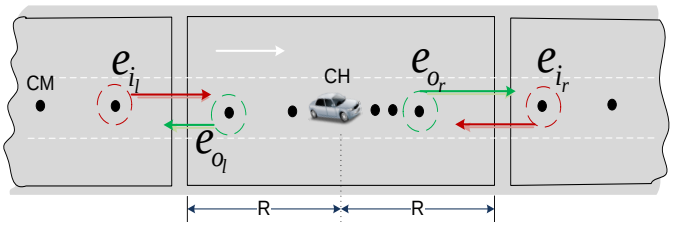

Figure 4.3: Illustration of the events that cause changes in cluster-membership.

be the first occurrence time of the first change in cluster-membership (after cluster formation) due to a vehicle leaving and entering the cluster from the right and the left side of the CH, respectively. Therefore, $T_{CM1} = \min\{T_{CM1_r}, T_{CM1_l}\}$. Since T_{CM1_r} and T_{CM1_l} are independent, the cdf of the time for the first change in cluster-membership to occur after cluster formation is given by $F_{T_{CM1}}(m) = 1-(1-F_{T_{CM1_r}}(m))(1-F_{T_{CM1_l}}(m))$. Notice that T_{CM1_r} and T_{CM1_l} are i.i.d.. Therefore, we focus on calculating only one of them, say T_{CM1_r}.

4.2.1 Time to the first change of cluster-membership

Let N_{CM_r} be the number of CMs on the right side of the CH, and assume that $N_{CM_r} > 0$ [3]. Let $\mathbb{X}_{CM} = \{X_i\}_{i=0}^{N_{CM_r}}$ be the set of distance headways of the CH and the N_{CM_r} nodes as illustrated in Figure 4.4, where $\mathbb{X}_{CM}(m) \subseteq (s_0, s_1, \ldots, s_{N_{CM_r}}) \equiv [X_i(m) \in s_i, \forall i \in [0, N_{CM_r}]]$. The system, $\mathbb{X}_{CM}$, can be represented by an $(N_{CM_r}+1)$-dimensional Markov chain. Suppose that set $\mathbb{X}_{CM}$ is in super state $I_{CM} = (k_0, k_1, \ldots, k_{N_{CM_r}})$ when the clusters are initially formed, *s.t.*, $\sum_{i=0}^{N_{CM_r}-1} k_i < N_R$, $\sum_{i=0}^{N_{CM_r}} k_i \geq N_R$, and $I_{CM} \in \Omega_k$. Let the time period until a node enters/leaves the cluster from one side be $T_{CM1_{r(\Omega_k)}}$, given that $\mathbb{X}_{CM} \in I_{CM} \in \Omega_k$. Then this time period is equal to the first passage time for the system, $\mathbb{X}_{CM}$, to transit from super state I_{CM} to a super state $(k'_0, k'_1, \ldots, k'_{N_{CM_r}})$ such that $\sum_{i=0}^{N_{CM_r}} k'_i < N_R$ (i.e., a node enters the cluster) or $\sum_{i=0}^{N_{CM_r}-1} k'_i \geq N_R$ (i.e., a node leaves the cluster). That is, $T_{CM1_{r(\Omega_k)}} = \min\Big\{m > 0; \mathbb{X}_{CM}(m) \in (k'_0, k'_1, \ldots, k'_{N_{CM_r}}), \Big\{\sum_{i=0}^{N_{CM_r}} k'_i < N_R \cup \sum_{i=0}^{N_{CM_r}-1} s_i \geq N_R\Big\} \mid \mathbb{X}_{CM} \in I_{CM}\Big\}$.

[3]When $N_{CM_r} = 0$, the problem reduces to a single distance headway, with only the event of a node entering the cluster causing the cluster-membership change. In this case, the first passage time analysis for one dimensional chain can be used.

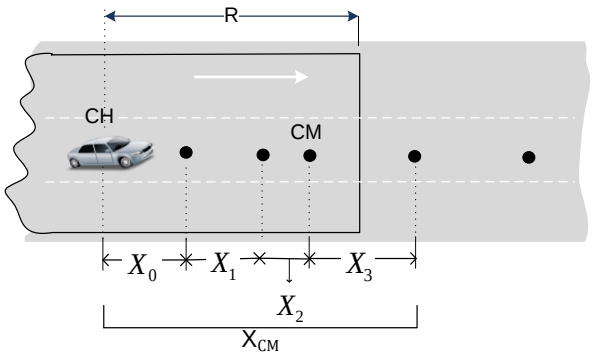

Figure 4.4: A cluster with $N_{CM_r} = 3$ and $\mathbb{X}_{CM} = \{X_0, X_1, X_2, X_3\}$.

Since the change in cluster-membership occurs at the edge of the cluster, the value of $X_{N_{CM_r}}$ in the system, $\mathbb{X}_{CM}$, is critical to identify the change. Notice that, initially, the distance headway $X_{N_{CM_r}}$ can only be in a state $k_{N_{CM_r}} \in [N_R - \sum_{i=0}^{N_{CM_r}-1} k_i, N_{\max}]$. Therefore, we propose to lump the $(N_{CM_r}+1)$-dimensional Markov chain into partitions (lumped states) $\Omega'_0, \Omega'_2, \ldots \Omega'_{N_L-1}$, such that each lumped state $\Omega'_i = \{(s_0, s_1, \ldots, s_{N_{CM_r}})\}$ contains all super states that have the first N_{CM_r} states, i.e., $(s_0, s_1, \ldots, s_{N_{CM_r}-1})$, as permutations of each other[4]. We refer to this chain as *edge lumped Markov chain*. Furthermore, divide the lumped states into three sets, Ω_I, Ω_L and Ω_E, such that a lumped state $\Omega'_i = \{(s_0, s_2, \ldots, s_{N_{CM_r}})\}$ belongs to *i)* Ω_I, if $\sum_{i=0}^{N_{CM_r}-1} s_i < N_R$, and $\sum_{i=0}^{N_{CM_r}} s_i \geq N_R$; *ii)* Ω_L, if $\sum_{i=0}^{N_{CM_r}-1} s_i \geq N_R$; and *iii)* Ω_E, if $\sum_{i=0}^{N_{CM_r}} s_i < N_R$. Let $M_{N_{CM}}$ be the transition probability matrix of the described lumped markov chain. The time for the first cluster-membership change to occur, $T_{CM1_r(\Omega_k)}$, is the first passage time for system $\mathbb{X}_{CM}$ to transit from super state $I_{CM} \in \Omega_k \in \Omega_I$ to any state in Ω_L (i.e., when a node leaves the cluster) or Ω_E (i.e., when a node enters the cluster). To find the distribution of $T_{CM1_r(\Omega_k)}$, we force the lumped states in Ω_E and Ω_L to become one absorbing state. Following the same steps as in Section 4.1, the cdf of $T_{CM1_r(\Omega_k)}$ can be derived as

$$F_{T_{CM1_r(\Omega_k)}}(m) = \tilde{M}_{N_{CM}}(\Omega_k, \Omega_{\tilde{N}_L-1}) + \sum_{\substack{j \\ \Omega_j \in \Omega_I}} \tilde{M}_{N_{CM}}(\Omega_k, \Omega_j) F_{T_{CM1_r(\Omega_j)}}(m-1), \quad m \geq 1 \tag{4.10}$$

where $\tilde{M}_{N_{CM}}$ is the probability transition matrix of the new absorbing lumped Markov chain

[4]Since the $(N_{CM_r}+1)$-dimensional Markov chain is lumpable into partitions $\Omega_1, \Omega_2, \ldots \Omega_{N_L-1}$, $\Omega_i = \{(s_0, s_1, \ldots, s_{N_{CM_r}})\}$ contains all super states that are permutations of each other according to Theorem 1. Then, it is lumpable into partitions that are subsets of $\Omega_0, \Omega_2, \ldots \Omega_{N_L-1}$.

with $\tilde{N}_L$ states, such that the $(\tilde{N}_L - 1)^{\text{th}}$ state is the single absorbing state containing all states in Ω_E and Ω_L.

For a random initial state of $\mathbb{X}_{CM}$, the probability that $\mathbb{X}_{CM}$ is initially in lumped state $\Omega'_i = \{(s_0, s_2, \ldots, s_{N_{CM_r}})\}$ is given by $\frac{\mho_i}{\sum_{j\Omega_j \in \Omega_I} \mho_j} \times \frac{\pi_{s_{N_{CM_r}}}}{\sum_{k=K_i}^{N_{\max}} \pi_k}$, $K_i = N_R - \sum_{u=0}^{N_{CM_r}-1} s_u$, where $\mho_i$ is the stationary distribution of lumped state $\Omega_i = \{(s_0, s_2, \ldots, s_{N_{CM_r}-1})\}$ of the N_{CM_r}-dimensional Markov chain lumped according to Theorem 1. Hence, the cdf of the time interval between the time instant when the cluster is initially formed till the first cluster-membership change is given by

$$F_{T_{CM1_r}}(m) = \frac{1}{\sum\limits_{\substack{j \\ \Omega'_j \in \Omega_I}} \mho_j} \sum_{\substack{i \\ \Omega'_i \in \Omega_I}} \frac{\pi_{(i, s_{N_{CM_r}})} \mho_i F_{T_{CM1_r(\Omega'_i)}}(m)}{\sum_{k=K_i}^{N_{\max}} \pi_k} \tag{4.11}$$

where $(i, s_{N_{CM_r}})$ is the state index of the distance headway of the $N_{CM_r}^{\text{th}}$ CM in the i^{th} lumped state.

4.2.2 Time period between successive changes of cluster- membership

In the previous subsection, we have analysed the time interval from initial cluster formation to the first cluster-membership change. In order to have a better measure of internal cluster stability, we analyse the time interval between two successive cluster-membership changes in this subsection. Let T_{CM} denote the time interval between two consecutive membership changes of a cluster. Notice that the cluster-membership change rate, i.e. the rate at which nodes enter or leave the cluster, is the reciprocal of T_{CM}. We focus on one side of the cluster in this subsection, since a similar derivation for the other side can be done.

To derive the distribution of T_{CM}, the first step is to find the distribution of I_{CM} at the time when the first cluster-membership change occurs. In order to do this, first we make the lumped states in sets Ω_E and Ω_L of the lumped Markov chain absorbing, without combining them into one state. The result is an absorbing markov chain and let M'_{CM} be its probability transition matrix. Then the probability of absorption in lumped state $\Omega_e \in \Omega_E$ and the probability of absorption in lumped state $\Omega_l \in \Omega_L$ are given respectively

by

$$\delta_{E_e} = \frac{1}{\sum\limits_{\substack{j \\ \Omega'_j \in \Omega_I}} \mho_j} \sum_{\substack{i \\ \Omega'_i \in \Omega_I}} \frac{\pi_{(i,s_{N_{CM_r}})} \mho_i}{\sum_{k=K_i}^{N_{\max}} \pi_k} \lim_{m \to \infty} {M'}^{(m)}_{N_{CM}}(\Omega_i, \Omega_e)$$

and

$$\delta_{L_l} = \frac{1}{\sum\limits_{\substack{j \\ \Omega'_j \in \Omega_I}} \mho_j} \sum_{\substack{i \\ \Omega'_i \in \Omega_I}} \frac{\pi_{(i,s_{N_{CM_r}})} \mho_i}{\sum_{k=K_i}^{N_{\max}} \pi_k} \lim_{m \to \infty} {M'}^{(m)}_{N_{CM}}(\Omega_i, \Omega_l)$$

where ${M'}^{(m)}_{N_{CM}}(\Omega_i, \Omega_E)$ denotes the $(\Omega_i, \Omega_E)^{\text{th}}$ entry of the m^{th} power of matrix ${M'}_{N_{CM}}$. Note that $\sum\limits_{\substack{e \\ \Omega_e \in \Omega_E}} \delta_{E_e}$ and $\sum\limits_{\substack{l \\ \Omega_l \in \Omega_L}} \delta_{L_l}$ are the probabilities that the first cluster-membership change occurs due to a vehicle entering the cluster and leaving the cluster, respectively. When calculating the time interval between successive cluster-membership changes, the examined system changes. Let $\mathbb{X}_{CM_E}$ and $\mathbb{X}_{CM_L}$ be the systems of distance headways of the CH and the nodes on one side of the cluster when the first cluster-membership change occurs due to a node entering the cluster and a node leaving the cluster, respectively. For example, if system $\mathbb{X}_{CM}$ is absorbed in lumped state $\Omega_i = \{(s_0, s_1, \dots s_{N_{CM_r}})\}$, then the initial lumped state for system $\mathbb{X}_{CM_L}$ is $\{(s_0, s_1, \dots s_{N_{CM_r}-1})\}$ if $\Omega_i \in \Omega_L$ and the initial lumped state for system $\mathbb{X}_{CM_E}$ is $\{(s_0, s_1, \dots s_{N_{CM_r}}, s_{N_{CM_r}+1})\}$ if $\Omega_i \in \Omega_E$, where $s_{N_{CM_r}+1} \in [N_R - \sum_{i=0}^{N_{CM_r}} s_i, N_{max}]$. Let Ω'_e be the lumped state for system $\mathbb{X}_{CM_E}$ corresponding to lumped state Ω_e for $\mathbb{X}_{CM}$, and let Ω'_l be the lumped state for system $\mathbb{X}_{CM_L}$ corresponding to lumped state Ω_l for $\mathbb{X}_{CM}$. Additionally, let $\delta_{E'_e}$ equal δ_{E_e} weighted by the stationary distribution (B.2) to account for the added distance headway in the system, $\mathbb{X}_{CM_E}$. The cdf of the time interval between two successive cluster-membership changes is approximated by

$$F_{T_{CM}}(m) = \sum_{\substack{e \\ \Omega_e \in \Omega_E}} \delta_{E'_e} F_{T_{CM1_{e(\Omega'_e)}}}(m) + \sum_{\substack{l \\ \Omega_l \in \Omega_L}} \delta_{L_l} F_{T_{CM1_{l(\Omega'_l)}}}(m). \tag{4.12}$$

4.3 Numbers of common CMs and unclustered nodes between clusters

In Section 4.1, the time for the first change in cluster-overlap state along with the cluster-overlapping and cluster-non-overlapping time periods are studied. Despite the importance

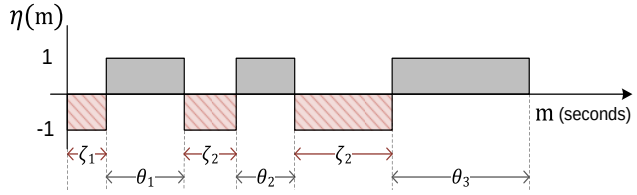

Figure 4.5: Illustration of the alternating renewal process between overlapping and non-overlapping time periods.

of the change in overlap-state as a measure of external cluster stability, it is a binary metric. A quantitative metric that describes in detail the level of external stability is desired. One quantitative measure is the number of nodes located between the clusters. That is, the number of nodes shared between overlapping clusters and the number of nodes left unclustered between disjoint clusters. The number of common nodes between neighboring clusters is an indicator of the level of intercluster communication interference that can occur during the overlapping period. On the other hand, during the non-overlapping period, the number of unclustered nodes between disjoint clusters is an indicator of the portion of network nodes that are left unserved by the clustered structure.

Given initially overlapping neighboring clusters, vehicles can enter and leave the overlapping/unclustered region. Additionally, the cluster-overlap state may change over time. Therefore, in this section we investigate the system of two neighboring clusters in terms the change of the numbers of common CMs and unclustered nodes between the two clusters along with the change in the cluster-overlap state. Since the system of distance headways between the neighboring clusters, $\mathbb{X}_c$, constructs a finite irreducible lumped Markov chain, there exists an infinite sequence of cluster-overlapping and cluster-non-overlapping time periods [72]. Therefore, the overlap state between clusters fluctuates between overlapping and non-overlapping scenarios.

Let $\{\eta(m), m = 0, 1, \dots\}$ be a stochastic process with state space $\{-1, 1\}$. If $\sum_{i=0}^{N_c} X_i(m) < 2R$, i.e., the clusters overlap, then $\eta(m) = -1$; otherwise, $\eta(m) = 1$. Denote by $\zeta_1, \theta_1, \zeta_2, \theta_2, \dots$ the lengths of successive intervals spent in states -1 and 1, respectively, where $\zeta_1, \zeta_2, \dots$ are i.i.d. and $\theta_1, \theta_2, \dots$ are i.i.d.. The process $\{\eta(m)\}$ alternates between states -1 and 1, as shown in Figure 4.5, which is referred to as alternating renewal process [70]. Since we assume that the clusters are initially overlapping, then $\eta(0) = -1$ and $\zeta_k = T_{ov}^k$, and $\theta_k = T_{nov}^k$, i.e., k^{th} cluster-overlapping period and the k^{th} cluster-non-overlapping period, respectively. We assume that the T_{ov}^k's are i.i.d. with cdf (4.5) and the T_{nov}^k's time periods are i.i.d. with cdf (4.7) and they are independent of one another[5]. The

[5]Index k is dropped from T_{ov}^k and T_{nov}^k to refer to an arbitrary overlapping and non-overlapping period,

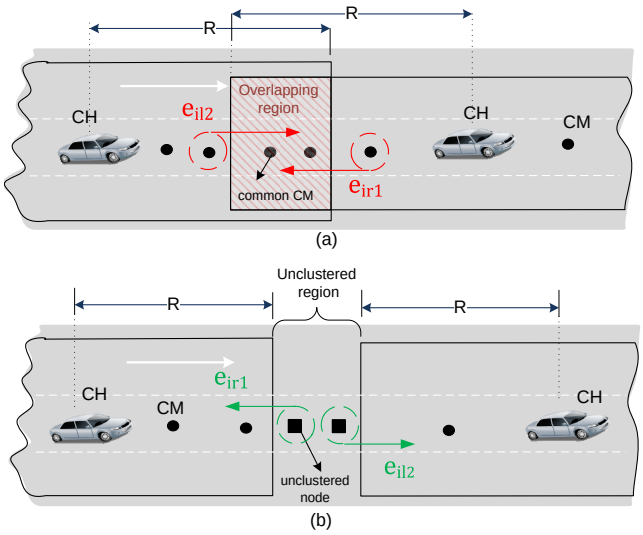

Figure 4.6: Illustration of the events that cause a vehicle to (a) enter the overlapping region and (b) leave the unclustered region between neighboring clusters.

k^{th} cycle is composed of ζ_k and θ_k.

4.3.1 Node interarrival time during an overlapping/non- overlapping period

During an overlapping/non-overlapping period, vehicles enter and leave the overlapping/ unclustered region resulting in a change in the number of common/unclustered nodes between neighboring clusters. Consider two overlapping clusters. A vehicle can enter the overlapping region from either of the clusters. Let T_i and T_{Ii} be the first arrival time and the interarrival time of nodes to the overlapping region, respectively. We are interested in the arrival times that cause an increase in the number of common nodes in the two clusters. The time for the first node entering the overlapping region is $T_i = \min(T(e_{i_r1}), T(e_{i_l2}))$, where e_{i_r1} is the event that a vehicle enters the following cluster from the right side of its CH, and e_{i_l2} is the event that a vehicle enters the leading cluster from the left side of its CH as illustrated in Figure 4.6(a). Note that $T(e_{i_r1})$ and $T(e_{i_l2})$ have the same probabilistic behaviors.

respectively.

We assume that $T(e_{i_r1})$ and $T(e_{i_l2})$ are independent. The times, $T(e_{i_r1})$ and $T(e_{i_l2})$ can then be calculated independently by applying the first passage time analysis on two edge lumped Markov chains, each identifying the hop edge node of its corresponding cluster, as in Subsection 4.2.1. However, we propose to approximate the distributions of $T(e_{i_r1})$ and $T(e_{i_l2})$ by calculating them from a fully lumped Markov chain with the initial distribution calculated from the state space of the edge lumped Markov chain. Since the distributions of $T(e_{i_r1})$ and $T(e_{i_l2})$ are the same, we will focus on one of them only, say $T(e_{i_r1})$. Let $\mathbb{S}_E$ be a set of states of the edge lumped Markov chain for a cluster with N_{CM_r} nodes, such that a lumped state $\Omega_i = \{s_0, s_1, \ldots, s_{N_{CM_r}}\}$ belongs to $\mathbb{S}_E$ if $\sum_{i=0}^{N_{CM_r}-1} s_i < N_R$ and $\sum_{i=0}^{N_{CM_r}} s_i \geq N_R$. Let $\{\pi_{E,i}\}_{i=1}^{|\mathbb{S}_E|}$ be the stationary distribution of the edge lumped Markov chain. Furthermore, divide the lumped states of the fully lumped Markov chain representing system $\mathbb{X}_{CM}$ into two sets, Ω_R and Ω_{R^c}. A lumped state $\Omega_i = \{s_0, s_1, \ldots, s_{N_{CM_r}}\}$ belongs to Ω_R if $\sum_{i=0}^{N_{CM_r}} s_i < N_R$ and to Ω_{R^c} otherwise. Let $T(e_{i_r1}, \Omega_k)$ be the first occurrence time of event e_{i_r1} given that system $\mathbb{X}_{CM}$ is initially in lumped state $\Omega_k \in \Omega_R$. Using the recursive formula (4.1), we have $F_{T(e_{i_r1},\Omega_j)}(m) = \tilde{M}_{N_{CM}}(\Omega_j, \Omega_{\tilde{N}_L-1}) + \sum_{\substack{k \\ \Omega_k \in \Omega_R}} \tilde{M}_{N_{CM}}(\Omega_j, \Omega_k) F_{T(e_{i_r1},\Omega_k)}(m-1)$. The cdf of $T(e_{i_r1})$ is approximated by

$$F_{T(e_{i_r1})}(m) \approx \sum_{\substack{j \\ \Omega_j \in \Omega_R}} \omega_j F_{T(e_{i_r1},\Omega_j)}(m), \quad m \geq 1 \tag{4.13}$$

where $\omega_j = \sum_{\substack{i \\ O(\Omega_i)=\Omega_j}} \pi_{E,i}$ is the initial probability distribution of states $\Omega_j \in \Omega_R$ and $O(\Omega_i)$ is a function that maps a lumped state from edge lumped markov chain to the corresponding one in the fully markov chain, note that $\omega_j = 0$ if $\nexists \Omega_i \in \mathbb{S}_E \; s.t. O(\Omega_i) = \Omega_j \; \forall \Omega_i \in \mathbb{S}_E$ and $\Omega_j \in \Omega_R$.

In order to calculate the probability distribution of node interarrival time to the overlapping region, the probability distribution of the state of the system when a node first enters the cluster needs to be calculated. Consider a cluster with $N_{CM_r} - 1$ nodes at time zero. When a node enters the cluster, system $\mathbb{X}_{CM}$ representing the N_{CM_r} CMs can only be in an edge lumped state $\Omega_i = \{s_0, s_1, \ldots, s_{N_{CM_r}}\}$ s.t. the first N_{CM_r} states construct a lumped state, $\Omega_k = \{s_0, s_1, \ldots, s_{N_{CM_r}-1}\}$, in a fully lumped Markov chain for system $\mathbb{X}_{CM}$, that satisfies *i)* $\Omega_k \in \Omega_R$ and *ii)* $\tilde{M}_{N_{CM}}(\Omega_k, \Omega_{\tilde{N}_L-1}) > 0$. That is, $\Omega_k \in \Omega_R$ is directly accessible from a lumped state in Ω_{R^c}. As a result, the node interarrival time to the

overlapping region from one cluster can be approximated by

$$F_{T(e_{Ii_r1})}(m) \approx \sum_{\substack{j \\ \Omega_j \in \Omega_R}} \omega_{I_j} F_{T(e_{i_r1},\Omega_j)}(m), \quad m \geq 1 \tag{4.14}$$

where $\omega_{I_j} = \frac{\sum_{\substack{i \\ O(\Omega_i)=\Omega_j}} \tilde{M}_{N_{CM}-1}(\Omega_i,\Omega_{\tilde{N}_L-1})\pi_{E,i}}{\sum_{\substack{j \\ \Omega_j \in \Omega_R}} \sum_{\substack{i \\ O(\Omega_i)=\Omega_j}} \tilde{M}_{N_{CM}-1}(\Omega_i,\Omega_{\tilde{N}_L-1})\pi_{E,i}}$ is the probability distribution of the initial state when a node just entered the cluster, and $\tilde{M}_{N_{CM}-1}$ is the probability transition matrix of the absorbing lumped Markov chain that represents system $\{X_0, X_1, \ldots, X_{N_{CM_r}-1}\}$. The cdf of the node interarrival time to the overlapping region is given by

$$F_{T_{Ii}}(m) = 1 - (1 - F_{T(e_{Ii_r1})}(m))^2. \tag{4.15}$$

When two clusters become disjoint, vehicles enter and leave the unclustered region. Let us consider the node interdeparture time from the unclustered region that causes the number of unclustered nodes to decrease, denoted by T_{Io}. Nodes can leave the unclustered region and enter either of the two clusters. It can be concluded that the time for a node to leave the unclustered region is equal to the minimum of two time intervals $T(e_{i_r1})$ and $T(e_{i_l2})$, as illustrated in Figure 4.6(b). Notice that the events that cause the node departure from the unclustered region during a non-overlapping period are the same as those causing the node arrival to the overlapping region during the overlapping period. Therefore, the distribution of T_{Io} can be calculated accordingly.

4.3.2 Steady-state distributions of the numbers of common CMs and unclustered nodes

In this section we investigate the limiting behavior of the external cluster stability. Considering clusters initially formed to be partially overlapping, we examine the external cluster stability under the assumption that cluster maintenance is not implemented. That is, we want to answer two questions: *After a long time, what is the probability that two neighboring clusters are overlapping (non-overlapping)? What is the probability distribution of the number of common CMs (unclustered nodes) in the overlapping (unclustered) region?*

The first question can be answered using the theory of alternating renewal process. The limiting overlapping and non-overlapping probability is given by $P_{ov} = \frac{E[T_{ov}]}{E[T_{ov}]+E[T_{nov}]}$ and

$P_{nov} = \frac{E[T_{nov}]}{E[T_{ov}]+E[T_{nov}]}$, respectively [70]. For the second question, we propose to model the problem as a storage buffer with a two-state random environment [73]. The buffer content represents the number of nodes in the overlapping/unclustered region between neighboring clusters. The two random states of the buffer are the overlapping and the non-overlapping states which fluctuate according to the alternating renewal process as described earlier. Let $N_i(\zeta_k)$ ($N_o(\theta_k)$) be the numbers of nodes entering (leaving) the buffer during the k^{th} overlapping period (non-overlapping period), respectively. Let $N_i(\Delta t)$ ($N_o(\Delta t)$) be the numbers of nodes entering (leaving) the overlapping (unclustered) region during an arbitrary time period, Δt, respectively. The numbers $N_i(\Delta t)$ and $N_o(\Delta t)$ are point processes corresponding to the i.i.d. interrenewal periods T_{Ii} and T_{Io}, and representing the input process (output process) of nodes to (from) the buffer, respectively. The mean and the variance of the input process during an overlapping period and the output process during a non-overlapping period are given by [70]

$$E[N_i(\zeta_k)] = \frac{E[T_{ov}]}{E[T_{Ii}]}, \quad Var[N_i(\zeta_k)] = \frac{c_{T_{Ii}}^2}{E[T_{Ii}]}E[T_{ov}], \tag{4.16}$$

$$E[N_o(\theta_k)] = \frac{E[T_{nov}]}{E[T_{Io}]}, \quad Var[N_o(\theta_k)] = \frac{c_{T_{Io}}^2}{E[T_{Io}]}E[T_{nov}], \tag{4.17}$$

respectively, where $c_{T_{Ii}}$ and $c_{T_{Io}}$ are the coefficients of variation of T_{Ii} and T_{Io}, respectively. Consider the k^{th} cycle. The buffer content at the beginning of the cycle is given by[6] $B_k = [B_{k-1} + N_i(\zeta_{k-1}) - N_o(\theta_{k-1})]^+$. Assuming that the processes $N_i(\zeta_{k-1})$ and $N_o(\theta_{k-1})$ are non-decreasing for all k, the buffer content model can be associated with a G/G/1 queue [73]. In the queueing model, the service time of customer $k-1$ is $S_{k-1} = N_i(\zeta_{k-1})$ and the interarrival time between customers $k-1$ and k is $A_{k-1} = N_o(\theta_{k-1})$. Then the buffer content at the beginning of the k^{th} cycle is the waiting time of the k^{th} customer. Therefore, the buffer content at an arbitrary time step, m, is equal to the virtual waiting time (or the workload) of this G/G/1 queue [73] [74]. The virtual waiting time depicts the remaining service time of all customers in the system at an arbitrary time step. Let $V(m)$ denote the virtual waiting time (buffer content) at an arbitrary time step m. The relation between the virtual waiting time at the m^{th} time step and the customer waiting time at the beginning of a cycle is given by [73]

$$V(m) = \left[B_{n(m)} + S_{n(m)} - m + \sum_{k=1}^{n(m)-1} A_k \right]^+ \tag{4.18}$$

[6] $y = [x]^+$ is equivalent to $y = \max(0, x)$

where $n(m) = \max\{k \geq 0 : \sum_{i=1}^{k} A_k \leq m\}, m \geq 0$.
To find the limiting probability distribution of the buffer content (i.e., the number of common/unclustered nodes between two neighboring clusters) a diffusion approximation is used. The diffusion approximation is a second order-approximation that uses the first two moments of the service and interarrival times of the G/G/1 queue [75]. Let $\rho = E[S_k]/E[A_k]$ be the intensity factor. A steady-state distribution of the buffer content exists if $\rho < 1$ and it is approximated by a geometric distribution with parameter equal to $\left(1 - \frac{\lambda_g^2}{\lambda_g^2 - 2\chi_g}\right)$. The approximated pmf is given by [75] [76]

$$P_V(n) \approx \left(1 - \frac{\lambda_g^2}{\lambda_g^2 - 2\chi_g}\right)\left(\frac{\lambda_g^2}{\lambda_g^2 - 2\chi_g}\right)^n, \quad n \geq 0 \tag{4.19}$$

where $\chi_g = \rho - 1$ and $\lambda_g^2 = \frac{E[S_k^2]}{E[A_k]}$ which can be calculated from (4.16) and (4.17). The limiting probability distribution of the numbers of common CMs and unclustered nodes between the two clusters can be described by the pmf (4.19) with probability P_{ov} and P_{nov}, respectively. Let P_{C0} and P_{U0} denote the limiting probabilities that there are zero common CMs and zero unclustered nodes between neighboring clusters, respectively. These probabilities are given by $P_{C0} = P_{ov}P_V(0) + P_{nov}$, and $P_{U0} = P_{nov}P_V(0) + P_{ov}$.

4.4 Results and Discussion

This section presents numerical results for the analysis of the proposed external and internal cluster stability metrics. The external cluster stability metrics are the time to the first change of cluster-overlap state, T_{ov1} and the time interval between successive changes of cluster-overlap state (cluster-overlapping period, T_{ov} and cluster-non-overlapping period, T_{nov}). The internal cluster stability metrics are the time to the first change of cluster-

Table 4.1: System parameters in simulation and analysis of Chapter 4

Traffic flow condition	**D(veh/km)**	$\mathbf{E[N_{CM_r}]}$	$\mathbf{E[N_c]}$
Uncongested	9	2	3
Near-capacity	26	4	5
Congested	42	6	8
R (meter)	$\mathbf{N_{max}}$	$\mathbb{X}_{\boldsymbol{c}}(\mathbf{0})$	$\mathbb{X}_{\boldsymbol{CM}}(\mathbf{0})$
160	9	{0,1,1,1,1,2}	{1,1,1,1,5}

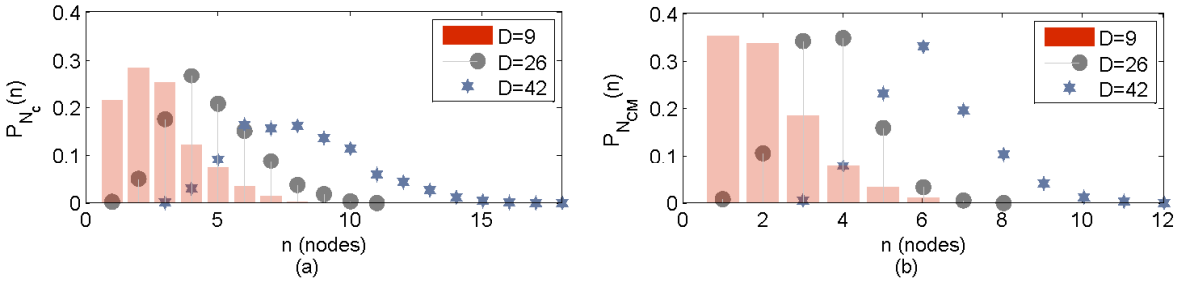

Figure 4.7: The pmfs of (a) the number of nodes between two neighboring CHs, N_c and (b) the number of nodes in a cluster N_{CM_r}, calculated from simulating a simple weighted clustering of vehicles.

membership, T_{CM1}, and the time between successive cluster-membership changes, T_{CM}. Additionally, numerical results are presented for pmfs of the steady-state numbers of common CMs and unclustered nodes between two neighbouring clusters. We consider a connected VANET in three traffic flow conditions, uncongested, near-capacity, and congested, each corresponding to a set of parameters listed in Table 4.1. For values of N_c and N_{CM_r} at the 0^{th} time step, we simulate a simple weighted clustering algorithm, where CHs are chosen with the minimum average relative speed to its one-hop neighbors, such that each vehicle belongs to a cluster and no two CHs are one-hop neighbors (i.e., similar to the use of mobility information for clustering in [12, 22]). The distance headways of vehicles on the highway follow a truncated exponential, gamma, and Gaussian distributions for the uncongested, near-capacity, and congested traffic flow conditions, respectively. The vehicles' speeds are i.i.d. and are normally distributed with mean 100 kilometer per hour and standard deviation of 10 kilometer per hour [1]. Figure 4.7 plots the probability distributions of N_c and N_{CM_r} for the resulting clusters from simulating the clustering algorithm. Initially, we set N_c to its average value from the cluster formation results. For $D = 42$ vehicles per kilometer (veh/km), we set I_c and I_{CM} to the states with highest probability of occurrence at the cluster formation stage. The Markov-chain distance headway model has the following parameters: $N_{\max} = 9$, each state covers 20 meters range of distance headways, the time step is equal to 2 seconds, and the transition probabilities are tuned according to the results in [51]. Based on these parameters, we generate time series of distance headway data according to the microscopic mobility model, using MATLAB. Each simulation consists of 20,000 iterations.

Figure 4.8 compares the distribution of the state of system $\mathbb{X}_c$, when the second overlapping state occurs, calculated using the exact derivation (4.4) and the proposed approx-

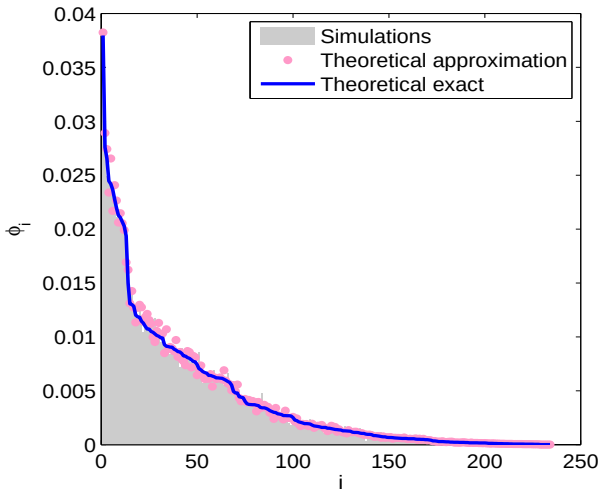

Figure 4.8: The pmf, $\phi_i = P(I_c \in \Omega_i)$, of system $\mathbb{X}_c$ being in lumped state $\Omega_i \in \Omega_{OV}$ at the instant when the second overlapping cluster state occurs.

imation (4.6). The values on the x-axis represent arbitrary IDs given to the lumped states $\Omega_i \in \Omega_{OV}$. The results from the proposed approximation shows close agreement with the exact and the simulation results.

Figure 4.9 plots the pmf of the time interval for the first change in cluster overlapping state, for (a) a given initial state of $\mathbb{X}_c$ and (b) when averaging over random initial states, respectively. The theoretical results for the pmfs of the cluster-overlapping period are calculated from the cdf in (4.5). The calculated pmf of T_{ov} in Figure 4.9(c) is based on the approximation given in Figure 4.8. The distribution of $T_{ov1}(\Omega_k)$ changes with I_c belonging to different lumped states Ω_k. The distribution of T_{ov1} describes the average time before the first cluster-overlap change for a randomly picked cluster in the network. When clusters overlap, the cluster-overlapping period is equal to the time period between two successive cluster-ovelap state changes (i.e., the time period of invariant cluster-overlap state). Note that the average time for the first change of cluster-overlap state is larger than the average time period between successive changes of cluster-overlap state. When the second overlapping state occurs between neighouring clusters, the clusters state is closer to non-overlapping than that when the clusters are initially formed, on average. That is, the clusters state can only be in the accessible lumped states (Ω_{OV1} in Figure 4.2).

Figure 4.10 plots the pmf of the time period from the cluster formation till the time step that a first change in cluster-membership occurs for (a) a given initial state $I_{CM} \in \Omega_k$

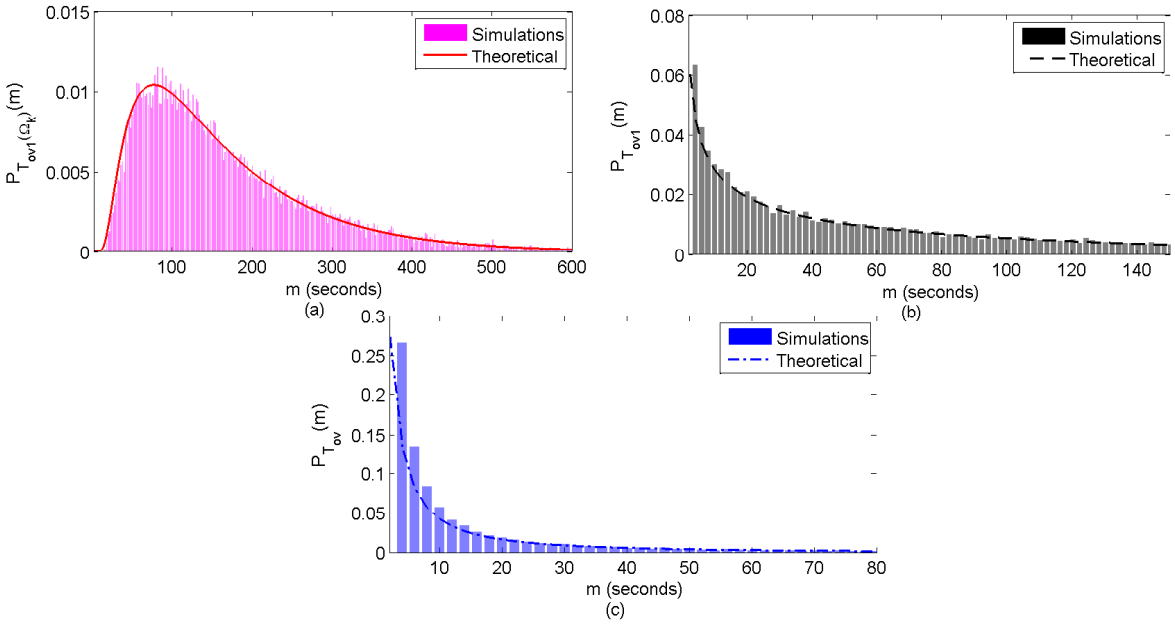

Figure 4.9: The pmfs of (a) the time to the first change in cluster-overlap state, $T_{ov1}(\Omega_k)$, for $I_c = \{0, 1, 1, 1, 1, 2\} \in \Omega_k$ when the clusters are initially formed; (b) the time to the first change in cluster-overlap state T_{ov1}; and (c) the cluster-overlapping time period, T_{ov}, when $D = 26$ veh/km.

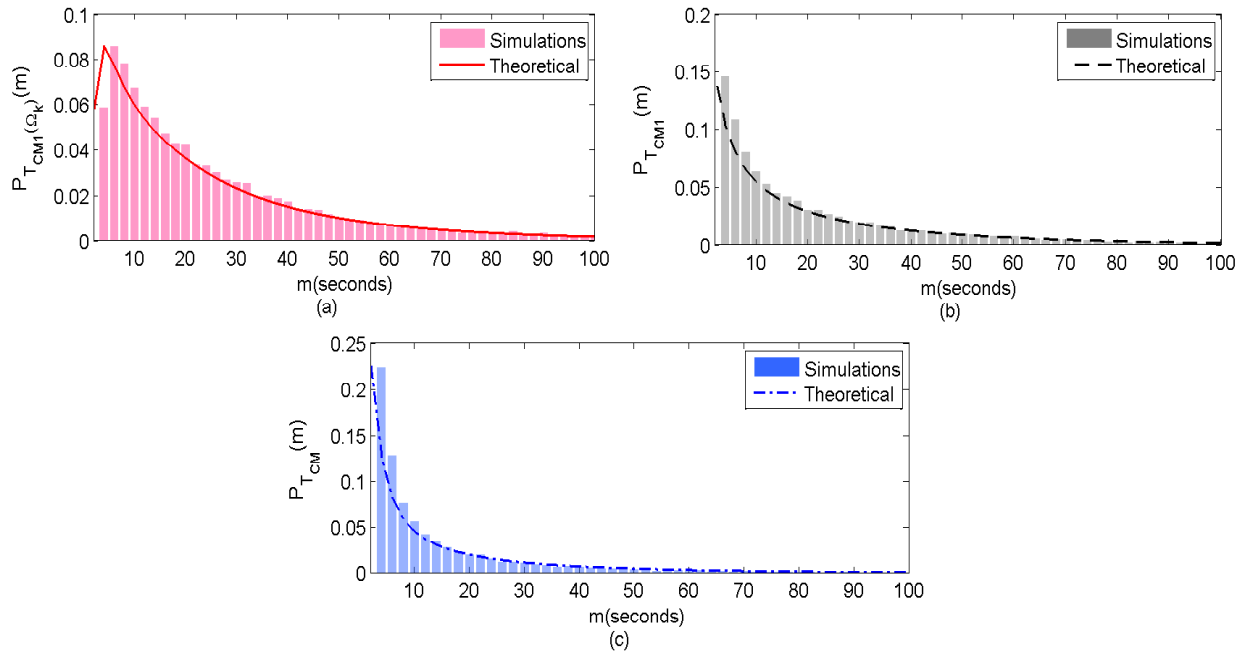

Figure 4.10: The pmfs of (a) the time to the first change in cluster-membership, $T_{CM1}(\Omega_k)$, for $I_{CM} = \{1, 1, 1, 1, 5\} \in \Omega_k$ when the cluster is initially formed; (b) the time to the first change in cluster-membership, T_{CM1}; and (c) the time period between two successive cluster-membership changes, T_{CM}, when $D = 26$ veh/km.

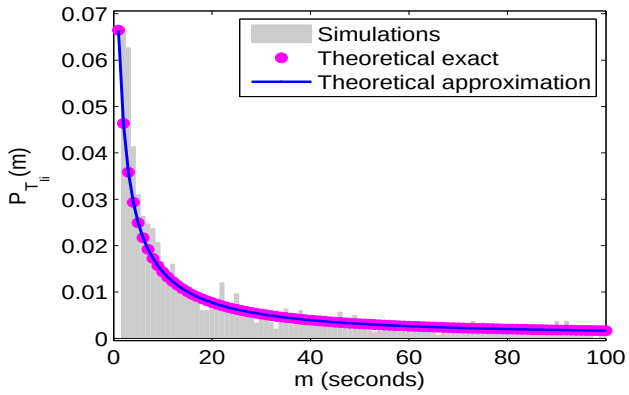

Figure 4.11: The pmf of the interarrival time of nodes to the overlapping region when $N_c = 5$ and $D = 26$ veh/km.

and (b) a random initial state, and (c) the pmf of the time period between successive cluster-membership changes. The theoretical results for the pmfs of $T_{CM1}(\Omega_k)$ and T_{CM1} are calculated from the cdfs in (4.10) and (4.11), respectively. The pmf of the time period between successive cluster-membership changes is calculated from the cdf in (4.12) and is plotted in Figure 4.10. The simulation results closely agree with the theoretical calculations. It is observed that, when the first change in cluster membership occurs after the cluster formation, the second change in cluster membership has a higher probability of occurring in a shorter time period. This reflects the effect of a wireless link between a CM and CH fluctuating between connecting and disconnecting states in a short period of time. The impact of this fluctuation can lead to frequent re-clustering that drains the precious VANET radio resources. Some clustering algorithms for VANETs aims to localize the impact of this fluctuation within the clusters [12, 15, 36][7]. Figure 4.11 plots the pmf of the first arrival time of nodes into the overlapping region $T_{e_{ir1}}$, for a near-capacity traffic flow condition. The exact theoretical value is calculated from the edge Markov chain as explained in Appendix A.4, whereas the approximated value is calculated from the fully lumped Markov chain using (4.13). The results show that approximating the node-arrival time to the overlapping/unclustered region using the fully lumped Markov chain is adequate.

Figure 4.12 and (Figure B.2 in the Appendix) plot the pmfs of the cluster-overlapping, T_{ov}, and the cluster-non-overlapping, T_{nov}, time periods for different vehicle densities when N_c is set to the average values in Table 4.1. The time interval between successive changes of

[7]Figure B.1, in Appendix B, plots the pmfs of the time interval between two successive cluster-membership changes for different vehicle densities.

cluster-overlap state is equal to T_{ov} (T_{nov}) when the two clusters are overlapping (disjoint). Notice that the vehicle density has little impact on the distribution of the overlapping/non-overlapping periods when N_c is set to the average value. However, this is not true for all N_c. Figure 4.13 plots the average cluster-overlapping and the average cluster-non-overlapping time periods for different numbers of nodes between neighbouring clusters, N_c. The average values are calculated using (4.8) and the values of N_c are from the clustering results in Figure 4.7. For a fixed N_c, the average cluster-overlapping period is larger for a larger density, whereas the average cluster-non-overlapping period is smaller for a larger density. The reason is that, in a congested traffic flow conditions, the distance headways are small when compared to those in an uncongested traffic flow condition. Therefore, for the same N_c, the cumulative distances are smaller for a high density. It should be noted that the large values of average cluster-overlapping time periods for $N_c = 1$ are due to the connected network assumption. Figure 4.13 shows that, as N_c increases, the average cluster-overlapping period reduces and the average cluster-non-overlapping period increases for the same traffic flow condition.

To investigate the limiting behavior of the number of vehicles in the overlapping/unclustered region, we first calculate the two parameters χ_g and λ_g^2 for the three vehicle densities. Notice that the distributions (4.5), (4.7), and (4.15) are all conditional on the initial cluster state in terms of N_c and N_{CM_r}. Therefore, in the calculation of χ_g and λ_g^2, we use the law of total expectation to calculate $E[T_{ov}] = \sum_n P_{N_c}(n)E[T_{ov}(n)]$ and $E[T_{Ii}^2] = \sum_n P_{N_c}(n)E[T_{Ii}^2(n)]$, where $T_{ov}(n)$ is the cluster-overlapping time period for two clusters separated by $N_c = n$ nodes and $T_{Ii}(n)$ is the node interarrival time for a cluster with $N_{CM_r} = n$ nodes, respectively. The calculations are done for near-capacity and congested traffic flow conditions only. The reason is that the diffusion approximation assumes that the point processes $N_i(\zeta_k)$ and $N_o(\theta_k)$ are normally distributed according to the central limit theorem. This assumption is not satisfied for an uncongested traffic flow, due to a relatively small number of vehicles between two clusters as shown in Figure 4.7. The intensity factor is found to be $\rho = 1.0143$ and 1.3172 for $D = 26$ and 42 veh/km, respectively. As a result, the steady-state distribution does not exist. However, consider only $N_c \geq E[N_c]$ for both cases, we find that $\rho = 0.33$, and 0.64 for $D = 26$, and 42 veh/km, respectively. Figure 4.14 plots the steady-state probability distributions for the non-zero number of vehicles in the overlapping/unclustered region when $N_c \geq E[N_c]$ for near-capacity and congested traffic flow conditions. The theoretical results are normalized to the value $1 - P_V(0)$, since the probability distributions in Figure 4.14 represent the non-zero number of common CMs with probability P_{ov} and the non-zero number of unclustered nodes with probability P_{nov}. The simulation results closely agree with the theoretical calculations. However, there exist slight differences between simulation and theoretical results especially at the

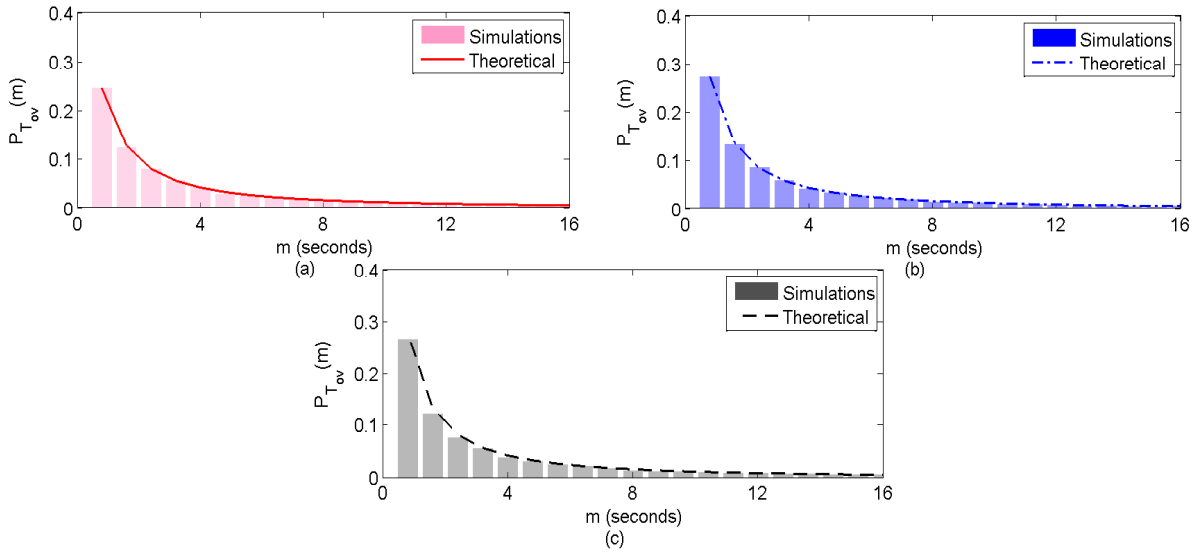

Figure 4.12: The pmf of cluster-overlapping time period with vehicle density of (a) $D = 9$, (b) $D = 26$, and (c) $D = 42$ veh/km.

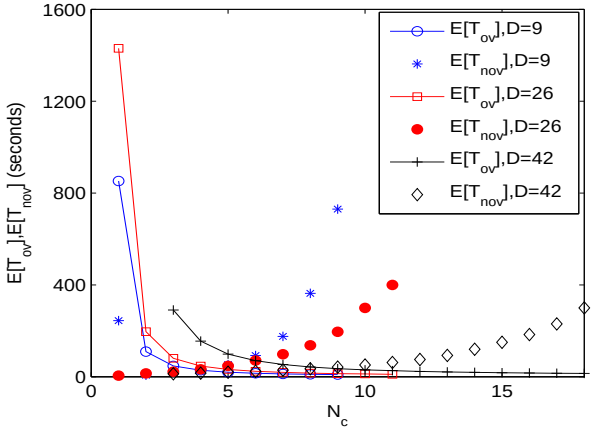

Figure 4.13: Average cluster-overlapping and cluster-non-overlapping time periods for different N_c values with vehicle density $D = 9, 26,$ and 42 veh/km. The values of N_c are those in Figure 4.7.

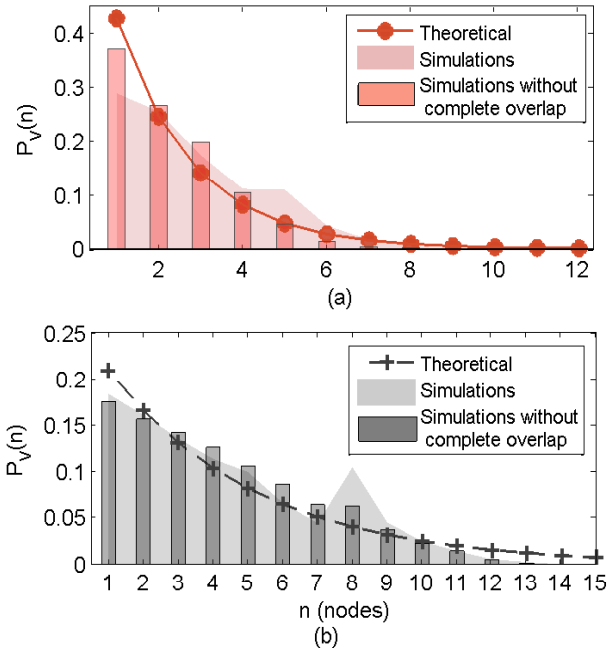

Figure 4.14: The steady-state pmfs of buffer content, i.e., the number of non-zero nodes in the overlapping/non-overlapping period, for (a) $D = 26$ and (b) $D = 42$ veh/km.

values of $n = 5$ and $n = 8$, for $D = 26$ and 42 veh/km, respectively. This is mainly due to complete overlapping between neighboring clusters. When two clusters completely overlap, i.e., become one hop neighbors, all the nodes between them become common nodes, however no additional nodes can enter the overlapping region. This is not accounted for in our model. According to many clustering algorithms, when two CHs become one hop neighbors, they merge into a single cluster [12, 15, 23]. Figure 4.14 shows that the simulation results excluding the complete cluster overlapping data are in closer agreement with the theoretical results in comparison with simulation results that include the complete cluster overlapping data. Additionally, the numerical and simulation results for the limiting probabilities of having zero common CMs and zero unclustered nodes are given in Table 4.2.

Table 4.2: Limiting probabilities of zero common CMs/unclustered nodes

	D(veh/km)	**Simulation**	**Theoretical**
P_{C0}	26	0.86	0.78
P_{C0}	42	0.69	0.67
P_{U0}	26	0.57	0.47
P_{U0}	42	0.52	0.56

4.5 Summary

This chapter presents a stochastic analysis of single-hop cluster stability in a highway VANET with focus on a single lane. The time periods of invariant cluster-overlap state and cluster-membership are proposed as measures of external and internal cluster stability, respectively. A stochastic mobility model that describes the time variations of individual distance headways is adopted in the analysis. The system of distance headways that govern the changes in the overlap state and the cluster membership is modeled by a discrete-time lumped Markov chain. The first passage time analysis is employed to derive the distributions of the proposed cluster stability metrics. The analysis provides insights about the time periods during which a cluster is likely to remain unchanged in terms of its cluster-membership and its overlap state with neighboring clusters. Additionally, the limiting probability distributions of the numbers of common and unclustered nodes between neighboring clusters are approximated using queuing theory and diffusion approximation. The probability distributions derived for the proposed cluster stability metrics can be utilized in the development of efficient clustering algorithms for VANETs.

Chapter 5

Cluster-based routing overhead

Node clustering is an approach to improve the scalability of routing protocols in VANETs as discussed in Section 1.5. Cluster-based routing protocols proposed in the literature aim to minimize the routing overhead and scale to an increased node density. In the first part of this chapter we analyze the impact of steady-state cluster characteristics in terms of the cluster size and the cluster-overlap on the routing overhead. Mesoscopic vehicle mobility models are adopted to analyze the overhead for four generic cluster-based routing protocols, each using either proactive and reactive routing strategies for inter- or intra- cluster routing protocols. Additionally, we calculate the steady-state cluster characteristics that minimize the average routing overhead.

The second part of this chapter presents analysis of the impact of cluster instability on control signalling overhead for one of the four generic routing protocols. We assume that the clusters are formed with cluster characteristics that minimize the average routing overhead for the considered generic routing protocol. The cluster stability model presented in Chapter 4 is used to capture the time variations of the cluster structure in terms of the rates of change in cluster membership and the cluster-overlap state. The probability distribution of the intracluster routing overhead is derived using the cluster membership change rate. Furthermore, the intercluster routing overhead is modeled as a rooted tree with the tree-nodes representing the value of the overhead and the tree-edges weighted by the probability of cluster-overlap state changes. Numerical results are presented to evaluate the proposed models, which demonstrate a close agreement between analytical and simulation results.

5.1 Steady-state cluster characteristics for generic routing

In this section, we analyze the impact of the cluster characteristics (K and l_o) and the corresponding cluster parameters ($L_c, L_o, N_{CM},$ and N_{CCM}) on the performance of generic routing protocols on a stationary network scenario. To capture the effect of cluster characteristics on the network protocol performance, we use mesoscopic vehicle mobility models.

Consider the system model described in Chapter 2. Every node generates information packets with a constant rate of ω packets per second (pkt/s) and the destination is equally likely to be any other node in the network. We consider both generic proactive and reactive routing strategies for inter- and intra- cluster routing protocols. For example, a protocol that uses reactive intercluster routing and proactive intracluster routing is referred to as a reactive-proactive cluster-based routing protocol. As a result, we have four generic cluster-based routing protocols, *i.e.,* proactive-proactive (pp), reactive-reactive (rr), proactive-reactive (pr), and reactive-proactive (rp). When generic proactive routing is used in a flat network, every node has complete information of the network topology. This is achieved by flooding local node information with every other node in the network and maintaining the topology information by frequent updates. The nodes send out topology updates at a fixed rate to account for location changes. In generic flat reactive routing, a source node initiates a route discovery process in which a route request packet is flooded throughout the network. Let $\psi_{f,n}$ denote the flooding overhead in terms of the number of packets needed to flood a packet to $n-1$ nodes, $n = 2, 3, \ldots, N_{HWY} - 1$. When a node floods a packet to the other $N_{HWY} - 1$ nodes, every receiving node regenerates and rebroadcasts the same message until all the $N_{HWY} - 1$ nodes receive it with a flooding overhead of $\psi_{f,N_{HWY}} = N_{HWY}$ packets.

5.1.1 Routing overhead components

We calculate the total routing overhead in terms of the number of exchanged packets per second that are necessary for the operation of the generic routing protocols. Note that a regenerated packet by an intermediate node contributes to the routing overhead. We divide the total routing overhead into the following three terms: *i)* the clustering overhead ψ_c, which represents the message signaling required to maintain the clusters while the routing protocol is in operation; *ii)* the intracluster routing overhead ψ_{Intra} corresponding to the portion of routing overhead needed within the cluster; and *iii)* the intercluster routing overhead ψ_{Inter}, which counts for the messaging needed between clusters. The

total routing overhead has the three main components and is given by

$$\psi_T = \psi_c + \psi_{Intra} + \psi_{Inter}. \tag{5.1}$$

Given a set of clusters, each CH will send a hello packet (CH-Hello) to all its CMs at the beginning of the cluster maintenance cycle. Upon receiving a CH-Hello packet, each CM replies with a CM-Hello packet. A CH-Hello/CM-Hello packet contains information about node's ID, position, speed, acceleration, and direction of movement. The exchange of hello packets between CH and its CMs and visa versa allows every CM to know its CH and every CH to know its CMs. No additional exchange of hello packets is required since all the nodes will know their single-hop neighbors from the cluster maintenance messaging. We use the same general computation for cluster maintenance overhead as in [6], where a CH floods a CH-Hello packet within its cluster with an overhead of $\psi_{f,N_{CM}}$, and every CM that is i ($\leq K$) hops away from the CH requires i packets to deliver its CM-Hello reply packet to its CH. Therefore the cluster maintenance overhead is given by

$$\psi_c = \delta_c(\Sigma_{i=1}^{K} N_i i + o_p N_{CM}) N_{CH}. \tag{5.2}$$

where δ_c is the rate of CH-Hello packets per CH (in pkt/s), N_i is the number of nodes that are i ($\leq K$) hops away from the CH, and $o_p \in (0, 1]$ is a protocol specific optimizing factor. A unity o_p corresponds to the simple flooding overhead, $o_p < 1$ reduces the overhead by a factor of o_p from that of the flooding overhead. The overhead calculations for ψ_{Intra} depend on the type of intracluster routing protocol used.

When a proactive intracluster routing is used, at the beginning of the topology update cycle, every CM shares its local topology information with every other CM in the same cluster, which requires $\psi_{f,N_{CM}}$ packets. With this exchange, every CM has the route information to every destination in the cluster. Each cluster contributes N_{CM}^2 packets per update cycle to the total overhead. Thus, the proactive intracluster routing overhead is given by

$$\psi_{Intra_p} = o_p \delta_{Intra} N_{CM}^2 N_{CH} \tag{5.3}$$

where δ_{Intra} is the intracluster topology update rate per node (in pkt/s). When a reactive protocol is used for intracluster routing, topology control messages need not be exchanged. However, when a source needs to transmit a packet to a certain destination, a route discovery process is triggered. If the source and destination are in the same cluster, which occurs with a probability $P_{Intra} = N_{CM}/N_{HWY}$, a route request packet is flooded throughout the cluster only, which requires $\psi_{f,N_{CM}}$ packets. Since there are ωN_{HWY} data packets to be

transmitted per second, the reactive intracluster routing overhead is

$$\psi_{Intra_r} = o_p \omega N_{HWY} P_{Intra} N_{CM}. \tag{5.4}$$

After the route is discovered, the information is unicasted to the source and flooding is not required. The number of route reply packets is usually much less than the number of packets required in the route discovery process and hence is not considered at this stage.

As for ψ_{Inter}, when proactive intercluster routing is used, each CH broadcasts local cluster topology information to other CHs. Let Φ_{CH} denote the number of packets needed to broadcast a CH packet to a neighboring CH. When the network is split into non-overlapping clusters, $\Phi_{CH} = 2k + 1$ packets are required to broadcast a packet from a CH to a neighboring CH. Note that a packet is required to cross the border of the cluster to the neighboring cluster. With the exchange of local cluster topology information among the CHs, the cluster-level route information is available at every CH (i.e., the sequence of clusters from the source to the destination). Hence, the proactive intercluster routing overhead is given by

$$\psi_{Inter_p} = o_p \delta_{Inter} \Phi_{CH} N_{CH}^2 \tag{5.5}$$

where δ_{Inter} is the rate at which the CH exchanges local cluster topology information. When reactive intercluster routing is used, only if the source and destination are in different clusters, which occurs with probability $P_{Inter} = 1 - P_{Intra}$, a route request packet is broadcasted on a cluster level, requiring $\Phi_{CH} N_{CH}$ packets. Thus the intercluster reactive routing overhead is given by

$$\psi_{Inter_r} = o_p \omega N_{HWY} P_{Inter} \Phi_{CH} N_{CH}. \tag{5.6}$$

Routing overhead with overlapping clusters

Consider two adjacent clusters that share a single node; in this case, $2k$ packets are required to broadcast a packet from a CH to a neighboring CH. In general, increasing the overlapping between clusters (in terms of hop number, distance (L_o) or node number (N_{CCM})) reduces the signalling between neighboring clusters. Let ξ be the overlapping gain, which is the decrease in the number of packets needed to broadcast a packet from a CH to a neighboring CH due to overlapping from that of the disjoint case. However, the increased overlapping not only increases the overall number of clusters, but also increases the intracluster messaging, since the common nodes in the overlapping region, N_{CCM}, should report back to both CHs. The number of clusters, N_{CH}, increases by a factor of $(1 - l_o)^{-1}$ from that in the disjoint case. Therefore, $N_{CH} = \frac{L}{(1-l_o)L_c}$. The only overhead component that

changes with the overlapping is the cluster level broadcast overhead, ψ_{CH}. Other components are affected by the increase of N_{CH} only. With the increase of the l_o, Φ_{CH} decreases according to the overlapping gain, ξ, which depends on the number of overlapping hops between clusters. The maximum allowed overlapping length between neighboring clusters is when neighboring CHs are K hops away from each other i.e., $L_o = {}^{L_c}/_2$ or $l_o = 0.5$. Hence, Φ_{CH} can be generalized to

$$\Phi_{CH} = 2k + 1 - \xi. \tag{5.7}$$

5.1.2 Total cluster-based routing overhead

Let $\psi_{pp}, \psi_{rr}, \psi_{pr}$, and ψ_{rp} denote the total routing overhead for proactive-proactive, reactive-reactive, proactive-reactive, and reactive-proactive cluster-based routing protocols, respectively. The total routing overhead for each of the four routing strategies can be calculated by summing ψ_c and the corresponding intra- and inter- cluster routing overhead components. In order to calculate the average total routing overhead, we derive the probability distributions of the cluster parameters L_c and N_{CM} in the next section. The remaining cluster parameters are functions of these two. The distributions are mapped from the distance headway distributions, i.e, the mesoscopic vehicle mobility models.

As defined in the system model (Section 2.1), the cluster length, L_c, extends to K hops on both sides of the cluster. Therefore, the probability distributions of the hops lengths are needed to derive the distribution of L_c. The length of the second hop H_2 is with respect to the node at the first hop edge (as shown in Figure 5.1), and so on. There exists an empty gap after the i^{th} hop with a length $G_i = R - H_i$, where H_i denotes the length of the i^{th} hop, $i \geq 1$. Given a mesoscopic model, the distance headways of vehicles are i.i.d. with pdf $f_X(x)$ and cdf $F_X(x)$. As discussed in Section 3.2, the pdf of H_1 is given by (3.4) and (3.5) for low and intermediate vehicle densities, respectively. The pdf of the length of the first gap, G_1, is given by $f_{G_1}(g_1) = |\frac{d}{dg_1}(R - g_1)| f_{H_1}(R - g_1) = f_{H_1}(R - g_1)$. The length of the second hop is dependent on the first gap since $(H_2 \geqslant G_1)$. Similar to the derivation of the first hop, the conditional cdf of the second hop length is equal to the probability that the length of the second hop is less than a value h_2, given that there exists at least one node in the first hop h_1. This can be generalized to the length of the i^{th} hop, $i > 1$ with the following conditional cdf

$$F_{H_i|G_{i-1}}(h_i|g_{i-1}) = \frac{P(C^c(R - h_i), C(h_i - g_{i-1}))}{P(C(R - g_{i-1}))}. \tag{5.8}$$

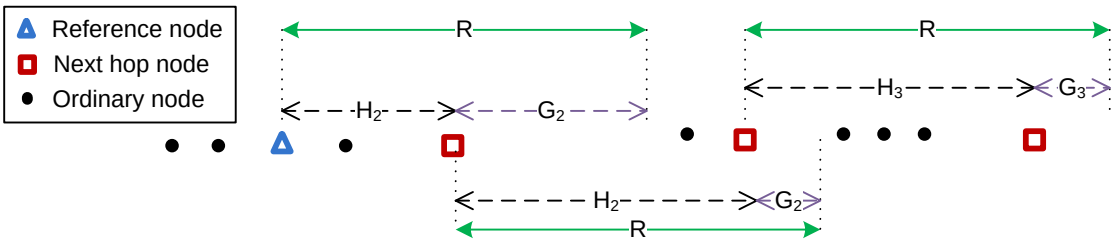

Figure 5.1: Illustration of the mapping of distance headways to three consecutive hops from a reference node, where H_i and G_i, $i = 1, 2, 3$ are the i^{th} hop and the i^{th} gap, respectively.

The conditional pdfs for the i^{th} hop (where $i > 1$) are given by [65]

$$f_{H_i|G_{i-1}}(h_1|g_{i-1}) = \frac{De^{-D(R-h_i)}}{1-e^{-D(R-g_{i-1})}}, \quad 0 < g_{i-1} < h_i \tag{5.9}$$

and

$$\begin{aligned} f_{H_i|G_{i-1}}(h_1|g_{i-1}) &= \frac{1}{\gamma(z, \lambda(R-g_{i-1}-\alpha))}[f_X(R-h_i)\gamma(z, \lambda(h_i-g_{i-1}-\alpha) \\ &\quad + f_X(h_i-g_{i-1})\Gamma(z, \lambda(R-h_i-\alpha))], \quad g_{i-1} \leq h_i \leq R-\alpha \end{aligned} \tag{5.10}$$

for low and intermediate vehicle densities, respectively. It can be shown, that the difference between the pdfs of successive hop lengths reduce as the number of hops increase. The reason is that the effect of the pdf of H_1 vanishes as we calculate the pdf of the length of further hops. However, when the product RD is large enough, the difference between the pdfs reduces. When $RD \to \infty$, $f_{H_i}(h_i) \to f_{H_1}(h_i)$ from (3.4) and (5.9) for low vehicle density and from (3.5) and (5.10) for intermediate vehicle density. Therefore, for large RD, the gap lengths are i.i.d. with pdfs that are approximated by (2.1) and (2.3) for low and intermediate vehicle densities, respectively.

The cluster length is upper bounded by $2kR$ since the length of the hop is upper bounded by R. The reference node for the first hop length H_1 is the CH. Consequently, the reference node for the second hop H_2 is the CM at the first hop edge (node A in Figure 5.2), and so on. The cluster length can be calculated by $L_c = 2\sum_{i=1}^{k} H_i + 2G_K$, where H_i is the length of the i^{th} from the CH, with conditional pdfs (5.9) and (5.10) for low and intermediate traffic densities, respectively. The K^{th} gap length, G_K, is included in the cluster length because the range of the K^{th} hop in the cluster extends to R. This is added

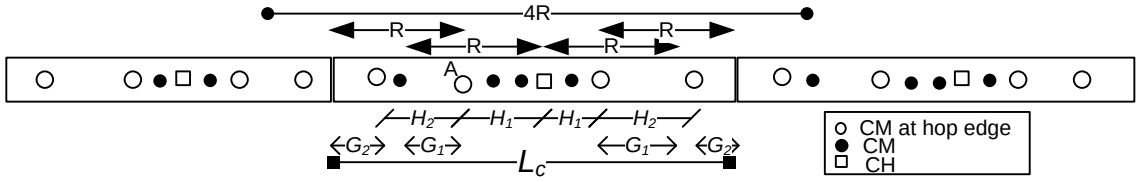

Figure 5.2: Three 2-hop disjoint clusters, each with a length of L_c which is upper bounded by $4R$.

to control the overlapping between clusters. Since $G_i = R - H_i$, L_c can be re-written as

$$L_c = 2kR - 2\sum_{i=1}^{K-1} G_i. \tag{5.11}$$

For a K-hop cluster, the distribution of the cluster length, L_c, depends on the distribution of the sum of $K-1$ gaps, $K > 1$. The length of a single hop cluster is fixed, i.e., $L_c = 2R$. For a low traffic density, we assume that DR is large enough such that the gaps lengths are i.i.d. with the pdf (2.1). Given that G_i's are i.i.d. and $G_i \sim Exp(D)$, the sum $\sum_{i=1}^{K-1} G_i$ is a random variable with an Erlang distribution, having shape and scale parameters equal to $K-1$ and D, respectively, denoted by $\sum_{i=1}^{K-1} G_i \sim Erlang(K-1, D)$. From (5.11), the pdf of the length of the cluster is given by $f_{L_c}(l) = \frac{1}{2} f_{\Sigma G_i}\left(\frac{2kR-l}{2}\right)$. Therefore, for a K-hop cluster, $K > 1$, and a low vehicle density the pdf of L_c is given by

$$f_{L_c}(l) = \frac{\lambda_l^{z_l}}{\epsilon(z_l-1)!}(\alpha_l - l)^{z_l-1} e^{-\lambda_l(\alpha_l - l)}, \quad 2R < l \leq \alpha_l \tag{5.12}$$

where $\lambda_l = \frac{D}{2}$, $z_l = K-1$, and $\alpha_l = 2kR$ are the scale, shape and location parameters of the L_c distribution, respectively, and $\epsilon = P(\sum_{i=1}^{K-1} G_i \leq (K-1)R)$ is a constant due to truncation. On the other hand, for an intermediate vehicle density, we assume that λR is large such that the gap lengths are i.i.d. with pdf (2.3). Using Laplace transform, the moment generation functions of the gap length and the sum of $K-1$ gap lengths are given by $M_{G_i}(s) = e^{-\alpha s}(1 + s/\lambda)^{-z}$ and $M_{\sum_i^{K-1} G_i}(s) = e^{-(K-1)\alpha}(1 + s/\lambda)^{-(K-1)z}$, respectively. The pdf of $\sum_i^{K-1} G_i$ is the inverse Laplace transform of $M_{\sum_i^{K-1} G_i}(s)$, and is given by $f_{\sum_{i=1}^{K-1} G_i}(l) = \frac{\lambda^{(K-1)z}}{\Gamma((K-1)z)}(l-(K-1)\alpha)^{(K-1)z-1} e^{-\lambda(l-(K-1)\alpha)}$, $(K-1)\alpha \leq l \leq \infty$. That is, the sum of $K-1$ Pearson type III (λ, z_i, α_i) distributed random variables is a random variable with a Pearson type III distribution and parameters $(\lambda, \sum_i^{K-1}(z_i), \sum_i^{K-1}(\alpha_i))$. As a result,

for an intermediate vehicle density the pdf of L_c for a K-hop cluster, $K > 1$, is given by

$$f_{L_c}(l) = \frac{\lambda_l^{z_l}}{\Gamma(z_l)}(\alpha_l - l)^{z_l - 1} e^{-\lambda_l(\alpha_l - l)}, \quad 2R + 2(K-1)\alpha < l \leq \alpha_l \tag{5.13}$$

where $\lambda_l = \frac{\lambda}{2}, z_l = (K-1)z$ and $\alpha_l = 2kR - 2\alpha(K-1)$ are the scale, shape, and location parameters for the distribution of L_c, respectively, and $\epsilon = P(\sum_{i=1}^{K-1} G_i \leq (K-1)(R-\alpha))$ is a constant due to truncation. According to our definition of the overlapping gain, ξ, in Section 5.1.1, ξ can be calculated by

$$\xi = \begin{cases} 0, & L_o < G_K \\ 1, & G_K \leq L_o < G_K + H_K \\ j+1, & G_K + \sum_{i=1}^{j} H_{K-i} \leq L_o < G_K + \sum_{i=1}^{j+1} H_{K-i} \\ K+1, & L_o = L_c/2. \end{cases} \tag{5.14}$$

The value of ξ can be seen as the integer component of the number of cluster hops covered by L_o. The discrete nature of the overlapping gain is due to the mapping between the number of hops and the overlapping length. The number of nodes in a cluster, N_{CM}, depends primarily on the inter-vehicle distances and the length of the cluster. Given the length of the cluster, the distribution of N_{CM} can be found by deriving the count distribution that corresponds to the inter-vehicle distance distribution. For a low vehicle density, the inter-vehicle distances are exponentially distributed ($\sim Exp\,(1/D)$); hence, the corresponding count distribution is Poisson ($\sim Pois(D)$). For a low vehicle density, the probability mass function (pmf) of the number of CM in a cluster of L_c is given by

$$P_{N_{CM}|L_c}(n|l) = \frac{(Dl)^n}{n!} e^{-Dl}. \tag{5.15}$$

For an intermediate vehicle density, the corresponding pmf is obtained using renewal theory. Let $\nu_n = \sum_{i=1}^{K-1} X_i$ be the sum of n consecutive inter-vehicle distances. The variable ν_n has a Pearson type III distribution ($\nu_n \sim Pears(\lambda, nz, n\alpha)$). Since the inter-vehicle distances are i.i.d., we have a renewal process. Let N_l be the number of nodes in a road segment of length l. For a renewal process, the events $N_l \leq n$ and $\nu_n > l$ are equivalent, therefore, $P(N_l \leq n) = P(\nu_n > l)$. Hence, the fundamental relation between the inter-distance distribution and the corresponding count distribution is given by $P(N_l = n) = F_{\nu_n}(l) - F_{\nu_{n+1}}(l)$ [70]. Given the cdf of $\nu_n \sim Pears(\lambda, nz, n\alpha)$ and cdf of $\nu_{n+1} \sim$

$Pears(\lambda,(n+1)z,(n+1)\alpha)$, the corresponding count distribution is given by

$$P(N_l=n)=\frac{\gamma(nz,\lambda(l-n\alpha))}{\Gamma(nz)}-\frac{\gamma((n+1)z,\lambda(l-(n+1)\alpha))}{\Gamma((n+1)z)}. \tag{5.16}$$

For a recurrent renewal process, the asymptotic distribution of the number of renewals in l, can be approximated by a normal distribution $N_l \sim Norm(\frac{l}{\mu},\frac{l\sigma^2}{\mu^3})$ [70]. Hence, given a cluster length $L_c=l$, the approximated pmf is given by

$$P_{N_{CM}|L_c}(n|l)=\frac{\mu}{\sigma}\sqrt{\frac{\mu}{2\pi}}e^{\frac{\mu(n\mu-l)^2}{2\sigma^2 l}}. \tag{5.17}$$

Using the derived distributions for N_{CM} and L_c, we calculate the average and the variance of the cluster-based routing overhead as discussed in the next Section.

5.1.3 Average cluster-based routing overhead

In this Section, we will find the average and variance of the cluster-based routing overhead for the four generic routing protocols. To calculate the average overhead, the distributions found in Subsection 5.1.2 are used to derive the statistical average for the overhead expressions (5.2)-(5.6). In our calculation of the averages and without loss of generality, we assume the following: *i)* N_{HWY} is independent of N_{CH} and N_{CM}; *ii)* N_i' s are i.i.d. and are independent of N_{HWY}, N_{CM} and N_{CH}; *iii)* the cluster design parameters, K and l_o, are constant; and *iv)* ξ is calculated using (5.14) average values. Hence, the average overhead for the generic protocols can be calculated by

$$E[\psi_c]=\delta_c\left(E\left[N_{CH}\sum_{i=1}^{K}iN_i\right]+o_pE[N_{CM}N_{CH}]\right) \tag{5.18}$$

$$E[\psi_{pp}]=E[\psi_c]+o_p\delta_{Intra}E\left[(N_{CM}-N_{CCM})^2N_{CH}\right]+o_p\delta_{Inter}\Phi_{CH}E\left[N_{CH}^2\right] \tag{5.19}$$

$$E[\psi_{rr}]=E[\psi_c]+o_p\omega E\left[N_{CM}^2\right]+o_p\omega\Phi_{CH}(E[N_{HWY}]E[N_{CH}]-E[N_{CH}N_{CM}]) \tag{5.20}$$

$$E[\psi_{pr}]=E[\psi_c]+o_p\omega E\left[N_{CM}^2\right]+o_p\delta_{Inter}\Phi_{CH}E\left[N_{CH}^2\right] \tag{5.21}$$

$$\begin{aligned}E[\psi_{rp}]=&E[\psi_c]+o_p\delta_{Intra}E\left[(N_{CM}-N_{CCM})^2N_{CH}\right]\\&+o_p\omega\Phi_{CH}\left(E[N_{HWY}]E[N_{CH}]-E[N_{CM}N_{CH}]\right).\end{aligned} \tag{5.22}$$

We assume that the routing protocol will eliminate the redundancy in relaying topology updates for the $N_{CCM}=l_oN_{CM}$ nodes in (5.19) and (5.22). We evaluate the average terms in the previous equations based on probability theory. For example,$E\left[N_{CM}N_{CH}\right]=$

$E\left[N_{CH}E\left[N_{CM}|L_c\right]\right] = \int_l \frac{L}{L_c(1-l_o)}\frac{l}{\mu}f_{L_c}(l)dl = \frac{L}{(1-l_o)\mu}$. Similarly $E\left[N_{CM}^2 N_{CH}\right] = E\left[N_{CH}E\left[N_{CM}^2|L_c\right]\right] = \frac{L}{\mu^2(1-l_o)}\left[\frac{\sigma^2}{\mu} + E(L_c)\right]$, for an intermediate vehicle density. In the same fashion, we can calculate the remaining averages of the product terms. Additionally, $E[N_{CM}^2] = \frac{\sigma^2}{\mu^3}E[L_c] + \frac{1}{\mu^2}\left(E(L_c^2)\right)$, $E[N_{CH}] = \frac{L}{1-l_o}E[L_c^{-1}]$, $E[N_{CH}^2] = \left(\frac{L}{1-l_o}\right)^2 E[L_c^{-2}]$.

From (5.19)-(5.22), we notice that increasing the cluster size K increases the intracluster routing overhead due to the increased number of nodes belonging to each cluster, from (5.3) and (5.4). On the other hand, increasing K reduces the average number of clusters N_{CH} and hence decreases the inter-cluster routing overhead according to (5.5) and (5.6). Increasing/decreasing the overlapping between neighboring clusters increases/decreases both ξ and N_{CH}, which have an opposite impact on the routing overhead, based on (5.7). Hence, the cluster characteristics that minimize the total routing overhead for the different generic cluster-based routing protocols should be further studied.

5.1.4 Numerical results

This section presents numerical results that show the impact of the cluster size and the cluster overlapping on the total routing overhead. We consider a single lane highway segment of length $L = 20km$ and a transmission range of $R = 250m$. The minimum distance headway for intermediate vehicle density is chosen to be $\alpha = 10m$. Without loss of generality, we fix the topology update rate to the value proposed in [77]: $\delta_{Inter} = \delta_{Intra} = 0.2$pkt/s. Since we focus on generic routing protocols, o_p is set to unity. We also fix the information packet generation rate and the cluster maintenance update rate at the same value as δ_{Inter} and δ_{Intra}, since our aim is to study the impact of clustering on the performance of the protocols for steady state conditions.

Figure 5.3 (a) and (b) plot the average total routing overhead, normalized to the average node number, versus the cluster size K for a low vehicle density of 15veh/km and an intermediate traffic density of 25veh/km with $\sigma = \frac{1}{2D}$, respectively. The node densities for different traffic flow condition are chosen according to Table 1.1. The cluster size K varies from $K = 0$ to $K = K_{max}$, where K_{max} is the size of a cluster that covers the entire road segment. Note that $K = 0$ and $K = K_{max}$ correspond to N_{HWY} single-node clusters and a single cluster containing N_{HWY} nodes on average, respectively. Hence, the four protocols at the two extreme limits of K behave as flat routing. The values at $K = 0$ and $K = K_{max}$ are equivalent to the overhead of a flat routing that is used in the inter- and intra- cluster routing, respectively. However, the difference in the total overhead between the two extremes is due to the clustering overhead ψ_c. When the network is a cluster of

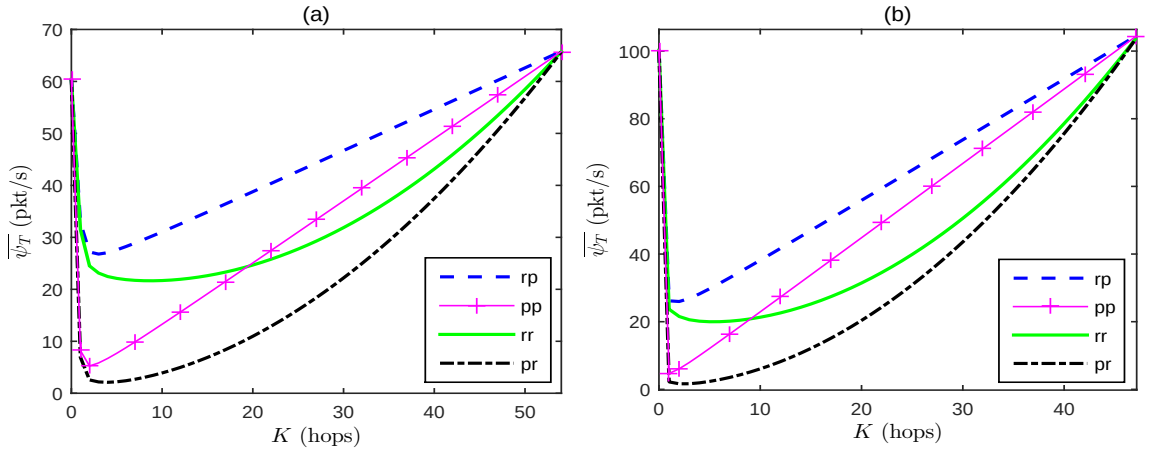

Figure 5.3: Average total routing overhead in pkt/s for four generic non-overlapping cluster-based routing protocols versus the cluster size (in hops) for $R = 250m$. The average overhead is normalized by the average number of nodes. (a) low vehicle density with $D = 15$veh/km and (b) intermediate vehicle density with $D = 25$veh/km and $\sigma = \frac{1}{2D}$

size K_{max}, the CH will flood a CH-Hello packet to an average of N_{HWY} CMs, where each CM replies with a CM-Hello packet. On the other hand, ψ_c for single-node clusters (at $K = 0$) is equivalent to the Hello messaging overhead used in flat routing.

It is apparent that clustering reduces the total routing overhead from that in flat routing. For small clusters, the inter-cluster routing overhead is dominant, making $E[\psi_{rr}]$ closer to $E[\psi_{rp}]$ than to the averages of the two other protocols, while for large clusters the intracluster routing overhead is dominant, thus making $E[\psi_{rr}]$ closer to $E[\psi_{pr}]$. This shows the trade-off between the inter- and the intracluster routing overheads as the cluster size increases. Hence, there exists a K^* value at which the routing overhead becomes minimum. However, when the node density increases, the increased number of nodes within a cluster will result in a larger intracluster routing overhead. As a result, K^* can change with node density.

Figure 5.4(a) plots the cluster size K^* that minimizes the average routing overhead versus the vehicle density for the four different protocols, for disjoint clusters. The K^* value is obtained using the low traffic flow calculations for densities < 26veh/km and the intermediate traffic flow calculations for densities > 25veh/km. The standard deviation σ is chosen to linearly decrease from 0.5μ to 0.3μ [1] with the increase of vehicle density (for the intermediate model only). This is realistic since, as the density increases, the inter-vehicle distance approaches a constant value. The K^* value decreases when the density

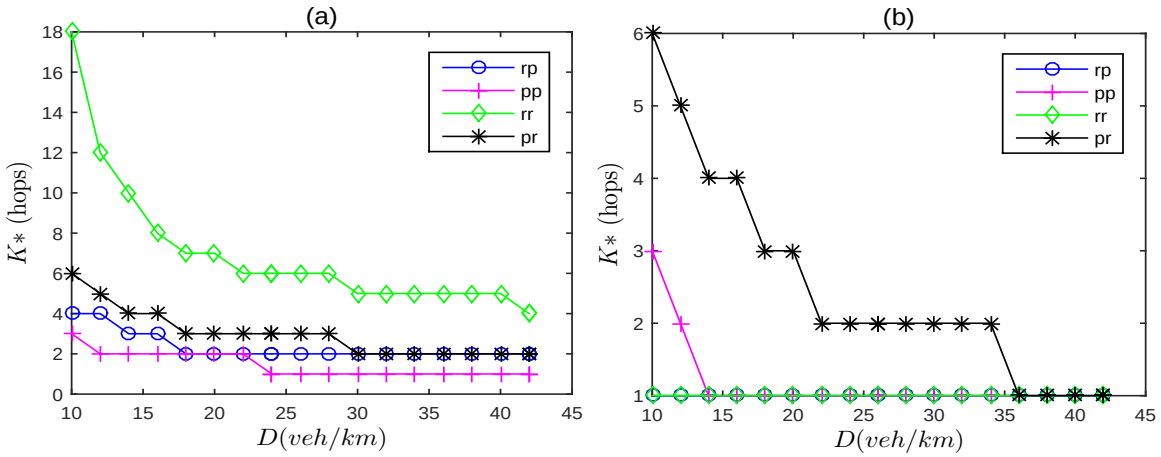

Figure 5.4: The cluster size K^* that minimizes the routing overhead versus vehicle density for $R = 250$meters when (a) $l_o = 0$ (b) $l_o = l_o^*$.

increases for all the protocols. When we allow overlapping and find K^* and l_o^* that minimize the average routing overhead using an exhaustive search, the average reactive-reactive and the average reactive-proactive routing overheads are minimized with completely overlapping single-hop clusters (i.e., $K^* = 1$, and $l_o^* = 0.5$), regardless of the vehicle density. On the other hand, both the average proactive-proactive and proactive-reactive routing overheads are minimized with partially overlapping clusters when $l_o^* < 0.1$, whereas K^* reduces with the vehicle density. Figure 5.4(b) plots the cluster size K^* that minimizes the average routing overhead versus the vehicle density for the four different protocols, when the overlapping factor is l_o^*. Although the overlapping gain (5.14) reduces the inter-cluster reactive routing overhead, the increased number of clusters due to overlapping has a stronger effect on the overhead for proactive inter-cluster routing protocols (by comparing (5.5) with (5.6)). Therefore, only those protocols with reactive inter-cluster routing benefit from complete overlap in reducing the average total overhead.

5.2 Impact of cluster instability on the routing overhead

In this section, we focus on one of the four generic routing protocols discussed in the previous section, which is reactive-proactive routing protocol. In a reactive intercluster routing protocol, a route discovery process is triggered when a source node has data to

send to a destination node outside of its cluster. The CHs and gateways are responsible of broadcasting the route request packet. When generic proactive routing is used for intracluster routing, every node has complete information of the cluster topology. This is achieved by sharing local topology information with cluster nodes via the CH. The cluster topology information is updated during the intracluster routing period whenever the local neighbourhood of a CM changes due to mobility [78]. As a result, proactive intracluster routing utilizes the local centralized management within the cluster, which is one of the main advantages of the clustered structure. We assume that the nodes on the highway are clustered by some clustering algorithm into possibly overlapping, single-hop clusters (according to the results in Subsection 5.1.4). Under the assumption that all the nodes have complete information about the network topology when the clusters are formed, we focus on the portion of routing overhead that is inflicted only by mobility.

Consider the system model described in Chapter 2. We assume that nodes access the control channel (CCH of the seven channels in the DSRC spectrum) according to a time division multiple access (TDMA)-based MAC protocol, in which time is divided into frames of constant duration τ_F seconds, and all nodes are synchronized to the beginning of the time frame. Each frame is partitioned into equal-duration time slots. We assume that the number of slots in the Hello-beaconing (Join-cluster) set is equal to the maximum number of nodes in the cluster. The time slots in a frame are partitioned into the following five sets [18, 29, 33]: *i)* two *intercluster routing* sets, in which route request (RREQ) packets are broadcast among clusters; *ii)* a *Hello-beaconing* set in which nodes broadcast their Hello messages to their one-hop neighbors; *iii)* an *intracluster routing* set, in which nodes transmit their local topology update messages; and *V)* a *Join-cluster* set, during which a newly arriving node transmit its Hello packet in order to join the cluster. Figure 5.5(a) illustrates the structure of the time frame. The time slots in the first intercluster routing set are assigned to the two gateways of the cluster. The gateways use these slots to relay RREQ packets, received from neighbouring clusters, to the CH. During the second intercluster routing set, the CH transmits RREQ packets to its gateways which relay RREQ packets to neighboring clusters. The CH builds a slot assignment table, which includes the time slots assigned for each CM for both the Hello-beaconing and the intracluster routing sets, and broadcasts it to its CMs during the CH Hello slot. Each cluster uses a unique frame from the two different frames used by its neighbouring cluster. That is, the time frame is reused every two clusters as illustrated in Figure 5.5(b)-(c). This is done to avoid intercluster interference that may be caused when clusters overlap as discussed in Appendix C.1. A cycle is the time period between two points in time that refer to the same time slot of the same time frame. That is, a cycle equals $3\tau_F$ seconds.

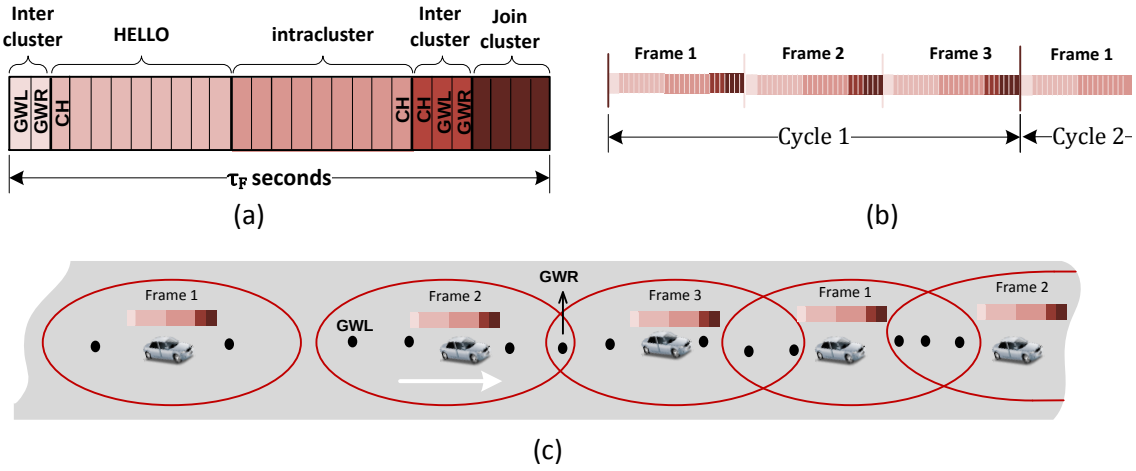

Figure 5.5: (a) Partitioning of a time frame into intercluster routing, Hello-beaconing, intracluster routing, and Join-cluster sets. (b) Time division into cycles each containing three consecutive frames. (c) Spatial reuse of frames within one cycle. GWR and GWL are the right and the left gateways of a cluster.

5.2.1 Intracluster routing overhead

At the beginning of the cluster's time frame and in the Hello beaconing period, each CM transmits its Hello message in the slot assigned by the CH. The CH assigns slots based on its cluster topology information from the previous cycle. If a CM detects a change in its local neighborhood during the cycle, the CM will broadcast a topology update message during the intracluster routing set[1]. Let $\Psi_{intra,i}$ be the intracluster routing overhead for node i in packets per frame. The value of $\Psi_{intra,i}$ depends on the node type. A node can be one of four types: *1)* CH; *2)* CM if it belongs to one cluster; *3)* common cluster member (CCM), CM that belongs to two neighboring clusters; or *4)* unclustered node (UN), if it is positioned in the unclustered region between two non-overlapping clusters.
If the node is a CM that belongs to one cluster, $\Psi_{intra,i}$ is either one or zero, depending on whether or not the node's local neighborhood changes during a cycle (of $3\tau_F$ seconds). Let P_H be the probability that a CM's local neighborhood changes during a cycle. A CM's neighborhood changes when *i)* a node leaves its neighborhood, leading to a disconnected communication link from the node to the CM; or *ii)* a node enters the CM's neighborhood, establishing a new link between the node and the CM. Let T_H be the time period between

[1]A CM detects a change in its neighborhood from the Hello beaconing period.

two successive changes in the node's one-hop neighborhood. The value of T_H is equal to the minimum of the first occurrence times for event *i)* and event *ii)*. Event *i)* occurs when the distance between the reference node and the hop edge node becomes larger than the transmission range, i.e, when the sum of distance headways $\{X_i\}_{i=0}^{N_H-1}$ becomes greater than the transmission range, where N_H is the number of nodes between the reference node and the hop edge node. On the other hand, event *ii)* occurs when the sum of distance headways of the set $\mathbb{X}_H = \{X_i\}_{i=0}^{N_H}$ becomes less than the transmission range. Let $F_{T_H}(m)$ be the cumulative distribution function (cdf) of T_H. $F_{T_H}(m)$ can be calculated by implementing first passage time analysis on a (N_H+1)-dimensional Markov chain that represents a system of (N_H+1) distance headways as discussed in Chapter 4. Therefore,

$$P_H = F_{T_H}\left(\tau \left\lfloor \frac{3\tau_F}{\tau} \right\rfloor\right). \tag{5.23}$$

If the node is a CM that belongs to one cluster, $\Psi_{intra,i}$ is either zero with probability $1-P_H$ or one packet per frame (pkt/f) with probability P_H. Upon receiving the local topology updates from its CMs, the CH updates the cluster topology information and broadcast it to its CMs at the end of the intracluster set. Therefore, the effect of mobility on the intracluster routing overhead can be measured by the number of topology update messages per frame. At the end of the intracluster set, a CH broadcasts a cluster topology update if at least one of its CMs and/or CCMs detects a change in their local neighborhood. Therefore, for a CH with a total of n CMs and CCMs, $\Psi_{intra,i}$ is either zero with probability $(1-P_H)^n$ or 1 pkt/f with probability $1-(1-P_H)^n$. Due to vehicle mobility, neighboring CHs may move apart from each other and the clusters may become disjoint, resulting in some CMs to become unclustered. Unclustered nodes are left without service and, therefore, they do not contribute to the intracluster routing overhead. When a node is unclustered, it stops receiving CH hello messages. Upon receiving a CH-Hello message, an unclustered node joins the cluster during the Join cluster period. The intracluster routing overhead for a common cluster member is similar to that of an ordinary CM. In the absence of mobility, two frames are sufficient to prevent intercluster interference. However, since an extra third frame is allocated to prevent intercluster interference that is caused by common cluster members, the Hello beaconing generated by the common cluster members between neighboring clusters is also considered to be mobility-induced overhead. As a result, for a CCM, $\Psi_{intra,i}$ is either 1 pkt/f with probability $1-P_H$ or 2 pkt/f with probability P_H.

In a highly dynamic VANET, vehicles approach or move apart from one another, resulting in changes in the cluster structure. The time variations of the distance between neighboring CHs, due to vehicle mobility, can cause the coverage ranges of the clusters to overlap or to become disjoint. During an overlapping/non-overlapping period, vehicles enter

and leave the overlapping/unclustered region, resulting in a change in the number of common/unclustered nodes between neighboring clusters. The number of common/unclustered nodes between neighboring clusters affects the intracluster routing overhead. In Section 4.3, we investigate the system of two neighboring clusters in terms the change of the numbers of common CMs and unclustered nodes between the two clusters along with the change in the cluster-overlap state. Assume that every two neighboring clusters are independent and have the same statistical behaviours. That is, T_{ov}'s (T_{nov}'s/N_{UN}'s/$N'_{CCM}s$) are i.i.d. for all pairs of neighboring clusters. The steady-state pmf of the number of common cluster members between neighboring clusters is approximated by a weighted geometric distribution with parameter equal to $p_g = \left(1 - \frac{\lambda_g^2}{\lambda_g^2 - 2\chi_g}\right)$ and a weight $p_s = p_{ov}$. The pmf of N_{CCM} is given by (4.19) and can be re-written as

$$P_{N_{CCM}}(n) = \begin{cases} p_s \left(1 - \frac{\lambda_g^2}{\lambda_g^2 - 2\chi_g}\right) \left(\frac{\lambda_g^2}{\lambda_g^2 - 2\chi_g}\right)^n, & n > 0 \\ (1 - p_s) + p_s \left(1 - \frac{\lambda_g^2}{\lambda_g^2 - 2\chi_g}\right), & n = 0 \end{cases} \tag{5.24}$$

where χ_g, λ_g^2, $E[T_{Ii}]$, and $c_{T_{Ii}}$ are given in Section 4.3. The value of p_s depends on the the overlap-state between neighboring clusters. The steady-state pmf of the number of unclustered nodes between two neighboring clusters, $P_{N_{UN}}(n)$, is given by (5.24) with weight $p_s = p_{nov}$.

Intracluster routing overhead per node

In this subsection, we investigate the intracluster routing overhead for a randomly chosen node from the network. Since the intracluster routing overhead varies with the node type, we first calculate the limiting probabilities of different node types in the network. Let P_{CH}, P_{CCM}, P_{UN}, and P_{CM} denote the limiting probabilities of the randomly selected node being a cluster head, a common cluster member, an unclustered node, and a cluster member, respectively. Since the number of CHs do not change in the system, $P_{CH} = \frac{N_{CH}}{N_{HWY}}$. The value of P_{CCM} depends on the total number of common nodes in the network which equals $\sum_{i=1}^{N_{CH}} N_{CCM}$ and has a negative binomial distribution with parameters p_g and N_{CH} (since N_{CCM} is geometrically distributed). Using the law to total probability, $P_{CCM} = \sum_{n=1}^{\infty} \frac{n}{N_{HWY}} p_{ov} \binom{n+N_{CH}-1}{n} (1-p_g)^{N_{CH}} p_g^n$. Therefore,

$$P_{CCM} = \frac{2p_{ov}N_{CH}\left(1 - \frac{E[T_{ov}]}{E[T_{nov}]}\right)}{\lambda_g^2 N_{HWY}}. \tag{5.25}$$

Similarly, $P_{UN} = \frac{2p_{nov}N_{CH}\left(1-\frac{E[T_{ov}]}{E[T_{nov}]}\right)}{\lambda_g^2 N_{HWY}}$. As a result, $P_{CM} = 1 - \frac{N_C H}{N_{HWY}} - \frac{2N_{CH}\left(1-\frac{E[T_{ov}]}{E[T_{nov}]}\right)}{\lambda_g^2 N_{HWY}}$. The intracluster routing overhead for a random node in the network is given by

$$P_{\psi_{intra,i}}(m) = \begin{cases} P_{CM}(1-P_H) + P_{CH}P_{Hn} + P_{UN}, & m = 0 \\ P_{CM}P_H + P_{CH}\left(1-P_{Hn}\right) + P_{CCM}(1-P_H), & m = 1 \\ P_{CCM}P_H, & m = 2 \\ 0, & otherwise \end{cases} \tag{5.26}$$

where $P_{Hn} = \sum_i P(N_{CM} = i)(1-P_H)^i$ is the probability that none of the nodes in the cluster detect a change in their one-hop neighborhood.

Total intracluster routing overhead of a random node sample

Suppose now we want to find the total intracluster routing overhead for n nodes randomly sampled from the network, and denote this overhead by $\Psi_{intra,n}$. We assume that the sampling probabilities are independent of the number of nodes sampled and they equal the node type probabilities[2]. Each node from the n selected nodes contributes to the total overhead by $\Psi_{intra,i}$ pkt/f, i.e., either 0,1, or 2 pkt/f. Let $\mathbb{A}_{\Psi_{intra,n}} = \{(a_0(i), a_1(i), a_2(i))\}_{i=1}^{|\mathbb{A}_{\Psi_{intra,n}}|}$ be a matrix of three columns, where each row represents a possible number of occurrences of overhead 0,1, or 2 pkt/f for the n sampled nodes. That is, $a_2(i)$ nodes from the n nodes contribute 2 pkt/f to the total overhead, with $\sum_{j=0}^{2} a_j(i) = n\,\forall i$. The sequence $(a_0(i), a_1(i), a_2(i))$ is a 3-restricted ordered integer partition of a positive integer n. Here we allow the part to be zero. An ordered 3-restricted integer partition of an integer n is an integer partition of n into exactly 3 parts. Therefore, $\mathbb{A}_{\Psi_{intra,n}}$ is a set of all possible 3-restricted ordered integer partitions of n, where $a_j(i)$, $0 \le j \le 2$, is the j^{th} part of the i^{th} partition, $0 \le a_j(i) \le n$, $1 \le i \le |\mathbb{A}_{\Psi_{intra,n}}|$, and $|\mathbb{A}_{\Psi_{intra,n}}| = \binom{n+2}{2}$ is the total number of such partitions, i.e., the number of rows in $\mathbb{A}_{\Psi_{intra,n}}$. The probability of occurrence of rows in $\mathbb{A}_{\Psi_{intra,n}}$ follows a multinomial distribution with parameters n, $P_{\Psi_{intra,i}}(0)$, $P_{\Psi_{intra,i}}(1)$, and $P_{\Psi_{intra,i}}(2)$. The cdf of total overhead for n nodes selected randomly from the network can be derived to be

$$F_{\Psi_{intra,n}}(m) = \sum_{i=0}^{\sum_{k=0}^{m} I_{m,n}} \frac{n!}{\prod_{k=0}^{2}[a_k(i)]!} \prod_{j=0}^{2} \left[P_{\Psi_{intra,i}}(j)\right]^{a_j(i)}, \quad 0 \le m \le 2n \tag{5.27}$$

[2]This is true only when the number of clusters is large relative to the number of sampled nodes.

where $I_{m,n}$ is the number of rows in $\mathbb{A}_{\Psi_{intra,n}}$ that result a total overhead of m pkt/f, given by

$$I_{m,n} = \begin{cases} \lceil \frac{m+1}{2} \rceil, & m < n \\ \lceil \frac{2n-m+1}{2} \rceil, & m \geq n. \end{cases} \tag{5.28}$$

5.2.2 Intercluster routing overhead

In this section, we analyze the impact of vehicle mobility on the intercluster routing overhead. When a reactive intercluster routing protocol is used, only if the source and destination are in different clusters, a route discovery process is initiated. The CHs and gateways are responsible for disseminating the route request packet during the intercluster routing sets. When the destination is found, the route information (sent back to the source node) is composed of local cluster membership information of each cluster on the route. The data packets are then forwarded according to local topology information within each cluster on the route towards the destination cluster. Every CM maintains its cluster's topology map. The local cluster membership information changes whenever a node leaves or enters the cluster.

Let L denote the route length between a source-destination pair, in terms of number of clusters and Ψ_{inter} the intercluster routing overhead per route request measured in packets[3]. As discussed in Subsection 5.1.1, the number of packets needed to broadcast a packet from one CH to a neighboring CH, Φ_{CH}, depend of the cluster-overlap state. When two neighboring CH overlap and share common cluster members, $\Phi_{CH} = 2$ packets. On the other hand, $\Phi_{CH} = 3$ packets when the two clusters are disjoint and the clusters' gateways are one-hop neighbors. After clusters are initially formed, the clusters are connected via gateways. However, due to vehicle mobility, clusters may move apart from each other resulting in the breakage of the link between the two gateways and, therefore, the two clusters become disconnected. Here, vehicle mobility imposes changes in route availability and cluster overlap state along the route, affecting the intercluster routing overhead. Consider two neighboring disjoint clusters in a connected network. The clusters' gateways are connected if and only if the distance between them is less than the transmission range. Let N_E be the number of nodes between the two gateways. Let $\mathbb{X}_{\mathbb{N}_\mathbb{E}}$ denote the system of distance headways between the two gateways. The time variations of $\mathbb{X}_{\mathbb{N}_\mathbb{E}}$ can be represented as a lumped Markov chain with a transition matrix $\tilde{M}_E$ (Theorem 1 in Section 4.1).

[3]Since disseminating the RREQ depends on the sequential delivery to the next relay node, we calculate the intercluster routing overhead in terms of packets. The spatial reuse of the time frame is irrelevant in this case.

Two neighboring clusters are connected if they overlap or if their gateways are connected. According to corollary 1 (in Section 4.1, the probability that two neighbouring clusters are connected via gateways is given by

$$P_E = p_{ov} + \sum_{n=1}^{N_{UN,\max}} P(N_{UN} = n) \sum_{\substack{i \\ \Omega_i \in \Omega_R}} \mho_{i,n+1} \tag{5.29}$$

where $N_{UN,\max}$ is the maximum number of unclustered nodes between two neighboring cluster[4] and $\mho_{i,n+1}$ is the steady-state probability that the system of $n+1$ distance headways, $\mathbb{X}_{n+1}$, is in lumped state $\Omega_i \in \Omega_R$, where Ω_R is a set of lumped states, s.t. $\Omega_i\{s_0, s_2, \ldots, s_n\} \in \Omega_R$, s.t. $\sum_{i=0}^{n} s_i \leq N_R$. The steady-state distribution, $\mho_{i,n+1}$, is a multinomial distribution with parameters $n+1$ and the stationary distribution of one-dimensional Markov chain X (corollary 2 in Section 4.1).

Reactive routing protocols may utilize a caching process, during which past discovered routes are stored in node's cache and used whenever the node needs to send data to the same destination. However, the dynamic topological changes in VANETs can lead to invalid caches. For example, in DSR/AODV protocol [49], a route error message is sent in the direction of the source to eliminate the invalid cache entries, when a link in a cached route is broken [49]. As a result, only when a cache is invalid a route discovery process is triggered[5]. Let τ_L denote the time interval between successive route requests of the same source-destination pairs. The probability that a route of length L clusters is cached is given by $P_{che} = (1 - F_{T_{CM}}(\tau_L))^L$, where T_{CM} is the time interval between successive changes in cluster membership and is given by (4.12). When a source node requests a route that is not cached, a route discovery process is triggered. At the end of the time frame, an RREQ is broadcasted to the gateway node within the source cluster during the second intercluster routing set. If the gateway is connected to the neighboring cluster's gateway/CH, it forwards the RREQ to the neighboring cluster; otherwise, a route to the destination is not found. The RREQ propagation continues to the next cluster with probability P_E, and the total intercluster routing overhead increases by 3 packets or 2 packets with probabilities P_{C0} and $1 - P_{C0}$, respectively. This can be illustrated by a probabilistic rooted tree starting at the root node representing the source cluster as shown in Figure 5.6. Each tree-node represents the number of packets that can be added to the total intercluster routing overhead. A link between a parent tree-node and a child tree-

[4]We assume that the value of $1 - F_{N_{UN}}(N_{UN,\max})$ is negligible

[5]We do not consider the control signaling overhead associated with route repairs in our calculation of intercluster routing overhead.

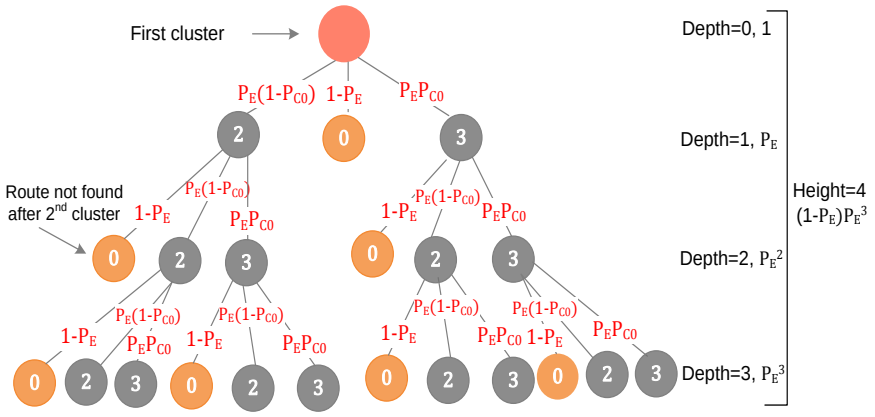

Figure 5.6: An illustration of the intercluster routing overhead for a route of length L. The route discovery process halts when two neighbouring clusters are disconnected with probability $1 - P_E$.

node is weighted by the probability of reaching the child tree-node given that the sample path (or realization) passed through the parent tree-node. The depth of the tree increases with probability P_E. When the tree hits a tree-node with value zero, the route does not exist. The height of the tree can be at most L. A leaf-node is a node that the tree stops, i.e., a tree-node with a value zero or a tree-node at depth L. To find the distribution of the intercluster routing overhead for a route of length-L clusters, Ψ_{inter}, the occurrence probabilities of all possible sample paths from the root node to every leaf node in the tree need to be found. The occurrence probability of a sample path is the product its links' weights. The length of the path from the root node to a leaf node follows a truncated geometric distribution and the pmf is given by

$$P_{Lf}(l) = \frac{P_E^l(1 - P_E)}{1 - P_E^L}, \quad 0 \leq l \leq L - 1. \tag{5.30}$$

For a path of length l, the number of tree-nodes of value 3 follow a binomial distribution with parameters l and P_{C0}. The minimum and the maximum total routing overhead resulting from a path of length l are $2l$ and $3l$, respectively. Let $\mathbb{B}_m$ be a matrix of two columns. The elements in row $\{b_{m,1}(i), b_{m,2}(i)\}$ represent the frequencies of parts 2 and 3, respectively, in the i^{th} integer partition of m into at most L parts, where each part is either 2 or 3. The pmf of the intercluster routing overhead per route request of length-L

clusters is given by

$$P_{\Psi_{inter}}(m) = \begin{cases} P_{che}, & m = 0 \\ (1 - P_{che}) \sum_{l=\lceil \frac{m}{3} \rceil}^{\min(\lfloor \frac{m}{2} \rfloor, L)} P_{Lf}(l-1) \binom{l}{b_{m,2}(l-\lceil \frac{m}{3} \rceil+1)} & \\ P_{C0}^{b_{m,2}(l-\lceil \frac{m}{3} \rceil+1)} (1 - P_{C0})^{l - b_{m,2}(l-\lceil \frac{m}{3} \rceil+1)}, & 2 \leq m < 3L \\ 0, & \text{otherwise.} \end{cases} \tag{5.31}$$

The vehicle mobility effect on the intercluster routing overhead is conveyed in P_{che}, P_{Lf}, and P_{C0}.

5.2.3 Numerical results and Discussion

This section presents numerical results for the analysis of the proposed cluster-based routing overhead. Consider a connected VANET with an intermediate vehicle density of 26 vehicles per kilometer [1] and transmission range R of 160 meters. For the initial clusters, we use a simple weighted clustering algorithm, where CHs are chosen with the minimum average relative speed to its one-hop neighbors, such that each vehicle belongs to a cluster and no two CHs are one-hop neighbors (i.e., similar to the use of mobility information for clustering in [12, 22]). The vehicle speeds are i.i.d. and are normally distributed with mean 100 kilometer per hour and standard deviation of 10 kilometesetr per hour [1]. The parameters of the limiting behavior of the overlapping/non-overlapping period and the number of common/unclustered nodes are set according to the results in [53] and listed in Table 5.1. Table 5.1 also lists the parameters of the Markov-chain distance headyway model and the transition probabilities which are tuned according to the results in [51]. Based on these parameters, we generate time series of distance headway data according to the microscopic mobility model, using MATLAB. Each simulation consists of 20,000 iterations.

Table 5.1: System parameters in simulation and analysis of Chapter 5

Parameter	value	Parameter	value
R (meter)	160	N_{CH}	120
τ_F	1 [79]	τ	2
$N_{\max}$	9	N_{HWY}	962
$E[T_{Io}]$	0.71	$E[T_{Ii}]$	0.71
$E[T_{nov}]$	38.52	$E[T_{ov}]$	12.61
$c^2_{T_{Ii}}$	5.35	P_{C0}	0.86
P_H	0.28	P_{U0}	0.57

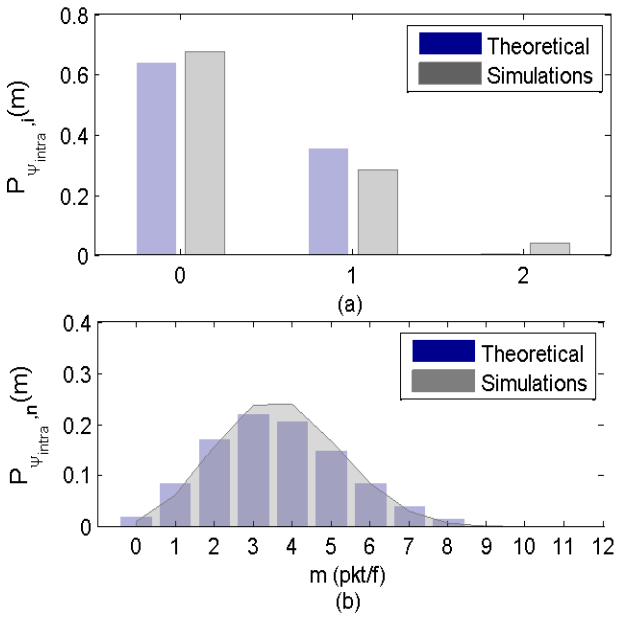

Figure 5.7: The pmfs of (a) the intracluster routing overhead for a random node $\Psi_{intra,i}$ and (b) the total intracluster routing overhead for $n = 10$ nodes sampled randomly from the network, $\Psi_{intra,n}$.

Figure 5.7 (a) plots the probability distribution of intracluster routing overhead per node, $P_{\Psi_{intra,i}}$. The theoretical value of $P_{\Psi_{intra,i}}$ is calculated using (5.23)-(5.26). The simulation value of $P_{\Psi_{intra,i}}$ is calculated using frequency count by taking into consideration the type of nodes in the cluster and the frame ID to access the network. Figure 5.7 (b) plots the intracluster routing overhead for $n = 10$ nodes randomly selected from the network. The results from the theoretical calculation have close agreement with the simulation results. Note that the theoretical calculation is based on the independent sampling probability. As a result, the proximity between theoretical and simulation results increases as the number of vehicles sampled from the network decreases relative to the number of clusters in the network.

Figure 5.8 plots the pmf of the intercluster routing overhead for a route of length $L = 20$ clusters. The irregular shape of the pmf, $P_{\Psi_{inter}}$, is due to the difference in the value of Φ_{CH} from one cluster to another along the route and the link availability due to vehicle mobility. Consider a clustering algorithm that forms connected overlapping clusters. Without the

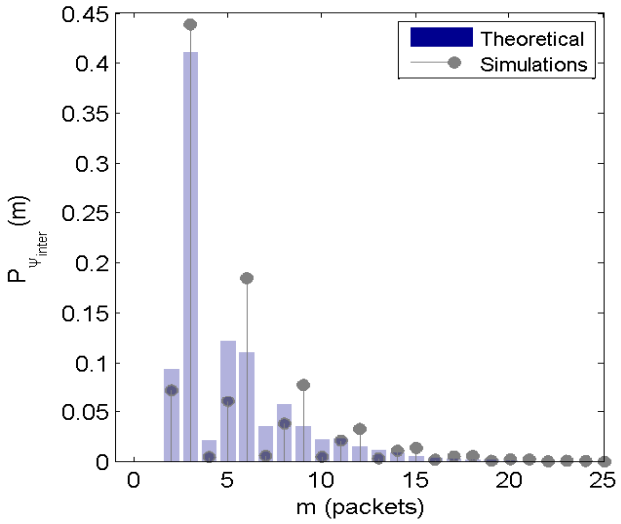

Figure 5.8: The pmf of the intercluster routing overhead for a route of length $L = 20$.

mobility effect, the intercluster routing overhead for a route of length L is equal to $2L$, since $P_{C0} = 0$ and $P_E = 1$. However, due to vehicle mobility, the cluster overlap state can change and so can the connectivity of the clusters. As a result, the availability of the cluster-level route and the value of Φ_{CH} between neighboring clusters change over time. Moreover, if $P_E = 1$, i.e., there is always a route of length L to the destination, the shape of the pmf $P_{\Psi_{inter}}$ becomes regular.

The intracluster routing overhead results show that the increase in the total overhead due to common cluster members is low. As a result, we can infer that two time frames can be made sufficient for the medium access of nodes (e.g., the use of spatial node assignment method [29]). The probability distributions of $\Psi_{intra,i}$ and Ψ_{inter}, derived in this work, provide measures for the impact of cluster instability on the routing overhead. They can be used to determine the size of the intracluster routing set in the time frame are to determine whether slot allocation should be contention-free or contention-based. Additionally, the cache timeout period can be chosen such that the probability of using an out-of-date route information is less than a desired probability threshold [49].

5.3 Summary

In this chapter, the impact of cluster structure and vehicle mobility on generic routing overhead is analyzed. The first part of this chapter presents a preliminary investigation on the impact of cluster structure in terms of cluster size and cluster-overlap on the average routing overhead when the network is stationary. Numerical results show the tradeoff between having smaller clusters and fewer clusters. For disjoint clusters, the cluster size that minimizes the overhead decreases when the density increases. However, when clusters are allowed to overlap, single-hop clusters minimize the routing overhead when reactive routing is used for intercluster routing strategy.

Considering a VANET that is clustered into possibly overlapping single-hop clusters at the cluster formation stage. The second part of this chapter presents a stochastic analysis of cluster instability impact on reactive-proactive routing overhead. These analysis are concerned with the impact of microscopic vehicle mobility on the cluster-based routing overhead, after cluster formation. The probability distributions of the rates of change in cluster membership and cluster-overlap state are utilized as measures of cluster instability. The limiting probability distributions of the numbers of common and unclustered nodes between neighboring clusters are used to determine the probabilities of four node types, which are then used to calculate the probability distribution of the proactive intracluster routing overhead for a single node and that for n randomly selected nodes from the network. Additionally, the intercluster routing overhead per route request is represented as a rooted tree from which its probability distibution is derived. The probability distributions for the cluster-based routing overhead can be helpful in the development of efficient cluster-based routing protocols for VANETs.

Chapter 6

Conclusions and Future work

6.1 Conclusions

VANETs are promising additions to our future intelligent transportation systems, which support various safety and infotainment applications. Recent years have witnessed extensive R&D activities world wide from auto companies, academics, and government agencies that have been working to develop VANETs on the transport infrastructure. VANETs are prone to large number of nodes, traffic jams, and variable traffic density. As a result, the network protocols designed for VANETs should be scalable. Node clustering is a potential approach to enhance scalability of network protocols in VANETs. However, the highly dynamic nature of VANETs imposes new challenges on forming and maintaining node clusters. The movements of vehicles with high and variable speeds cause frequent changes in the network topology, which increase the clustering cost. The main objective of this research is to study the effectiveness of node clustering for VANETs. To achieve the objective, this thesis presents stochastic analysis of node cluster stability in a highway VANET.

Due to vehicle mobility, communication links between network nodes switch between connection and disconnection. The change in VANET topology, caused by vehicle mobility, is a major contributor to cluster instability. To capture the changes in VANET topology, the communication link length and its lifetime are analyzed. A microscopic vehicle mobility model is proposed that describes the time variations of a distance headway. It models the distance headway as a discrete-time Markov chain that preserves the realistic dependency of distance headway changes at consecutive time steps. This dependency is consistent with highway traffic patterns from empirical NGSIM and simulated VISSIM data sets. The

proposed mobility model is a promising candidate vehicle mobility model to be utilized for traceable mathematical analysis in VANETs. The microscopic mobility model is used to analyze the communication link lifetime between a reference node and its hop edge node. Results indicate that on average, congested traffic flow conditions can cause communication links to break faster than in free traffic flow conditions.

The node cluster stability model characterizes two cluster stability metrics: the change rate in the overlap state between neighboring clusters as a measure of external cluster stability and the change rate in cluster-membership as a measure of internal cluster stability. The proposed microscopic mobility model is mapped into a lumped mobility model that describes the mobility of a group of vehicles. The proposed lumped mobility model facilitates the calculation of the probability distributions of the cluster stability metrics for a large number of vehicles within a cluster (or between two neighboring CHs). Additionally, the system of two neighboring clusters is investigated in terms of the change in the numbers of common CMs and unclustered nodes between the two clusters along with the change in the cluster-overlap state. The limiting behavior of this system is approximately characterized by a simple quantitative measure of the steady-state external cluster stability.

As an application of node clustering, a clustered VANET creates a virtual backbone that can be made responsible for the discovery and maintenance of routing paths, thus limiting the amount of control signalling overhead of routing protocols. The impact of cluster characteristics (cluster size and cluster overlap state) on the average routing overhead is analyzed. Results show a tradeoff between having smaller clusters and fewer clusters. Additionally, the cluster characteristics that minimize the average routing overhead are found to be dependent on the node density and/or the strategy used for inter- and intra- cluster routing. Furthermore, clusters formed with a structure that minimizes the routing overhead for a stationary network are considered. Then, the impact of the cluster instability, inflicted by node mobility, on the routing overhead is analyzed using the proposed cluster stability metrics. While the clusters can be initially formed to minimize the routing overhead, node mobility can change the originally formed clusters. The variation of clusters over time increase the control overhead and thus need to be taken into account.

The results of this research will help to develop guidelines for node clustering design in VANETs.

Firstly, the cluster stability analysis is a candidate tool for evaluating proposed clustering algorithms for VANETs. Given the distribution of the initial clusters formed by a clustering algorithm, the probability distributions of the cluster stability measures in terms of the cluster's relation with its CMs and its relation with neighboring clusters can be found. Secondly, the probability distributions derived for the proposed cluster stability

measures can be utilized for efficient parametrization of clustering algorithms for VANETs. For example, the distribution of the cluster-overlapping period can be utilized to dynamically choose the value of the time threshold used to avoid frequent merging and splitting of neighbouring clusters in VANETs [12, 15, 36]. The time period between successive cluster-membership changes provides a lower bound on the cluster-membership duration. This can be used to choose the time threshold value that determines when an unclustered node can create its own cluster after it has disconnected from its CH, thus minimizing re-clustering frequency [12, 15, 36]. Thirdly, the analysis of the impact of cluster instability on generic routing overhead can be utilized to determine the effectiveness of node clustering for routing in VANETs. This can be done by comparing the control overhead of a flat routing protocol with that of a cluster-based routing.

Despite the simplicity of the system model considered in this thesis, the results can be utilized for more general systems. The thesis focuses on vehicle traffic flow in one direction only. However, this is applicable to most clustering algorithms in the VANET literature. To enhance cluster stability, only vehicles moving in the same direction can be clustered together [12, 23]. Clusters on a single direction highway can be utilized for safety applications. For example, when a sudden break or an accident occurs, safety messages are generated by the source vehicle. Using the cluster backbone nodes, the safety message is disseminated upstream to vehicles travelling in the same direction as the source vehicle [80, 81]. In this case, the safety messages are only relevant to vehicles travelling in the same direction as they are in the danger zone. Although this thesis focuses on a single lane only, the lane is considered to be from a multi-lane highway. Therefore, the results of this thesis account for the majority of highway traffic scenarios in reality, rather than the limited case of a single lane highway.

This research has mainly addressed the effect of vehicle mobility, in terms of changing intervehicle distance headways over time, on communication link lifetime, on the external/internal cluster stability measures, and on cluster-based routing overhead. The resulting analyses of this research can still be insightful in the early stages of VANET implementation, i.e., when the penetration rate of the V2V technology is low. This is because the effect of mobility is independent of the penetration rate of the V2V technology. For example, the communication link between two equipped vehicles separated by a number of non-equipped vehicles is the same as that calculated in Chapter 3.

6.2 Future research direction

Our communication link analysis (and, therefore, the node cluster stability model) depends only on the link distance. In reality, the communication link between two nodes depends not only on the distance between the two nodes, but also on the communication channel condition. Although the distance between two nodes may be less than the communication range, poor channel conditions can result in inability of the two nodes to communicate. Both vehicle mobility and vehicle density affect the communication channel conditions. Additionally, as the vehicle density increases to a traffic jam situation, the network data load increases. In this case, the communication between two nodes (and, therefore, the link lifetime) is controlled by the network data traffic congestion rather than by vehicle mobility. Extending our communication link analysis to account for the communication channel condition and the network data load needs further investigation.

To date, VANET analysis and protocol design are mainly based on vehicle mobility models and/or vehicle traffic patterns on urban roads and highways, irrespective of the communication effect on the vehicle traffic. How VANETs implementation affect the vehicle traffic patterns and how to account for the changes in vehicle traffic pattern in the protocol design is an important research topic.

In the first part of our cluster-based routing overhead analysis, the cluster structure that minimizes the routing overhead is investigated for a stationary network. In the second part, the cluster instability impact on the routing overhead is analyzed based on initial clusters with structure from results of the first part. An effective cluster structure should take account of both costs at the same time. One promising node clustering algorithm for VANETs is *evolutionary clustering*, that aims to optimize a combination of a snapshot quality and a temporal smoothness cost.

Appendix A

A.1 Hop length distribution for intermediate vehicle density

From (2.3), the pdf of the inter-vehicle spacing X $\sim Pears(\lambda, z, \alpha)$, and the corresponding cdf is

$$\begin{aligned} F_X(x) &= \int_{\alpha}^{x} f_X(x)dx \\ &= \int_{\alpha}^{x} (x-\alpha)^{z-1} e^{-\lambda(x-\alpha)} dx. \end{aligned}$$

Letting $u = \lambda(x-\alpha)$,

$$\begin{aligned} F_X(x) &= \frac{\lambda^z}{\Gamma(z)} \int_0^{\frac{x-\alpha}{\lambda}} \left(\frac{u}{\lambda}\right)^{z-1} e^{-u} \lambda du \\ &= \frac{1}{\Gamma(z)} \int_0^{\lambda(x-\alpha)} u^{z-1} e^{-u} du \\ &= \frac{\gamma(z, \lambda(x-\alpha))}{\Gamma(z)}. \end{aligned}$$

From (3.3), we have

$$\begin{aligned} F_H(h) &= \frac{P\left(A^c(R-h)\right)\left(1-P(A^c(h))\right)}{1-P\left(A^c(R)\right)} \\ &= \frac{(1-F_X(R-h))F_X(h)}{F_X(R)}. \end{aligned}$$

Substituting (A.1),

$$\begin{aligned} F_H(h) &= \frac{\left[1-\frac{\gamma(z,\lambda(R-h-\alpha))}{\Gamma(z)}\right]\left[\frac{\gamma(z,\lambda(h-\alpha))}{\Gamma(z)}\right]}{\frac{\gamma(z,\lambda(R-\alpha))}{\Gamma(z)}} \\ &= \frac{\left[1-\frac{\gamma(z,\lambda(R-h-\alpha))}{\Gamma(z)}\right]\gamma(z,\lambda(h-\alpha))}{\gamma(z,\lambda(R-\alpha))}. \end{aligned}$$

Therefore, $\frac{d}{dh}\frac{\gamma(z,f(h))}{\Gamma(z)} = \frac{f^{z-1}(h)e^{-f(h)}}{\Gamma(z)}\frac{d}{dh}f(h)$. The corresponding pdf $f_H(h) = \frac{d}{dh}F_H(h)$, which leads to

$$f_H(h) = \frac{1}{\gamma(z,\lambda(R-\alpha))}[f_X(R-h)\gamma(z,\lambda(h-\alpha))+f_X(h)\Gamma(z,\lambda(R-h-\alpha))], \quad \alpha \le h < R-\alpha.$$

Appendix B

B.1 Proof of Theorem 1

Let $M_N = \{M_N(S_i, S_j)\}$, $0 \leq S_i, S_j \leq N_{\max}^N - 1$, be the transition matrix of the N-dimensional Markov chain that represents the system of N independent copies of the 1-dimensional Markov chain, X, with transition matrix $M = \{M(u_i, u_j)\}$, $0 \leq u_i, u_j \leq N_{\max} - 1$. A discrete-time Markov chain with stochastic transition matrix M_N is lumpable with respect to the partition Ω if and only if, for any subsets Ω_i and Ω_j in the partition, and for any super states S_1 and S_2 in subset Ω_i [71],

$$\sum_{S \in \Omega_j} M_N(S_1, S) = \sum_{S \in \Omega_j} M_N(S_2, S). \tag{B.1}$$

Consider the left hand side (LHS) of (B.1). Since X is a birth-death process, the super state $S_1 = (u_0, u_1, \ldots, u_{N-1})$, $0 \leq u_i \leq N_{\max} - 1$, can transit to any super state in set $\mathbf{A} = \{(u'_0, u'_1, \ldots, u'_{N-1})\}$, where state $u'_i \in \{u_i - 1, u_i, u_i + 1\}$, i.e., $|\mathbf{A}| \leq 3^{N_{\max}}$. Let subsets $\mathbf{A_i} = \mathbf{A} \cap \mathbf{\Omega_i}$ and $\mathbf{A_j} = \mathbf{A} \cap \mathbf{\Omega_j}$. Since $M_N(S_1, S) = 0 \ \forall S \notin \mathbf{A}$, the LHS of (B.1) reduces to $\sum_{S \in \mathbf{A_j}} M_N(S_1, S)$.

Similarly, for the right hand side (RHS) of (B.1), the super state $S_2 = (v_0, v_1, \ldots, v_{N-1})$, $0 \leq v_i \leq N_{\max} - 1$, can transit to any super state in set $\mathbf{B} = \{(v'_0, v'_1, \ldots, v'_{N-1})\}$, where state $v'_i \in \{v_i - 1, v_i, v_i + 1\}$, i.e., $|\mathbf{B}| \leq 3^{N_{\max}}$. Let subsets $\mathbf{B_i} = \mathbf{B} \cap \mathbf{\Omega_i}$ and $\mathbf{B_j} = \mathbf{B} \cap \mathbf{\Omega_j}$. Since $M_N(S_2, S) = 0 \ \forall S \notin \mathbf{B}$, the RHS of (B.1) reduces to $\sum_{S \in \mathbf{B_j}} M_N(S_2, S)$.

Consider two sequences, S_i and S_j, that are permutations of each other, and define $\varrho(S_i, O_{ij}) = S_j$ to be the permutation operator on sequence S_i under index order O_{ij} that gives S_j, i.e., $S_j = (S_i(O_{ij}(k)))_{k=1}^{|S_j|}$. For example, if $S_i = (1, 0, 2)$ and $S_j = (0, 2, 1)$, then $O_{ij} = (2, 3, 1)$.

Let $S'_1 = (u'_0, u'_1, \ldots, u'_{N-1})$ be a super state in subset $\mathbf{A_j}$. Therefore, $M_N(S_1, S'_1) = \prod_{n=0}^{N-1} M(u_i, u'_i)$. Since $S_1, S_2 \in \Omega_i$, there exists an index order O_{12}, s.t. $\varrho(S_1, O_{12}) = S_2$. Additionally, $\exists S'_2 = (v'_0, v'_1, \ldots, v'_{N-1})$ s.t. $S'_2 = \varrho(S'_1, O_{12})$. Note that $S'_2 \in \mathbf{B_2}$. As a result, $M_N(S_2, S'_2) = \prod_{n=0}^{N-1} M(v_i,\, v'_i) = \prod_{n=0}^{N-1} M(u_{O_{12}(n)}, u'_{O_{12}(n)})$. Since the product operation is commutative, we have $M_N(S_2, S'_2) = M_N(S_1, S'_1)$. In general, $\forall S_1, S_2 \in \Omega_i \; s.t. \varrho(S_1, O_{12}) = S_2$ and $\forall S'_1 \in \mathbf{A_j}$, $\exists S'_2 \in \mathbf{B_j} \; s.t. S'_2 = \varrho(S'_1, O_{12})$ and $M_N(S_2, S'_2) = M_N(S_1, S'_1)$. Hence, $\sum_{S \in \mathbf{A_j}} M_N(S_1, S) = \sum_{S \in \mathbf{B_j}} M_N(S_2, S)$, which ends the proof.

B.2 Proof of Corollary 1

Consider the tri-diagonal probability transition matrix of the Markov chain, X, as described in Subsection 3.1. The stationary distribution of the chain, X, is given by

$$\pi_i = \prod_{k=0}^{i-1} \left(\frac{p_k}{q_{k+1}} \right) \pi_0, \quad 1 \leq i \leq N_{\max} - 1 \tag{B.2}$$

where $\pi_0 = \left[1 + \sum_{i=1}^{N_{\max}-1} \prod_{k=0}^{i-1} \left(\frac{p_k}{q_{k+1}} \right) \right]^{-1}$. Consider the i^{th} lumped state $\Omega_i = \{s_0, s_1, \ldots, s_N\}$. Let N_D be the number of distinct states in $\{s_0, s_1, \ldots, s_{N-1}\}$ in which $(u_1, u_2, \ldots\ u_{N_D})$ and $(n_{u_1}, n_{u_2}, \ldots, n_{N_D})$ are the sequences of distinct states and their corresponding frequencies, respectively, where $0 \leq u_i \leq N_{\max} - 1$ and $\sum_{i=1}^{N_D} n_{u_i} = N$. Note that the size of the lumped state is equal to the number of super states that are permutations of each other, i.e., $1 \leq |\Omega_i| \leq N!, 0 \leq i \leq N_{\text{L}} - 1$. Therefore, the lumped states result from all possible outcomes of choosing N states from $N_{\max}$ different states independently, where choosing state s_i has the probability π_i, $0 \leq s_i \leq N_{\max} - 1$. This is a generalization of the Bernoulli trial problem. Hence, the stationary distribution for the lumped state Ω_i is given by

$$\mho_i = \frac{N!}{\prod_{k=1}^{N_D} n_{u_k}!} \prod_{k=1}^{N_D} \pi_{u_k}^{n_{u_k}}. \tag{B.3}$$

That is, the stationary distribution of the lumped Markov chain is multi-nomial, which ends the proof.

B.3 Proof of Corollary 2

Let the lumped state $\Omega_j = \{s_0, s_1, \ldots, s_{N-1}\}$ be a lumped state such that, if the system enters this state, the event of interest occurs. Then, $\{s_0, s_1, \ldots, s_N\}$ is an N-restricted integer partition of an integer that is greater than or equal to N_{th}. In combinatorics, an integer partition of a positive integer n is a set of positive integers whose sum equals n. Each member of the set is called a *part*. An N-restricted integer partition of an integer n is an integer partition of n into exactly N parts. Therefore, $\forall \Omega_j = \{s_0, s_1, \ldots, s_{N-1}\} \in \Omega_{OV}$, $\{s_0, s_1, \ldots, s_{N-1}\}$ is an integer partition of an integer that is less than N_{th}. Since, an integer N_{th} can be partitioned into at most N_{th} parts (i.e. when all the parts equal to one) and the order of the N states in the lumped state is not important, the number of lumped states $\in \Omega_{OV}$ when $N > N_{th}$ is equal to that when $N = N_{th}$. Notice that Corollary.2 applies only on the lumped Markov chain and not the original N-dimensional one. This ends the proof.

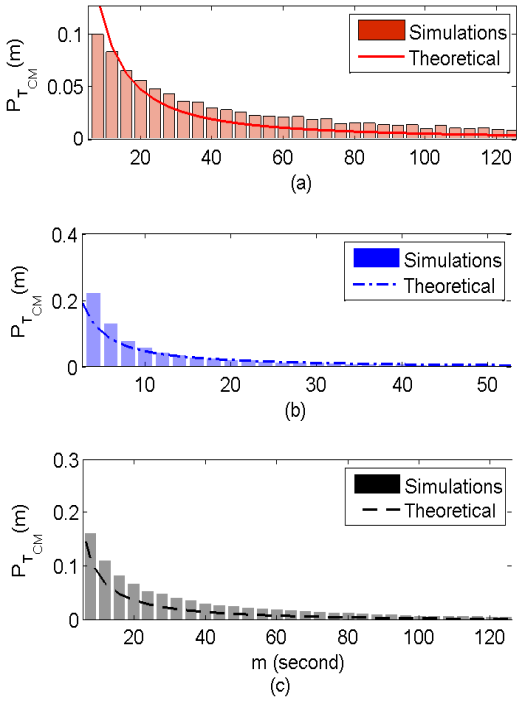

Figure B.1: The pmf of the time period between successive cluster-membership changes with vehicle density (a)$D = 9$, (b) $D = 26$, and (b) $D = 42$ veh/km.

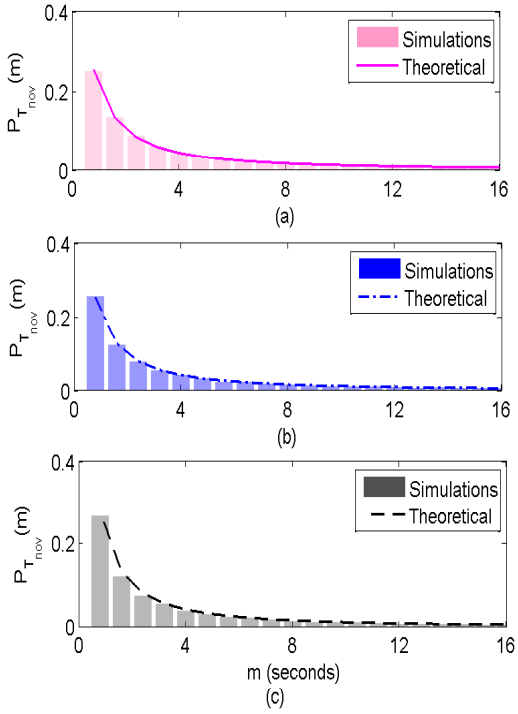

Figure B.2: The pmf of the cluster-non-overlapping time period with vehicle density (a) $D = 9$, (b) $D = 26$, and (c) $D = 42$ veh/km.

Appendix C

C.1 Intercluster interference due to cluster-overlap

A node broadcasts its Hello message during the Hello-beaconing set. Nodes within two hops from each other should be allocated different time slots. This is done to ensure that all the nodes within a node's one hop neighborhood receive the Hello message successfully. CMs of the same cluster are insured to be allocated different time slots by the CH. However, a strategy for avoiding intercluster interference should be adopted. Consider two disjoint neighboring clusters (cluster 1 and cluster 2 in Figure C.1) that are assigned the same time frame. One way to reduce intercluster interference is to use spatial slot assignment method [29]. In this method, the time slots in the Hello-beaconing set are further partitioned into a left set and a right set. The time slots of the left and the right Hello-beaconing set are spatially sorted and are assigned by the CH according to the CMs' positions [29]. However, this does not insure collision-free broadcasts. For example, if cluster 1 assigns a CM on its left the same slot assigned by cluster 2 to its left hop edge node, collision may occur at a node located in the right side of the cluster 1. Therefore, atleast two frames are required to ensure collision-free Hello message broadcast.

Consider three consecutive overlapping clusters (cluster 2, cluster 3, and cluster 4 in Figure C.1, and consider two frames assigned to neighboring clusters, as illustrated in the figure. Furthermore, assume that the spatial slot assignment method [29] is implemented. When overlapping between clusters increase, collision may still occur. This is illustrated in Figure C.1. If node B is allocated the same time slot in Frame 2 (by cluster 4) as node A (by cluster 2), a collision will occur at node C. It should also be noted that the spatial slot assignment method is sensitive to the positions of vehicles with respect to the CH and within the same side of the cluster. This makes the slot assignment method prone to failure in avoiding intercluster interference as discussed in this section. Since we assume

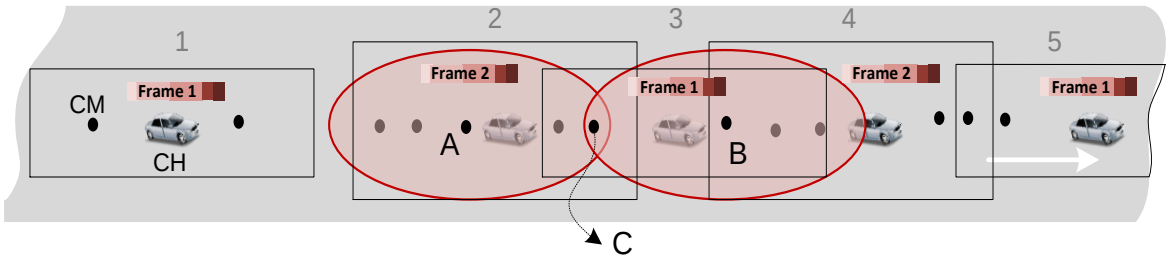

Figure C.1: Illustration of intercluster interference that may be caused when clusters overlap. Collision occurs at node C, when node A and B are allocated the same time slot during the Hello-beaconing set.

a collision free environment in our study, we consider the use of three unique frames (the minimum required).

References

[1] A. May, *Traffic Flow Fundamentals*. Prentice Hall, 1990.

[2] J. Harding, G. Powell, *et al.*, "Vehicle-to-vehicle communications: Readiness of V2V technology for application," Tech. Rep. DOT HS 812 014, U.S. Department of Transportation, 2014.

[3] H. T. Cheng, H. Shan, and W. Zhuang, "Infotainment and road safety service support in vehicular networking: From a communication perspective," *Mechanical Systems and Signal Processing*, vol. 25, no. 6, pp. 2020–2038, 2011.

[4] M. Xue, I. Er, and W. Sah, "Analysis of clustering and routing overhead for clustered mobile ad hoc networks," in *Proc. IEEE Distributed Computing Systems*, pp. 46–46, 2006.

[5] K. Sjoberg Bilstrup, E. Uhlemann, and E. Strom, "Scalability issues of the MAC methods STDMA and CSMA of IEEE 802.11 p when used in VANETs," in *Proc. IEEE ICC*, pp. 1–5, 2010.

[6] Z. Tao and G. Wu, "An analytical study on routing overhead of two-level cluster-based routing protocols for mobile ad hoc networks," in *Proc. IEEE Performance, Computing, and Communications*, 2006.

[7] L. Zhang, B. Soong, and W. Xiao, "An integrated cluster-based multi-channel MAC protocol for mobile ad hoc networks," *IEEE Trans. Wireless Communications*, vol. 6, no. 11, pp. 3964–3974, 2007.

[8] M. Jiang, J. Li, and Y. Tay, "Cluster based routing protocol (CBRP) functional specification," *IETF-Internet Draft*, 1999.

[9] D. Kim, S. Ha, and Y. Choi, "K-hop cluster-based dynamic source routing in wireless ad-hoc packet radio network," in *Proc. IEEE VTC*, vol. 1, pp. 224–228, 1998.

[10] Z. Chunhua and T. Cheng, "A multi-hop cluster based routing protocol for MANET," in *Proc. IEEE Information Science and Engineering*, pp. 2465–2468, 2009.

[11] O. Kayis and T. Acarman, "Clustering formation for inter-vehicle communication," in *Proc. IEEE ITS*, pp. 636–641, 2007.

[12] E. Souza, I. Nikolaidis, and P. Gburzynski, "A new aggregate local mobility (ALM) clustering algorithm for VANETs," in *Proc. IEEE ICC*, pp. 1–5, 2010.

[13] B. Hassanabadi, C. Shea, L. Zhang, and S. Valaee, "Clustering in vehicular ad hoc networks using affinity propagation," *Ad Hoc Networks*, vol. 13, pp. 535–548, 2014.

[14] S. Mohammad and C. Michele, "Using traffic flow for cluster formation in vehicular ad-hoc networks," pp. 631–636, 2010.

[15] S. Kuklinski and G. Wolny, "Density based clustering algorithm for VANETs," in *Proc. IEEE TridentCom*, pp. 1–6, 2009.

[16] J. Y. Yu and P. H. J. Chong, "A survey of clustering schemes for mobile ad hoc networks.," *IEEE Communications Surveys and Tutorials*, vol. 7, no. 1-4, pp. 32–48, 2005.

[17] J. Yu and P. H. Chong, "3hbac (3-hop between adjacent clusterheads): a novel non-overlapping clustering algorithm for mobile ad hoc networks," in *Proc. IEEE PACRIM*, vol. 1, pp. 318–321, 2003.

[18] Y. Gunter, B. Wiegel, and H. Großmann, "Cluster-based medium access scheme for VANETs," in *Proc. IEEE ITS*, pp. 343–348, 2007.

[19] L. Zhang, B.-H. Soong, and W. Xiao, "An integrated cluster-based multi-channel MAC protocol for mobile ad hoc networks," *IEEE Trans. Wireless Communications*, vol. 6, no. 11, pp. 3964–3974, 2007.

[20] N. MASLEKAR, M. BOUSSEDJRA, J. MOUZNA, and H. LABIOD, "A stable clustering algorithm for efficiency applications in VANETs," pp. 1188–1193, 2011.

[21] N. Maslekar, J. Mouzna, H. Labiod, M. Devisetty, and M. Pai, "Modified C-DRIVE: Clustering based on direction in vehicular environment," in *Proc. IEEE Intelligent Vehicles Symposium*, pp. 845–850, 2011.

[22] Z. Wang, L. Liu, M. Zhou, and N. Ansari, "A position-based clustering technique for ad hoc intervehicle communication," *IEEE Trans. Systems, Man, and Cybernetics, Part C: Applications and Reviews*, vol. 38, no. 2, pp. 201–208, 2008.

[23] G. Wolny, "Modified DMAC clustering algorithm for VANETs," in *Proc. IEEE Systems and Networks Communications*, pp. 268–273, 2008.

[24] D. Girinath and S. Selvan, "A novel cluster based routing algorithm for hybrid mobility model in VANET," *International Journal of Computer Applications*, vol. 1, no. 15, pp. 35–42, 2010.

[25] J. Luo, X. Gu, T. Zhao, and W. Yan, "A mobile infrastructure based VANET routing protocol in the urban environment," in *Proc. IEEE Communications and Mobile Computing*, pp. 432–437, 2010.

[26] T. Wang and G. Wang, "TIBCRPH: Traffic infrastructure based cluster routing protocol with handoff in VANET," in *Proc. IEEE Wireless and Optical Communications*, pp. 1–5, 2010.

[27] R. Aquino and A. Edwards, "A reactive location routing algorithm with cluster-based flooding for inter-vehicle communication,"

[28] D. Tian, Y. Wang, G. Lu, and G. Yu, "A VANETs routing algorithm based on Euclidean distance clustering," in *Proc. IEEE Future Computer and Communication*, vol. 1, pp. V1–183, 2010.

[29] Z. Rawashdeh and S. Mahmud, "Media access technique for cluster-based vehicular ad hoc networks," in *Proc. IEEE VTC*, pp. 1–5, 2008.

[30] A. Ahmad, M. Doughan, V. Gauthier, I. Mougharbel, and M. Marot, "Hybrid multichannel multi-hop MAC in VANETs," in *Proc. Advances in Mobile Computing and Multimedia*, pp. 353–357, 2010.

[31] G. Abdalla, M. Abu-Rgheff, and S. Senouci, "Space-orthogonal frequency-time medium access control (SOFT MAC) for VANET," in *Proc. IEEE Global Information Infrastructure Symposium*, pp. 1–8, 2009.

[32] L. Bononi and M. Di Felice, "A cross layered MAC and clustering scheme for efficient broadcast in vanets," in *Proc. IEEE MASS*, pp. 1–8, 2007.

[33] H. Trivedi, P. Veeraraghavan, S. Loke, A. Desai, and J. Singh, "SmartVANET: The case for a cross-layer vehicular network architecture," in *Proc. IEEE Advanced Information Networking and Applications Workshops*, pp. 362–368, 2011.

[34] T. Kim, S. Jung, and S. Lee, "CMMP: Clustering-based multi-channel MAC protocol in VANET," in *Proc. IEEE Computer and Electrical Engineering*, pp. 380–383, 2009.

[35] N. Chandra Rathore, R. Tomar, S. Verma, and G. Tomar, "CMAC: A cluster based MAC protocol for VANETs," in *Proc. IEEE CISIM*, pp. 563–568, 2010.

[36] H. Su and X. Zhang, "Clustering-based multichannel MAC protocols for QoS provisionings over vehicular ad hoc networks," *IEEE Trans. Vehicular Technology*, vol. 56, no. 6, pp. 3309–3323, 2007.

[37] M. Spiliopoulou, I. Ntoutsi, Y. Theodoridis, and R. Schult, "MONIC: modeling and monitoring cluster transitions," in *Proc. ACM KDD*, pp. 706–711, 2006.

[38] Z. Y. Rawashdeh and S. M. Mahmud, "A novel algorithm to form stable clusters in vehicular ad hoc networks on highways," *EURASIP J. Wireless Communications and Networking*, vol. 2012, no. 1, pp. 1–13, 2012.

[39] G. Palla, I. Derényi, I. Farkas, and T. Vicsek, "Uncovering the overlapping community structure of complex networks in nature and society," *Nature*, vol. 435, no. 7043, pp. 814–818, 2005.

[40] Y. Harikrishnan and J. He, "Clustering algorithm based on minimal path loss ratio for vehicular communication," in *Proc. IEEE Computing, Networking and Communications*, pp. 745–749, 2013.

[41] M. Krbalek and K. Kittanova, "Theoretical predictions for vehicular headways and their clusters," *Physics: Data Analysis, Statistics and Probability (arXiv)*, 2012.

[42] L. Li, W. Fa, J. Rui, H. Jian-Ming, and J. Yan, "A new car-following model yielding log-normal type headways distributions," *Chinese Physics B*, vol. 19, no. 2, 2010.

[43] S. Hoogendoorn and P. Bovy, "State-of-the-art of vehicular traffic flow modelling," *Proceedings of the Institution of Mechanical Engineers, Part I: Journal of Systems and Control Engineering*, vol. 215, no. 4, pp. 283–303, 2001.

[44] G. Yan and S. Olariu, "A probabilistic analysis of link duration in vehicular ad hoc networks," *IEEE Trans. Intelligent Transportation Systems*, vol. 12, no. 4, pp. 1227–1236, 2011.

[45] R. Luttinen, "Statistical properties of vehicle time headways," *Transportation Research Record*, no. 1365, 1992.

[46] K. Nagel and M. Schreckenberg, "A cellular automaton model for freeway traffic," *Journal de Physique I*, vol. 2, no. 12, pp. 2221–2229, 1992.

[47] F. Li and Y. Wang, "Routing in vehicular ad hoc networks: A survey," *IEEE Vehicular Technology Magazine*, vol. 2, no. 2, pp. 12–22, 2007.

[48] J. Broch, D. Maltz, D. Johnson, Y. Hu, and J. Jetcheva, "A performance comparison of multi-hop wireless ad hoc network routing protocols," in *Proc. ACM/IEEE MobiCom*, pp. 85–97, 1998.

[49] F. Bai, N. Sadagopan, and A. Helmy, "BRICS: A building-block approach for analyzing routing protocols in ad hoc networks-a case study of reactive routing protocols," in *Proc. IEEE ICC*, vol. 6, pp. 3618–3622, 2004.

[50] K. Abboud and W. Zhuang, "Analysis of communication link lifetime using stochastic microscopic vehicular mobility model," in *Proc. IEEE Globecom*, pp. 383–388, 2013.

[51] K. Abboud and W. Zhuang, "Stochastic analysis of single-hop communication link in vehicular ad hoc networks," *IEEE Trans. Intelligent Transportation Systems*, vol. 15, no. 5, pp. 2297–2307, 2014.

[52] K. Abboud and W. Zhuang, "Impact of node mobility on single-hop cluster overlap in vehicular ad hoc networks," in *Proc. ACM MSWiM*, pp. 65–72, 2014.

[53] K. Abboud and W. Zhuang, "Stochastic modeling of single-hop cluster stability in vehicular ad hoc networks," *IEEE Trans. Vehicular Technology*, 2015 (to appear).

[54] K. Abboud and W. Zhuang, "Impact of node clustering on routing overhead in wireless networks," in *Proc. IEEE Globecom*, pp. 1–5, 2011.

[55] K. Abboud and W. Zhuang, "Impact of microscopic vehicle mobility on cluster-based routing overhead in VANETs," 2015 (to be submitted).

[56] L. C. Edie and R. S. Foote, "Traffic flow in tunnels," in *Highway Research Board Proceedings*, 1958.

[57] P. Izadpanah, *Freeway Travel Time Prediction Using Data from Mobile Probes*. PhD thesis, University of Waterloo, 2010.

[58] F. Hall, "Traffic stream characteristics," *Traffic Flow Theory. US Federal Highway Administration*, 1996.

[59] X. Chen, L. Li, and Y. Zhang, "A markov model for headway/spacing distribution of road traffic," *IEEE Trans. Intelligent Transportation Systems*, vol. 11, no. 4, pp. 773–785, 2010.

[60] Q. Gong, S. Midlam-Mohler, V. Marano, and G. Rizzoni, "An iterative markov chain approach for generating vehicle driving cycles," *SAE Inter. J. Engines*, vol. 4, no. 1, pp. 1035–1045, 2011.

[61] "Next generation simulation community, vehicle trajectory data sets." http://ngsim-community.org/. Accessed Nov. 4, 2012.

[62] M. Fellendorf and P. Vortisch, "Microscopic traffic flow simulator VISSIM," *Fundamentals of Traffic Simulation*, pp. 63–93, 2010.

[63] PTV, "VISSIM 5.40 user manual," *Karlsruhe, Germany*, 2012.

[64] T. Hou and V. Li, "Transmission range control in multi-hop packet radio networks," *IEEE Trans. Communications*, vol. 34, no. 1, pp. 38–44, 1986.

[65] Y. Cheng and T. Robertazzi, "Critical connectivity phenomena in multihop radio models," *IEEE Trans. Communications*, vol. 37, no. 7, pp. 770–777, 1989.

[66] J. Fill, "The passage time distribution for a birth-and-death chain: Strong stationary duality gives a first stochastic proof," *J. Theoretical Probability*, vol. 22, no. 3, pp. 543–557, 2009.

[67] Maple, *Maple (Version 13). Waterloo, Ontario, Canada: Waterloo Maple Software.* 2009.

[68] "The math forum, "Proof of ordered partioning of integers"." http://mathforum.org/. Accessed May 13, 2013.

[69] D. Mazkewitsch, "The n-th derivative of a product," *The American Mathematical Monthly*, vol. 70, no. 7, pp. 739–742, 1963.

[70] D. Cox, *Renewal Theory.* Methuen & Co., 1962.

[71] P. Buchholz, "Exact and ordinary lumpability in finite Markov chains," *J. Applied probability*, vol. 31, no. 1, pp. 59–75, 1994.

[72] G. Rubino and B. Sericola, "Sojourn times in finite Markov processes," *J. Applied Probability*, vol. 26, no. 4, pp. 744–756, 1989.

[73] O. Kella and W. Whitt, "A storage model with a two-state random environment," *Operations Research*, vol. 40, no. 3-Supplement-2, pp. S257–S262, 1992.

[74] J. Cohen, "Superimposed renewal processes and storage with gradual input," *Stochastic Processes and their Applications*, vol. 2, no. 1, pp. 31–57, 1974.

[75] L. Kleinrock, *Queueing Systems, Volume II: Computer Applications*. John Wiely & Sons, 1976.

[76] H. Kobayashi and B. L. Mark, *System Modeling and Analysis: Foundations of System Performance Evaluation*. Prentice Hall, 2009.

[77] C. Adjih, T. Clausen, P. Jacquet, A. Laouiti, P. Minet, P. Muhlethaler, A. Qayyum, L. Viennot, *et al.*, "Optimized link state routing protocol," *The Internet Engineering Task Force, IETF, RFC*, vol. 3626, 2003.

[78] X. Wu, H. R. Sadjadpour, and J. Garcia-Luna-Aceves, "Routing overhead as a function of node mobility: modeling framework and implications on proactive routing," in *Proc. IEEE MASS*, pp. 1–9, 2007.

[79] ETSI, "Intelligent transport systems (ITS); on the recommended parameter settings for using STDMA for cooperative ITS; Access layer part," 2011.

[80] K. Abboud and W. Zhuang, "Modeling and analysis for emergency messaging delay in vehicular ad hoc networks," in *Proc. IEEE Globecom*, pp. 1–6, 2009.

[81] H. T. Cheng, H. Shan, and W. Zhuang, "Infotainment and road safety service support in vehicular networking: From a communication perspective," *Mechanical Systems and Signal Processing*, vol. 25, no. 6, pp. 2020–2038, 2011.